HAL
open science

Modélisation Géométrique et Reconstruction de Surfaces

Luc Biard

To cite this version:

Luc Biard. Modélisation Géométrique et Reconstruction de Surfaces. Géométrie algorithmique [cs.CG]. Université de Grenoble, 2009. tel-00994789

HAL Id: tel-00994789

https://theses.hal.science/tel-00994789

Submitted on 22 May 2014

HAL is a multi-disciplinary open access archive for the deposit and dissemination of scientific research documents, whether they are published or not. The documents may come from teaching and research institutions in France or abroad, or from public or private research centers.

L'archive ouverte pluridisciplinaire **HAL**, est destinée au dépôt et à la diffusion de documents scientifiques de niveau recherche, publiés ou non, émanant des établissements d'enseignement et de recherche français ou étrangers, des laboratoires publics ou privés.

MEMOIRE d'HABILITATION

présenté par

Luc Biard

pour obtenir le grade de

L'Habilitation à Diriger des Recherches

de

L'UNIVERSITE JOSEPH FOURIER
GRENOBLE

Spécialité : Informatique et Mathématiques Appliquées

Modélisation Géométrique et Reconstruction de Surfaces

Date de soutenance : 30 novembre 2009

Composition du Jury

Pr.	Gudrun ALBRECHT	Rapporteur
Pr.	Pere BRUNET	Rapporteur
Pr.	Gerald FARIN	Rapporteur
Pr.	Dominique BECHMANN	Examinateur
DR	Frédéric CHAZAL	Examinateur
Pr.	Rida FAROUKI	Examinateur
Pr.	Stéfanie HAHMANN	Examinateur
Pr.	Bernard LACOLLE	Examinateur

Habilitation préparée au sein du laboratoire
LJK

Contents

Introduction **1**

Personal bibliography **5**

1 Pythagorean Hodograph curves and geometric design **8**
1.1 Rational planar PH Curves 9
1.2 G2 approximation by Tschirnhausen quartics 12
1.3 PH Ovals of Constant Width 16
1.4 Minkowski IH curves 23
1.5 Future works 29
Bibliography 31

2 Computing Geodesics on subdivision surfaces **35**
2.1 Geodesic path on a polyhedron 36
2.2 Geodesic paths on a subdivision surface 41
2.3 Myocardium and geodesic loops 43
2.4 Conlusion and future works 45
Bibliography 47

3 Surface reconstruction via geodesic interpolation and micro-sensors **49**
3.1 The Morphosense ribbon 51
3.2 Curve reconstruction 52
3.3 The Morphosense ribbon and geodesic curves 56
3.4 Geodesic interpolation of two curves 58
3.5 Existence conditions for patches interpolating geodesic boundary curves . 62
3.6 Geodesic interpolation of curvilinear rectangles and triangles 64
3.7 Geodesic Bézier interpolation 68
3.8 Future works 71
Bibliography 72

4 Variation Diminishing Property of Bézier Curves **75**
4.1 Polar derivative 75
4.2 Diminishing variation property for univariate polynomials 76
4.3 Variation diminishing property for parametric polynomials 78
4.4 Future work 80
Bibliography 82

5 Industrial activities **83**
The method 83
Bibliography 90

PART 1 : Mémoire

Introduction

L'ensemble des thématiques abordées s'inscrivent dans le contexte de la modélisation et du calcul géométrique. La géométrie duale basée sur la théorie des enveloppes a été au coeur de la thèse de R. Ait-Haddou (1996). Les résultats obtenus sont aussi bien de nature théorique (dualité en géométrie de Minkowski) qu'algorithmique (interpolation et approximation G2 sous contraintes, construction d'ovales à largeur constante). L'expertise faite de ces méthodes nous a permis par la suite de ré-investir ces outils au travers d'activités contractuelles (ELF, Total Fina ELF) pour la propagation de fronts d'ondes en optique géométrique. Le calcul effectif de chemins géodésiques avec la thèse de V. Pham-Trong (2001), s'inscrit encore résolument dans un cadre géométrique puisque les surfaces considérées sont les surfaces du monde de "l'image" (surfaces de subdivision). Les résultats obtenus ont là encore pu être exploités avec N. Szafran au travers d'un projet de détermination de géodésiques périodiques sur le myocarde. Nous travaillons maintenant depuis quelques années en collaboration avec le LETI sur la reconstruction de courbes et surfaces à partir de capteurs. Les méthodes développées au travers de la thèse de N. Sprynski (2007) sont prospectives dans le sens où les données à traiter sont d'un type nouveau, et de nature très applicative et numérique. A contrario, les outils développés sur cette même thématique en collaboration avec le professeur R. Farouki (suite à mon séjour à l'université de Davis) et N. Szafran sont de nature plus théorique et s'appuient sur les propriétés différentielles des surfaces et des géodésiques. Enfin, l'étude des courbes Bézier et de leurs propriétés par le biais des floraisons en collaboration avec R. Ait-Haddou est là encore un "classique" de la modélisation géométrique.

Chapitre 1 : Courbes à Hodographe Pythagorien et modélisation géométrique.

Les courbes à hodographe pythagorien (PH) sont caractérisées par la propriété que leur vitesse paramétrique est une fonction polynomiale ou rationnelle du paramètre de la courbe. De par leurs propriétés algébriques, les courbes PH jouent un rôle essentiel dans certaines applications de la CAO, en modélisation géométrique, en animation et dans le contrôle de la cinématique en robotique. En particulier, les courbes PH permettent de générer des courbes parallèles rationnelles utiles par exemple pour la modélisation des trajectoires d'outils pour les machines à commande numérique. Ces courbes ont été introduites au début des années 1990, en particulier par R. Farouki et T. Sakallis, et depuis ce sujet de recherche n'a cessé de se développer en s'appuyant notamment sur les outils de la géométrie tradionnelle.

Deux grandes stratégies ont vu le jour pour l'étude de ces courbes. Une approche algébrique, initiée par R. Farouki, permettant de caractériser les courbes planes PH à l'aide du théorème de Kubota/Pythagore. Précisément, une courbe plane polynomi-

ale est PH si son hodographe satisfait la relation de Pythagore $x'(t)^2 + y'(t)^2 = \sigma(t)^2$ où $\sigma(t)$ est un polynôme. Une deuxième approche, initiée par H. Pottmann, s'appuie sur la représentation duale des courbes consistant à les définir comme l'enveloppe de leur droites tangentes. Cette approche se généralise aux surfaces mais difficilement aux courbes gauches de l'espace. A contrario, l'approche algébrique a été généralisée depuis aux courbes gauches en s'appuyant notamment sur l'utilisation des quaternions et sur la représentation de Hopf. Ces nouveaux outils ont permis de caractériser les courbes à "rotation minimizing frame" (RMF) et les courbes polynomiales à "rational rotation minimizing frame" (RRMF) qui forment une sous-famille des courbes PH. Ces courbes sont très largement étudiées actuellement et sont utilisées pour la modélisation de surfaces tubulaires, le contrôle de déplacement... En pratique, l'utilisation de ces nouveaux "objets" géométriques nécessitent des algorithmes d'interpolation et d'approximation afin de les rendre accessibles pour des applications en modélisation géométrique.

La thèse de R. Ait-Haddou (1996) s'appuie essentiellement sur l'approche duale dans le cadre des courbes planes et a consisté dans un premier temps à développer des algorithmes d'interpolation G2 sous contraintes de courbure par des courbes PH (quartiques de Tschirnhausen). Ensuite, l'approche duale de Pottmann a été généralisée dans cette thèse au cas d'une géométrie non euclidienne. Ces méthodes ont permis de développer deux méthodes de construction d'ovales et rosettes PH à largeur constante, utiles pour la modélisation des cames.

References :

PHD Thesis, R. Ait-Haddou, 1996

[9], [13], [18], [22], [23]

Chapitre 2 : Détermination de géodésiques sur des surfaces de subdivision.

Un chemin géodésique entre deux points sur une surface de l'espace est un plus court chemin local. Un plus court chemin est porté par un chemin géodésique. La plupart des méthodes pour l'évaluation de ces chemins géodésiques s'appuient sur la résolution d'équations différentielles. Nous avons souhaité développer une méthode permettant de déterminer des géodésiques dans un cadre plus général, en nous appuyant sur les outils de la modélisation géométrique. Il s'agit d'une méthode itérative qui s'applique aux surfaces de subdivision, en particulier aux surfaces de Bézier et aux surface NURBS. A chaque étape de la méthode, un chemin géodésique exact est déterminé sur une surface polyédrique issue du réseau de contrôle subdivisé de la surface initiale. Cette géodésique exacte (ou ce plus court chemin) est obtenue par projection et mise à jour de la géodésique calculée à l'étape précédente. On détermine ainsi une suite de chemins géodésiques sur la suite des surfaces polyédriques issues des réseaux de contrôle successifs et convergeant vers la surface donnée.

Suite à ces travaux, une application spécifique a été développée avec N. Szafran dans le cadre de la modélisation des fibres du myocarde pour l'imagerie médicale. Le but de ce projet (commun aux laboratoires TIMC, LMC, L3S, Centre Hospitalo-Universitaire, à Grenoble, et coordonné par le Prof. A. Raoult) était de vérifier une conjecture de Streeter selon laquelle les fibres cardiaques sont organisées en courbes géodésiques sur des surfaces emboîtées. Une bonne connaissance de l'organisation fibreuse du myocarde étant à terme une aide essentielle au remodelage chirurgical après accident coronarien et à la détection

de pathologies cardiaques au stade néonatal. Il s'agissait ici, pour nous de modéliser et calculer des courbes géodésiques fermées, globalement $G2$, sur des surfaces fermées. Les outils précédents consistant à laisser évoluer sur la surface une courbe fermée soumise à sa propre contraction (principe de l'élastique) nous a permis d'obtenir des boucles géodésiques lisses sur des surfaces toroidales.

References :
PHD Thesis, V. Pham-Trong, 2001
[12], [17]

Chapitre 3 : Reconstruction et Modèles géométriques dédiés aux technologies de capteurs.

Cette activité a démarré au travers d'une collaboration avec le service des Micro-systèmes et Objets Communicants du CEA/LETI à Grenoble. Il s'agit de reconstruire des formes 2D et 3D à l'aide d'informations tangentielles estimées en des points de cette forme et transmises par des magnétomètres et accéléromètres miniaturisés. Il est à noter qu'il ne s'agit pas d'un problème d'interpolation ou d'approximation duale (type "Pottmann") puisque les informations tangentielles ne sont pas localisées dans l'espace, de sorte qu'à notre connaissance, ce type de problème est nouveau. Dans le cas des courbes planes et gauches (thèse de N. Sprynski) l'utilisation d'algorithmes géométriques spécifiques permet la reconstruction en temps réel de ces courbes dans l'espace. Les résultats ont été validés par un démonstrateur constitué de 32 capteurs répartis sur un ruban "Morphosense".

Plusieurs stratégies basées sur la reconstruction de courbes tracées sur une surface ont ensuite été développées pour la reconstruction de cette surface. Nous sommes en fait confrontés à plusieurs difficultés. En particulier, les distances entre capteurs étant fixes il est nécessaire de reconstruire un maillage curviligne de la surface respectant ces distances. Néanmoins, nous avons pu démontrer que ce ruban permettait l'acquisition de certaines courbes 3D caractéristiques sur une surface, à savoir des courbes géodésiques. Ce qui nous a permis de développer des méthodes spécifiques d'interpolation.

Cette nouvelle approche pour la reconstruction de surface à partir de géodésiques s'est poursuivi lors de mon séjour à UC Davis avec le professeur R. Farouki. Précisément, des conditions nécessaires et suffisantes pour la reconstruction de surfaces lisses interpolant des courbes géodésiques (par exemple, issues d'acquisitions par le ruban "Morphosense") ont été déterminées. Plusieurs méthodes de reconstruction ont ensuite été développées aussi bien dans le cadre "produit tensoriel" que triangulaire.

References :
PHD Thesis, N. Sprynski, 2007
[7], [7], [8], [10], [15], [15], [21]
Faits marquants de la DRT du CEA en 2005,
Patent no WO/2006/095109, N. Sprynski et al (CEA/LETI), 2006

Chapitre 4 : Diminution de la variation des courbes de Bézier.

Cette activité en collaboration avec R. Ait-Haddou concerne l'étude des courbes de Bézier en s'appuyant sur la notion de floraison d'un polynôme. Dans un contexte de modélisation géométrique, l'outil floraison permet de relier des informations de type géométrique à des résultats algébriques (nombre de racines) ou analytiques (extrémas) ou

même algorithmique. En particulier, le lien entre la concavité du polygone de contrôle d'un polynôme et le minimum de sa floraison sous contraintes symétriques linéaires a été étudié. Récemment, un raffinement de la propriété de minimisation des variations d'une courbe Bézier a été proposé.

References : [5], [11]

Chapitre 5 : Activités de recherche liées à des contrats industriels.

La nature des travaux réalisés au travers de ces contrats avec ELF EP puis TOTAL FINA ELF S.A. se découpe en 2 parties. D'une part la modélisation d'interfaces géologiques (par utilisation de quadriques par morceaux) sous contraintes d'approximation et de raccord $G1$ (B. Lacolle et N. Szafran). Pour ma part je me suis intéressé à la modélisation des fronts d'onde et à leur propagation dans un contexte d'optique géométrique. L'approche choisie s'appuie sur la géométrie duale qui permet naturellement de définir des courbes et des surfaces rationnelles dont les offsets (courbes et surfaces parallèles) se déduisent aisément en fonction du paramètre temps par enveloppe.

Cette approche s'inscrivait naturellement dans la suite des travaux initiés lors de la première thématique. Par ailleurs, ce formalisme permet une bonne approximation des fronts d'onde réfléchi après interaction avec les différentes interfaces du milieu et assure naturellement des raccords géométriques G^1 (ce qui évite les discontinuités de suivi dans les méthodes de lancer de rayons).

References : [24], [25]

Perspectives

Concernant l'activité conjointe avec le LETI des discussions sont actuellement en cours pour une collaboration autour d'une "*Plateforme matérielle et logicielle*". Les objectifs étant la reconstruction dynamique d'animations et de mouvements 3D de surfaces équipées de capteurs sur des topologies non régulières, ainsi que la validation des méthodes développées. Par ailleurs, la visite du professeur R. Farouki à l'automne 2009 devrait permettre de valider et développer plusieurs méthodes basées sur l'interpolation géodésique et s'appuyant sur des courbes PH quintiques pour la reconstruction surfacique sous contraintes de longueurs.

Depuis mon séjour à UC Davis (2007-2008), nous travaillons également avec R. Farouki sur un projet concernant les courbes RRMF et en particulier sur la reconstruction et l'interpolation par des surfaces rationnelles de lignes de courbure définies par des courbes RRMF. La construction de ces lignes de courbure s'appuie sur l'interpolation de Hermite par des courbes RRMF. En particulier, un algorithme d'interpolation d'Hermite généralisé dans l'espace par des courbes RRMF devra être développé.

Concernant notre activité "calcul" (collaboration avec N. Szafran), une nouvelle approche pour le calcul de géodésiques sur des polyèdres et des surfaces de subdivision est actuellement en cours. Cette méthode s'appuie sur les propriétés locales de la surface.

Enfin, la collaboration avec l'université d'Osaka et R. Ait-Haddou se poursuit. L'un des objectifs étant de développer un algorithme géométrique de localisation des racines réelles d'un polynôme.

Personal bibliography

PHD Thesis supervision

[1] PhD Thesis, Rachid Ait-Haddou,
Courbes à hodographe pythagorien en géométrie de Minkowski et modélisation géométrique, Applied Mathematics, University Joseph Fourier, Laboratory LMC-IMAG, 6 septembre 1996

[2] PHD Thesis, Valérie Pham-Trong,
Détermination géométrique de chemins géodésiques sur des surfaces de subdivision, Applied Mathematics, University Joseph Fourier, Laboratory LMC-IMAG, 28 septembre 2001

[3] PHD Thesis, Nathalie Sprynski,
Reconstruction de courbes et surfaces à partir de données tangentielles, Applied Mathematics, University Joseph Fourier / Laboratory LJK and CEA/LETI, 5 juillet 2007

My PHD Thesis

[4] Luc Biard, *Méthode algorithmique d'implicitisation et d'inversion. Application au lancer de rayons*, Thèse de l'Université Joseph Fourier, Grenoble I, Spécialité Mathématiques Appliquées, novembre 1990

Submitted in Revues

[5] Rachid Ait-Haddou, Taishin Nomura and Luc Biard, *A Refinement of the Variation Diminishing Property of Bézier Curves*, on Revision, Comput. Aided Geom. Design, May 2009

[6] Farouki R. T., N. Szafran, L. Biard, *Construction and smoothing of triangular Coons patches with geodesic boundary curves*, on Revision, CAGD, June 2009

Publications in Revues

[7] Farouki R. T., N. Szafran, L. Biard, *Construction of Bézier surface patches with Bézier curves as geodesic boundaries*, to appear in Computer-Aided Design, 2009

[8] Farouki R. T., N. Szafran, L. Biard, *Existence conditions for Coons patches interpolating geodesic boundary curves*, Computer Aided Geometric Design, Volume 26, Issue 5, pp. 599-614, June 2009

[9] Ait-Haddou Rachid, Walter Herzog and Luc Biard, *Pythagorean-hodograph ovals of constant width*, Computer Aided Geometric Design, Volume 25, 4-5, pp. 258–273, May 2008

[10] N. Sprynski, N. Szafran, B. Lacolle, L. Biard, *Surface reconstruction via geodesic interpolation*, Computer-Aided Design, Volume 40, Issue 4, pp. 480-492, April 2008

[11] R. Ait-Haddou, L. Biard, M.A. Slawinski, *Minimizing Blossoms Under Symmetric Linear Constraints*, Computer Aided Geometric Design Volume 19, Issue 6, June 2002, Pages 421-431

[12] V. Pham-Trong, N. Szafran and L. Biard, *Pseudo-geodesics on three-dimensional surfaces and pseudo-geodesic meshes*, Numerical Algorithms © Kluwer Academic Publishers, Volume 26, Issue 4, pp. 305-315, April 2001

[13] R. Ait-Haddou, L. Biard and M.A. Slawinski, *Minkowski isoperimetric-hodograph curves*, Computer Aided Geometric Design, Volume 17, Issue 9, October 2000, pp. 835-861

Proceeding of international conferences with reviewing

[14] N. Sprynski, B. Lacolle, D. David, and L. Biard, *Curve Reconstruction via a Ribbon of Sensors*, In Proceeding of the 14th IEEE International Conference on Electronics, Circuits and Systems, ICECS - 2007, Marrakech, Maroc, December 2007

[15] N. Sprynski, B. Lacolle, L. Biard, D. David, *Curve and Surface Reconstruction via Tangential Information*, "Curve and Surface Design : Avignon 2006", P. Chenin, T. Lyche, L. L. Schumaker (eds), Nashboro Press, pp. 254–263, 2007

[16] N. Szafran, S. Despréaux, L. Biard, and F. Blaise, *Sawing of logs in virtual trees using 3D intersection algorithms*, "International Symposium on Plant growth Modeling, simulation, visualization and their Applications 2003" - PMA'03, Beijing, China, In Bao-Gang Hu and Marc Jaeger editors, Plant Growth Modeling and Applications, Tsinghua University Press - Springer, October 2003, pages 372-383, ISBN 7-302-07140-3

[17] A. Mourad, L. Biard, D. Caillerie, P.-S. Jouk, A. Raoult, N. Szafran and Y. Usson, *Geometrical modelling of the fibre organization in the human left ventricle*, In Katila, Magnin, Clarysse, et Montagnat, editors, Functional Imaging and Modeling of the Heart, volume 2230 of Lecture Notes in Computer Sciences, pages 32–38, Helsinki, novembre 2001. Springer, 2001.

[18] R. Ait-Haddou and L. Biard, *G2-Approximation of an Offset Curve by Tschirnhausen Quartics*, in Mathematical Methods for Curves and Surfaces, M. Daehlen, T. Lyche, and L. Schumaker (eds), Vanderbilt University Press, pp. 1-10, 1995.

[19] Luc Biard, *Parametric Surfaces and Ray Tracing*, in "Photorealism in Computer Graphics", EurographicSeminars, Tutorials and Perspectives in Computer Graphics, K. Bouatouch and C. Bouville (Eds.), Springer-Verlag, pp. 33-53, 1992

[20] L. Biard and P. Chenin, *Ray Tracing Rational Parametric Surfaces*, in Curves and Surfaces, P.-J. Laurent, A. Le Méhauté, L. L. Schumaker (eds), Boston - London, Academic Press, Inc., pp. 37-43, 1991

Conférences invitées

[21] L. Biard, *Surface reconstruction from geodesics*, Séminaire Invité, Department of Mechanical Science and Bioengineering, Osaka University, Juillet 2009

[22] L. Biard, *Courbes PH et Surfaces PN, une sous classe des NURBS aux propriétés remarquables*, Conférencier Invité, Séminaire externe de DASSAULT Systèmes, Suresnes, 31 Mars 2000

[23] R. Ait-Haddou and L. Biard, *Rational Pythagorean Hodograph Rosettes and Ovaloids of Constant Width*, Fourth SIAM Conference on Geometric Design, Conférence invité au Minisymposium on "Pythagorean-Hodograph Curves". Nashville, Tennessee, November 6-9, 1995

Rapports de contrats industriels

[24] B. Lacolle, N. Szafran, L. Biard, *Approximations adaptatives par des quadriques et modélisation géométrique des interfaces en liaison avec le contexte optique*, Rapport de contrat TOTAL FINA ELF S.A., Juillet 2004

[25] B. Lacolle, N. Szafran and L. Biard, *Modélisation par paraboloïdes et Modélisation par surfaces duales*, Rapport de contrat ELF EP n° 11985, CNRS n° 721671/00, UJF n° 9025, Mars 2001

Chapter 1

Pythagorean Hodograph curves and geometric design

Construction of offset curves is fundamental to a variety of applications in geometric modeling, such as generation of tool path for numerical control machines, or definition of tolerance zone. Several methods have been proposed for approximating offset curves by piecewise polynomial or rational forms so that they may be incorporated into current CAD software (Farin [19]).

In 1990, R.T. Farouki and T. Sakkalis introduced a class of special polynomial curves with rational offsets, namely the *Pythagorean Hodograph* curves (PH curves) [22], and showed their capabilities in free-form design applications. However the degree of the offsets present some disadvantage. For example, the low degree PH solution of the C^1 Hermite interpolation problem involves a polynomial PH curve of degree 5 with rational offsets of degree 9 [21]. In order to remedy this drawback, H. Pottmann [42] described a full class of rational curves with rational offsets (*rational PH curves*) by use of the dual geometry and established their practical use and their low degree solution. For example, the rational PH solution of the G^2 approximation problem can be achieved by rational PH curves of algebraic class 4 (Pottmann [43]). In practice, for applications in which offset computations are needed, the PH curves with offsets of low degree are most appealing. Among these curves there are the Tschirnhausen cubics (T-cubic) which are, with circles, the only rational curves with a rational cubic PH parametrization (Farouki et al. [25]). The fact that these curves become one under a suitable scaling, rotation and linear parametrization [22] makes it of limited practical use. Therefore, the Tschirnhausen quartics (T-quartics) are particularly attractive since they are characterized by the lowest degree and are sufficiently flexible for practical design schemes.

The Ph.D thesis of Rachid Ait-Haddou [3] is related to the study of parallel curves in non-Euclidean geometry as well as the determination of algorithms of geometrical modeling under G^1 or G^2 constraints. According to the works of H. Pottmann, he introduced the concept of Pythagorean Hodograph curves in the Minkowski space and their geometrical characterizations within the formalism of Bézier curves. He then developed the differential geometry of Minkowski spaces, providing him with the theoretical framework necessary for the development of practical algorithms.

In a second part, R. Ait-Haddou [2] solved the G^2 approximation problem under

curvature constraints, with rational PH curves of dual degree 3, so that their offsets are of degree 4. This approach is based on G^2 Hermite interpolation of *special* curvature elements by two segments of Tschirnhausen quartics. This requires an additional appropriate new interpolation point. It turns out that the geometric characterization of Tschirnhausen quartics as involutes of Tschirnhausen cubics provides a simple localization of the added interpolation point.

Finally, two geometric constructions for rational ovals and rosettes of constant width formed by piecewise rational PH curves (Ait-Haddou et al. [5]) have been developed. The first construction models with rational PH curves of algebraic class 3 (T-quartics) and is based on the fact that T-quartics are exactly the involutes of T-cubic curves. The second construction models with rational PH curves of algebraic class $m > 4$ and is based on the dual control structure of offsets of rational PH curves.

This chapter is organized as follows. After reviewing some basic concepts concerning rational PH curves in Section 1.1, we present the main results obtained in (Ait-Haddou [3]). Section 1.2 is devoted to the G^2 approximation under curvature constraints by PH curves of dual degree 3 (Ait-Haddou et al. [2]). We then present in Section 1.3 the main ideas for the construction of ovals and rosettes of constant width formed by piecewise rational PH curves (Ait-Haddou et al. [5]). In Section 1.4 the main ideas about Pythagorean Hodograph curves in the Minkowski space and their geometrical characterizations within the formalism of Bézier curves (Ait-Haddou et al. [4]) are outlined. Finally, as a conclusion, Section 1.5 presents some future work.

1.1 Rational planar PH Curves

• **Dual Bézier curves**.

The approach of dual Bézier representation of rational Bézier curves, introduced by J. Hoschek [35], provides an elegant tool for studying rational PH curves from the view point of construction, interpolation and approximation [1, 43]. The fundamental idea of this approach is that any rational Bézier curve $C(t)$ can be described as the envelope of its tangent lines $L(t)$. The tangent lines $L(t)$ can be expressed as a linear homogeneous equation $< U(t), X >= 0$, with $X = (x_0, x_1, x_2)$ the homogeneous Cartesian coordinates, and $U(t)$ the vector of the homogeneous line coordinates.

For a rational curve $C(t)$, the vector $U(t)$ may be expressed in Bézier form

$$U(t) = \sum_{i=0}^{m} B_i^* B_i^m(t), \tag{1.1}$$

where $B_i^m(t)$ are the Bernstein polynomials of degree m. Such a representation is called the *dual Bézier representation* of the curve C, and the curve C is said to be of class m. The vectors B_i^* are the line coordinate vectors of the *Bézier lines*. The set of Bézier lines B_i^* form the *Bézier lateral* and the points $E_i = B_i^* \cap B_{i+1}^*$ for $i = 0, ..., m$ with $m + 1 \equiv 0$ are the *Bézier vertices*. The conversion expression from the dual form U to its standard representation as point set C, can be obtained by the formula

$$C(t) \equiv U(t) \wedge U'(t). \tag{1.2}$$

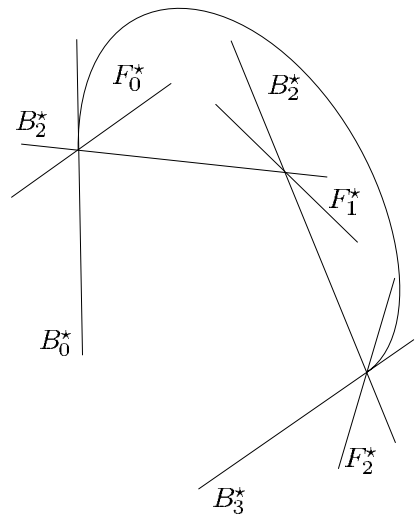

Fig. 1.1 - *Dual Bézier curve.*

The lines of the Bézier lateral do not determine a Bézier curve completely since the vectors B_i^* and any multiple λB_i^* with $\lambda \neq 0$, represent the same line. For a complete description J. Hoschek [35] associates a weight w_i with each normalized vector B_i^*. This increases the flexibility of dual curves but makes the scheme dependent on the origin. To avoid this limitation, Pottmann [42] introduced the Farin lines F_i^* (the analogue to Farin's auxiliary points of rational Bézier curves (Farin [19])) which are concurrent with B_i^* and B_{i+1}^* and are represented by the vectors

$$F_i^* = B_i^* + B_{i+1}^*. \tag{1.3}$$

Given the lines B_i^* for $i = 0, ..., m$ and the lines F_i^* for $i = 0, ..., m-1$, we can actualize the homogeneous coordinate vectors B_i^* such that (1.3) holds. Then (1.1) defines a unique dual curve U (see Figure 1.1).

• Rational PH Curves.

Given a planar curve C with a rational parametrization $C(t)$, its offset at a signed distance d is the parametric curve

$$C_d(t) = C(t) + d\, N(t), \tag{1.4}$$

where $N(t) = \big(N_1(t), N_2(t)\big)$ is the unit normal vector along the curve C. The parametrization $C(t)$ is said to be a *rational PH parametrization* of the curve C if the unit normal $N(t)$ is rational in the parameter t. In this case, for each real number d, the parametrization $C_d(t)$ of the offset curve is rational in parameter t. Notice that not all rational curves possess a rational PH parametrization.

If $C(t)$ is a rational PH parametrization, the curve C will be said to be a *rational PH curve*. In particular, we speak of a *polynomial PH curve* if $C(t)$ is a polynomial PH representation.

For a rational PH curve $C(t)$, the components of $N(t)$ must have the form (Pottmann [42]) :

$$N_1(t) = \frac{2\, a(t)\, b(t)}{a^2(t) + b^2(t)}, \quad N_2(t) = \frac{a^2(t) - b^2(t)}{a^2(t) + b^2(t)}, \tag{1.5}$$

with polynomials $a(t)$ and $b(t)$.

Furthermore, the dual representation provides an elegant way to characterize rational PH curves. More precisely, the tangent line $L(t)$ at $C(t)$ has the equation

$$N_1(t)\, x + N_2(t)\, y + h(t) = 0, \tag{1.6}$$

where $h(t)$ is a rational function if $C(t)$ is a rational PH parametrization. Then, by setting $h = -e/f$, we obtain Pottmann's [43] dual representation of rational PH curves, (i.e., rational curves with rational offsets) in terms of line coordinates

$$U(t) = \Big(-e\,(a^2+b^2),\ 2\,a\,b\,f,\ f\,(a^2-b^2)\Big), \tag{1.7}$$

where a, b, e and f are polynomials in t. Conversely, given polynomials a, b, e, f, the dual representation (1.7) defines a rational PH curve.

We can observe that $e \equiv -f$ in (1.7) leads to a dual representation $\mathbf{u}(t)$ of a segment $c(t)$ of the unit circle. The dual representation $\mathbf{u}(t)$ does not differ from (1.7) in the second and third coordinate. Therefore the Bézier and Farin lines of the circle segment $c(t)$ are parallel to the corresponding Bézier and Farin lines of the rational PH curve $C(t)$.

The same arguments show that the Bézier and Farin lines of the offset curve $C_d(t)$ are obtained by an appropriate translation of the corresponding Bézier and Farin lines of $C(t)$. More precisely the i-th Bézier and Farin line of C_d and C are parallel, and their oriented distance is d times the oriented distance of the i-th Bézier or Farin line of the circle segment c from its midpoint [42]. Notice that, a nice geometric characterization of the set of rational PH curves is given in (Fiorot et al. [30]).

• **Tschirnhausen quartic curves (T-quartics)**.

Particularly interesting is the family of rational PH curves with algebraic class 3 obtained by setting

$$a(t) = t, \quad b(t) = 1, \quad e(t) = \alpha t + \beta, \quad f(t) = \gamma t + \delta,$$

in (1.7), which leads to the following dual representation

$$U(t) = \Big(-(\alpha t^3 + \beta t^2 + \alpha t + \beta), \quad 2\gamma t^2 + 2\delta t, \quad \gamma t^3 + \delta t^2 - \gamma t - \delta\Big).$$

Each d-offset parametrization is obtained by substituting α by $\alpha + \gamma\, d$ and β by $\beta + \gamma\, d$ in the previous representations.

The curves $U(t) \wedge U'(t)$ yield a set of rational quartics of algebraic class 3 called *Tschirnhausen quartics* (or T-quartics). These curves are closed under offsetting, have five degrees of freedom included translations (same flexibility as conics) and are free of inflections. Furthermore, they are characterized by the fact that *they are exactly the involutes of the polynomial Pythagorean hodograph cubics* (*Tschirnhausen cubics*) [42]. Finally, notice that each regular segment of a T-quartic is of monotonous curvature.

• **Tschirnhausen Cubic Curves (T-cubics)**.

Let $r(t) = (x(t), y(t))$ be a plane polynomial curve of degree n. Offset curves of $r(t)$ are rational if and only if the hodograph components of $r(t)$ satisfy the Pythagorean relation $x'^2(t) + y'^2(t) = \sigma^2(t)$ with $\sigma(t)$ a polynomial of degree $n-1$, which is equivalent (Kubota [38]) to the following expression for the derivatives

$$x'(t) = w(t)\,[u^2(t) - v^2(t)] \quad \text{and} \quad y'(t) = 2\,w(t)u(t)v(t),$$

with polynomials $u(t), v(t)$ and $w(t)$.

A Tschirnhausen cubic curve (T-cubic) is a polynomial PH cubic curve. T-cubics are, with circles, the only rational curves with a rational cubic PH parametrization. They

possess rational offsets of degree 5, are free of inflections and can be obtained as caustics of a parabola for parallel light rays (which are not parallel to the axis of the parabola). Finally, notice that two Tschirnhausen cubic curves can be deduced, one from the other, by using a suitable scaling, rotation and linear reparametrization (Farouki et al. [21, 22]).

Farouki's expressions provide the following simple and elegant geometric characterization of polynomial PH cubic curves.

Theorem 1. [21] – *The Bézier cubic curve* $BP[P_0, P_1, P_2, P_3] = \sum_{i=0}^{3} P_i\, B_i^3(t)$ *is a T-cubic if, and only if*

$$\theta_1 = \theta_2 \quad \textit{and} \quad L_1^2 = L_0 L_2,$$

where $L_0 = |P_0P_1|$, $L_1 = |P_1P_2|$, $L_2 = |P_2P_3|$, *and where* θ_1, θ_2 *are the control polygon oriented angles at the interior vertices* P_1 *and* P_2 *respectively (see Figure 1.2 - Left).*

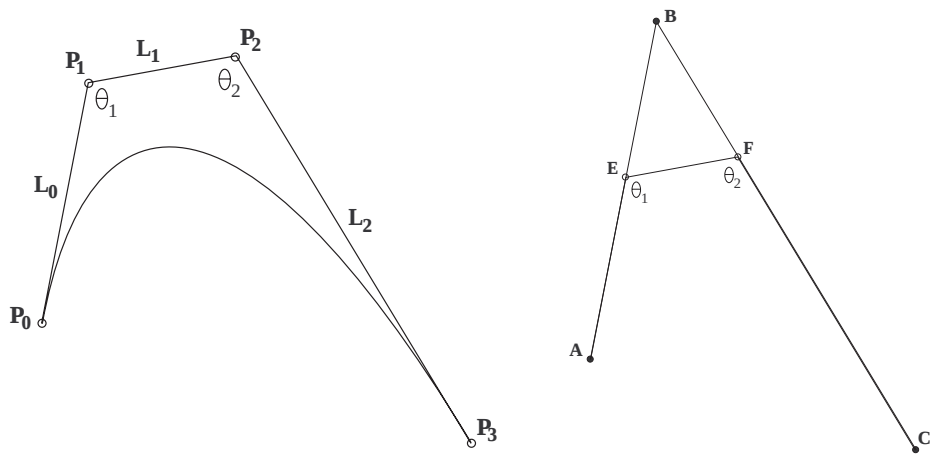

Fig. 1.2 - *Tschirnhausen cubic segment.*

Furthermore, we give the two following results (Ait-Haddou et al. [2]) which will be explicitly needed for the construction of section 1.2.

Proposition 1. [2] – *With notations of Theorem 1, the total arc-length* L *of a T-cubic curve* $BP[P_0, P_1, P_2, P_3]$ *is given by the formula*

$$L = L_0 + L_2 - L_1 \cos\theta_1.$$

Proposition 2. [2] – *Given a non-degenerate triangle* (ABC), *there is a unique point* E *on the segment* $[AB]$ *and a unique point* F *on the segment* $[BC]$ *(see Figure 1.2 - Right) such that the Bézier curve* $BP[A, E, F, C]$ *is a T-cubic curve denoted by* $T(ABC)$.

1.2 G2 approximation by Tschirnhausen quartics

Using the fact that rational PH curves of algebraic class 3 (Tschirnhausen quartics) can be regarded as the involutes of Tschirnhausen cubics, a geometric algorithm for approximating a given curve by a G2 piecewise rational PH curve of class 3 has been developed. The produced curve will also preserve the curvature variations of the initial curve. This

algorithm is based on a hierarchical segmentation of the initial curve and G^2 Hermite interpolation of *special* curvature elements by two segments of Tschirnhausen quartics. This requires an additional appropriate new interpolation point. It turns out that the geometric characterization of T-quartics as involutes of T-cubics provides a simple localization of the added interpolation point.

• **Segmentation**.

A *curvature element* (P, T, k) is composed of a point P, a unit tangent vector T at point P and a non zero curvature k. A G^2 curve defines curvature elements composed of a point on the curve, and of the tangent vector and the curvature at this point.

Two curvature elements (P_0, T_0, k_0) and (P_1, T_1, k_1) will be said to be *T-connected* if there exists a T-quartic segment which interpolates these curvature elements. Because of the degrees of freedom of T-quartics (five), two curvature elements are not T-connected in general.

Two curvature elements (P_0, T_0, k_0) and (P_1, T_1, k_1) will be said to be *admissible* if there exists a convex segment with continuous monotonous curvature and turning angle less than π, interpolating these two curvature elements.

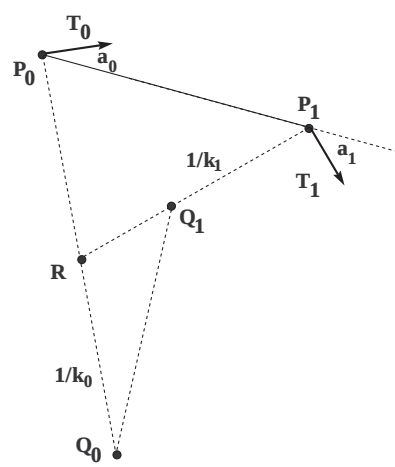

Fig. 1.3 -
Geometry of admissible curvature elements.

Theorem 2. (Guggenheimer & Ostrowski [31]). *Two curvature elements* (P_0, T_0, k_0) *and* (P_1, T_1, k_1) *are admissible (with increasing curvature) if*

$$
\begin{array}{ll}
i) & -\dfrac{\pi}{2} < a_1 < 0 < a_0 < \dfrac{\pi}{2}\,, \\
ii) & 0 < |Q_0Q_1| < |P_0Q_0| - |P_1Q_1| < |Q_0R| + |RQ_1| \\
iii) & \textit{the triangle } (Q_0, Q_1, R) \textit{ is positively oriented.}
\end{array}
$$

with oriented angles a_0 *and* a_1 *as defined in Fig. 1.3 and where* Q_0, Q_1 *are respectively the centers of curvature of the two curvature elements* (P_0, T_0, k_0) *and* (P_1, T_1, k_1).

Notice that each interpolating curve produced by Theorem 2 is an involute of a G^1 convex segment $r(t)$ of length $k_0^{-1} - k_1^{-1}$, with endpoints Q_0 and Q_1, with tangent vectors Q_0R at Q_0 and RQ_1 at Q_1, and inscribed in the triangle (Q_0RQ_1). Since Tschirnhausen quartics are exactly the involutes of Tschirnhausen cubics, we will now construct the

previous curve $r(t)$ as a tangent continuous curve composed of T-cubics.
Precisely, given a G^2 curve $s(t)$, the strategy is the following.

-1. Perform a geometric segmentation by computing all vertices (points with locally extremal curvature) of the curve $s(t)$.

-2. Evaluate additional points such that the turning angle of the tangents between two consecutive breakpoints is smaller than π. This leads to a sequence of admissible curvature elements.

-3. Construct a G^2 piecewise rational PH curve of class 3, with monotone curvature, which interpolates these curvature elements.

Consider now this last step.

• G^2 **interpolation by T-quartics**.

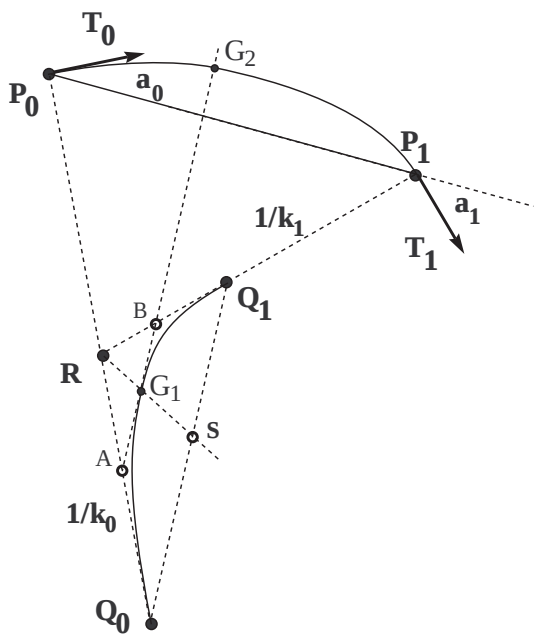

Fig. 1.4 -
G^2 Hermite interpolation of admissible curvature elements by two segments of T-quartics with G^2 contact and monotonous curvature.

Given two admissible curvature elements as in Fig. 1.4 and two real parameters $\alpha, \beta \in]0,1[$, we consider the two triangles (Q_0AG_1) and (G_1BQ_1) with points A, B, G_1 defined by

$$A = (1-\alpha)R + \alpha\, Q_0, \quad B = (1-\alpha)R + \alpha\, Q_1, \quad G_1 = (1-\beta)A + \beta\, B.$$

Then, using Proposition 2, we consider the two T-cubics $T(Q_0AG_1)$ and $T(G_1BQ_1)$, forming a G^1 T-cubic curve denoted by $T_{\alpha,\beta}(Q_0RQ_1)$.

Theorem 3. [2] – *Let l be a real number such that $|Q_0Q_1| < l < |Q_0R| + |RQ_1|$. Then, for each value of β in $]0,1[$, there exists an unique $\bar{\alpha}$ in $]0,1[$ such that the arc length of the G^1 T-cubic $T_{\bar{\alpha},\beta}(Q_0RQ_1)$ associated with the triangle (Q_0RQ_1) and the two reals $\bar{\alpha}$ and β is l.*

Thus, noting that for two admissible curvature elements (P_0, T_0, k_0) and (P_1, T_1, k_1), with increasing curvature, we have according to Theorem 2

$$|Q_0Q_1| < \frac{1}{k_0} - \frac{1}{k_1} < |Q_0R| + |RQ_1|,$$

a PH solution of our G^2 Hermite interpolation problem is obtained, for each value of β in $]0,1[$, as an involute of the G^1 T-cubic curve $T_{\bar{\alpha},\beta}(Q_0RQ_1)$, of length $k_0^{-1} - k_1^{-1}$, as specified in Theorem 3.
This construction (see Fig. 1.4) provides a new curvature element (G_2, T_{G_2}, k_{G_2}), with $k_{G_2} = |G_1G_2|^{-1}$, such that the curvature elements (P_0, T_0, k_0), (G_2, T_{G_2}, k_{G_2}) and (P_1, T_1, k_1) are T-connected.

Consider now the construction of dual Bézier control structure of the involute of a T-cubic curve (Ait-Haddou et al. [1, 2]).

• **Construction of involutes of a T-cubic**.

A simple and elegant method to construct the dual Bézier control structure of the involute of a T-cubic curve is based on the dual representation of the osculating circles of the involute at the endpoints (Pottmann [43]).

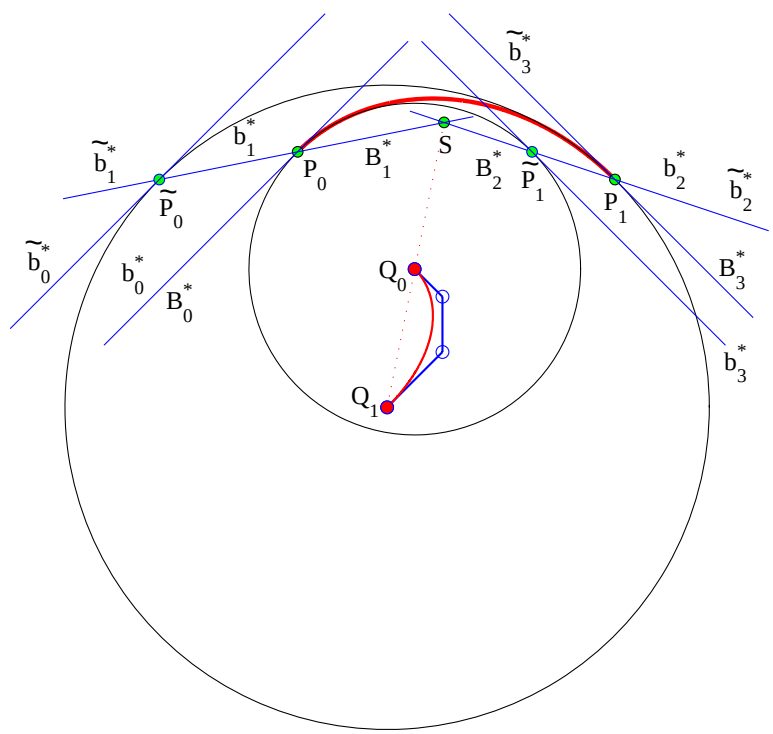

Fig. 1.5 - *Osculating circles at the endpoints of a T-quartic with their dual control structure.*

Theorem 4. *Consider two T-connected curvature elements (P_0, T_0, k_0) and (P_1, T_1, k_1). The Bézier lines B_1^* and B_2^*, of the dual representation of the interpolating T-quartic segment C, pass through the point S defined by :*

$$S = \frac{\rho_1}{\rho_1 - \rho_0} Q_0 + \frac{\rho_0}{\rho_0 - \rho_1} Q_1,$$

where $\rho_i = k_i^{-1}$, $i = 0, 1$ and where Q_0, Q_1 are respectively the centers of curvature of the two curvature elements (P_0, T_0, k_0) and (P_1, T_1, k_1).

Given a T-cubic curve, each of its involutes (T-quartics) yields connected curvature elements. The first and the last Bézier line of the involute are deduced from the tangent vectors of the T-cubic curve at the end-points, and the point S of the previous Theorem 4 is evaluated from the end-points of the T-cubic curve as centers of curvature. Hence, we get the second and third Bézier lines according to Theorem 4. Finally, the Farin lines of the involute are obtained by degree elevation of one corresponding circular arc in class 3, and by performing parallel translation of the Farin lines.

• **Results and concluding remarks**.

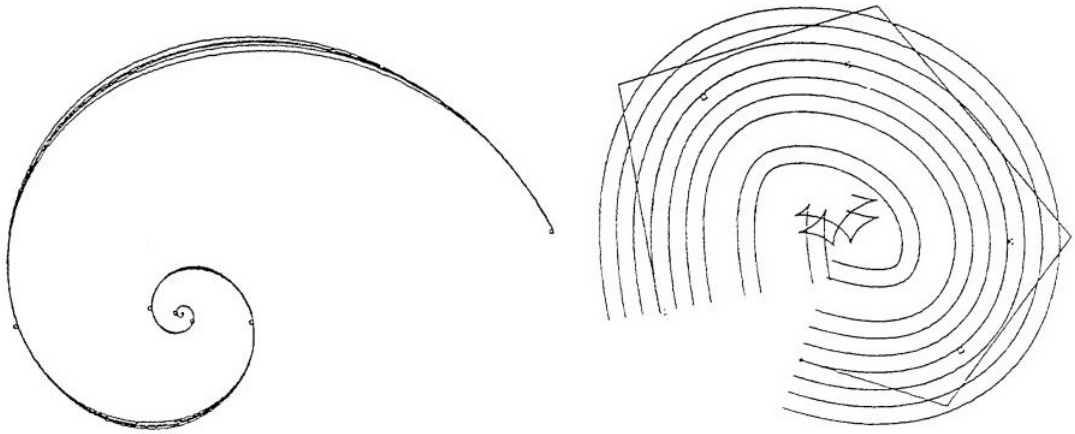

Fig. 1.6 - *Left : G^2 approximation with monotonous curvature of a logarithmic spiral with influence of parameter β. Right : G^2 approximation with monotonous curvature of a cubic B-spline together with its offsets.*

Because of the monotone curvature of the logarithmic spiral segment shown in Fig. 1.6 (left), we just have to verify that the turning angle between two consecutive breakpoints of the geometric segmentation is less than π. Furthermore, we can see the influence of the tension parameter β for the approximation of this logarithmic spiral segment. In Fig. 1.6 (right), some rational PH approximations of a cubic B-spline curve and of its offsets are shown. Since the Tschirnhausen quartics are closed under offsetting, PH approximation of each offset of a cubic spline segment involves just an appropriate translation of the dual Bézier control structure of the G^2 PH approximation of the initial curve.

1.3 PH Ovals of Constant Width

The theory of curves of constant width has generated an important literature, much of which is related to extremal phenomena or to the theory of convex bodies in general (Bonnensen [8]). Recently, the idea of constant width has been developed in a somewhat different spirit, as a topic of differential geometry, so that the nature of parametrization of these curves has not really been studied in great details.

The main objective in (Ait-Haddou et al. [5]) is to demonstrate the adequacy of using piecewise PH curves in constructing ovals and rosettes of constant width. The crucial element that brings PH curves into the scene of ovals of constant width is the fact that the interior offset of an oval Γ of constant width D at the distance D is the curve Γ itself.

Therefore, the characterization of offsets of PH curves in terms of simple manipulations on the dual Bézier structure of the original curve give an elegant method of construction of ovals of constant width. Another construction of ovals and rosettes of constant width is based on the idea of Hammer and Sobczyk [32], that generates plane curves of constant width as orthogonal trajectories of certain planar line families.

• **Motivating example**.

We are concerned in this section with modeling of cams. A cam is mechanical device allowing to transform a rotating motion $w(t)$ into a periodic longitudinal alternating motion $X(t)$. A camshaft is a system generally used in piston engines to control the opening of valves. It consists of a cylindrical axis with a number of oblong lobes protruding from it, one for each valve. As they rotate, the cams open the valves by pressing them.

Of course, this system requires a permanent contact between the cam and the valve. The contact is realized by mean of a spring pushing the axis against the cam (see Fig. 1.7).

From http://en.wikipedia.org/wiki/Camshaft

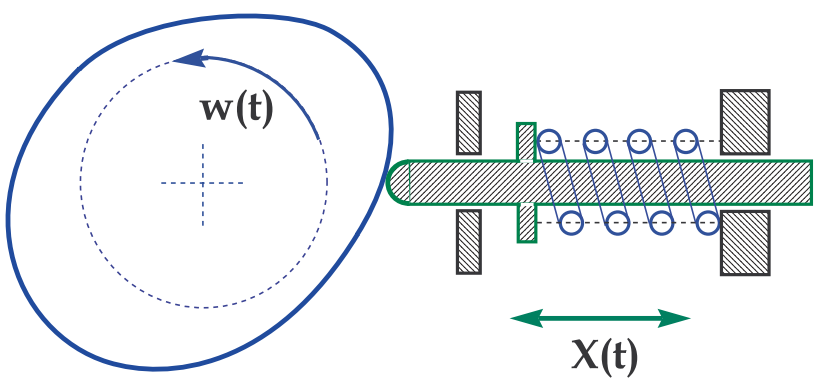

Fig. 1.7 - *Cam mechanism with spring.*

Another solution, avoiding the spring mechanism, would be to consider two sided opposite contacts of the cam with a **U**-device interdependent with the axis (see Fig. 1.8). But of course, such a mechanism requires that the cam is an oval of constant width D.

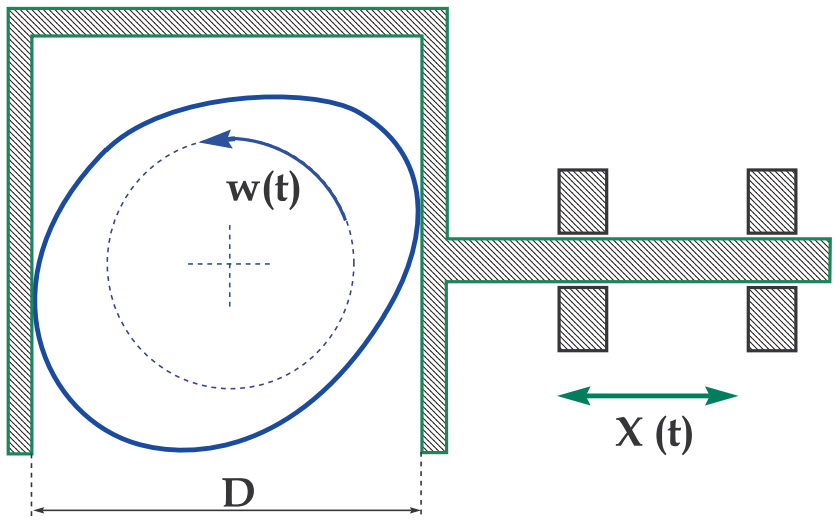

Fig. 1.8 - *Cam mechanism without spring.*

Thus, considering this second approach, we are concerned with the two following problems. The first one concerns the modeling and construction of rational ovals of constant width. For technological applications in which curves of constant width are needed (Drexler [18]), the piecewise polynomial or rational forms are preferred, so that they may be incorporated into current CAD software in order to be easily handled by numerical control milling machines for manufacturing.

The second problem concerns the construction of cams with respect to a given periodic longitudinal alternative motion $X(t)$. Precisely, assuming that the rotation of the cam is uniform, we are concerned by the approximation of a cam by a piecewise rational oval of constant width in order to produce a given periodic longitudinal alternating motion $X(t)$. This reverse problem has not been yet fully achieved.

We now consider in the following of this section two constructions of ovals of constant width involving T-quartic curves and rational PH curves of class $m > 4$.

• **Ovals and rosettes of constant width**.

A positively oriented rosette is a G^2 plane closed curve with positive curvature (Strubecker [45]). An oval is a *simple* rosette, i.e., a G^2 plane closed *simple* curve with positive curvature.

Let us consider a rosette C: $s \mapsto C(s)$, for $0 \leq s \leq L$, where s and L will denote respectively the arc length and the perimeter of the rosette. The tangent and normal vectors to C at $C(s)$ are denoted by $T(s)$ and $N(s)$ respectively while $k(s)$ will denote the curvature at point $C(s)$. We will consider the functions C, T, N and k to be periodic of period L. Furthermore, let us denote by $a \in [0, L]$ the smallest parameter such that $T(a) = -T(0)$. Then, for a positively oriented rosette C as above, let us consider $\psi : s \mapsto \psi(s)$, the real regular function such that $\psi(0) = a$ and $T \circ \psi(s) = -T(s)$, for $0 \leq s \leq L$, and the following vector and functions :

$$p_* = C \circ \psi^j - C, \quad \delta_* = < p_*, N >, \quad \Delta_* = < p_*, T >, \quad 2\lambda_* = \frac{1}{k} + (-1)^{j+1} \frac{1}{k \circ \psi^j},$$

where j is the index of C (notice that $j = 1$ for an oval C). The function δ_* will be called the *width function* of C.

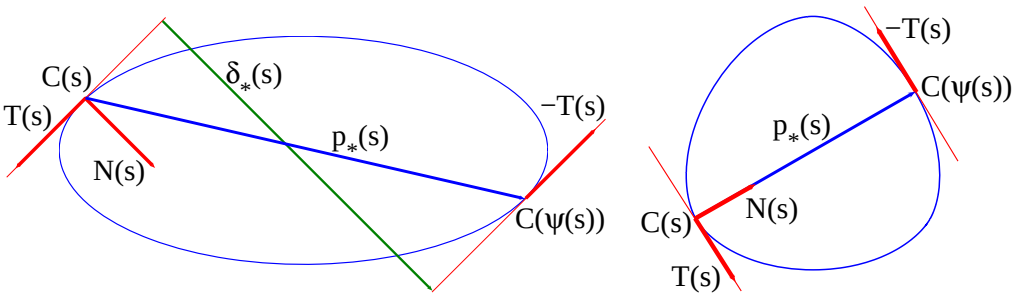

Fig. 1.9 - *Width function of an ellipse and of an oval of constant width.*

A pair of points of a rosette which have the same normal line will be called an *orthodiameter pair*. A rosette C is said to be of *constant width* if δ_* is a constant function.

Theorem 5. [16].
An oval is of constant width if and only if each of its points belongs to an orthodiameter pair. The index of a rosette C of constant width is an odd number and $\delta_* = ||p_*|| = 2\lambda_*$. A rosette is of constant width if and only if each of its points belong to an orthodiameter pair.

• **Construction of piecewise T-quartic rosettes of constant width**.

In this section we give a geometric construction of ovals and rosettes of constant width composed of piecewise rational PH curves of class 3 (T-quartics). These constructions are based on the fact that T-quartics are exactly the involutes of T-cubic curves and on a condition for the existence of orthogonal trajectories of a continuous family of lines.

A continuous family of lines $U(t)$ is said to be *k-simple* if there exists a circle $\mathcal{C}$ such that any point exterior to $\mathcal{C}$ is covered exactly k times by lines of $U(t)$. Then, as emphasized in [32, 33, 47], if k is an odd number, regular orthogonal trajectories of a k-simple family of lines exist and are rosettes of constant width. Each orthogonal trajectory of the family $U(t)$ is one involute of the envelope of this family. Therefore, to get piecewise T-quartic rosettes of constant width, we just have to find a piecewise T-cubic curve such that its tangent lines form a k-simple family of lines.

<u>Case $k = 1$</u> – Construction of ovals of constant width.

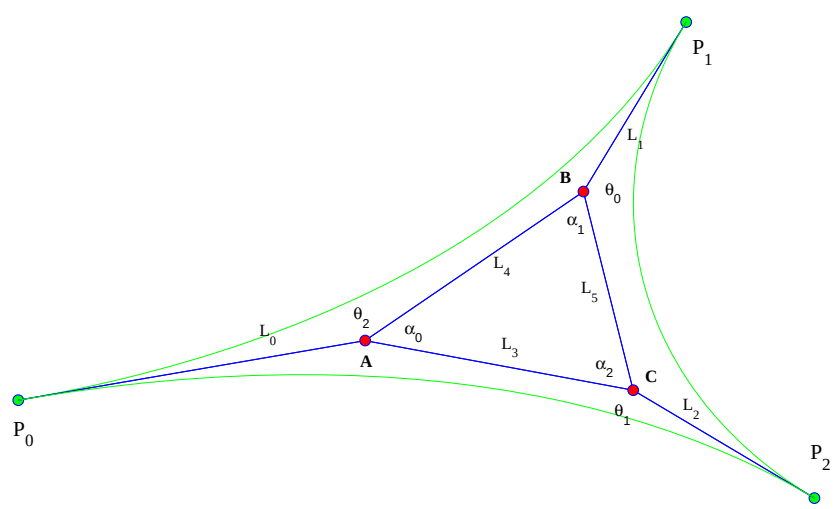

Fig. 1.10 - *Construction of a piecewise T-cubic curve.*

1. Consider a non-degenerate triangle (ABC) with interior angles less than $\pi/2$ (see Fig. 1.10). There exist unique points P_0, P_1 and P_2 exterior to the triangle (ABC), such that the Bézier curves $BP[P_0, A, B, P_1]$, $BP[P_1, B, C, P_2]$ and $BP[P_2, C, A, P_0]$ are T-cubic curves.

2. The family of the tangent lines to this piecewise T-cubic curve is simple.

3. Therefore, the involutes of this piecewise T-cubic curve provide ovals of constant width, which are composed of 6 T-quartic segments (see Fig. 1.11).

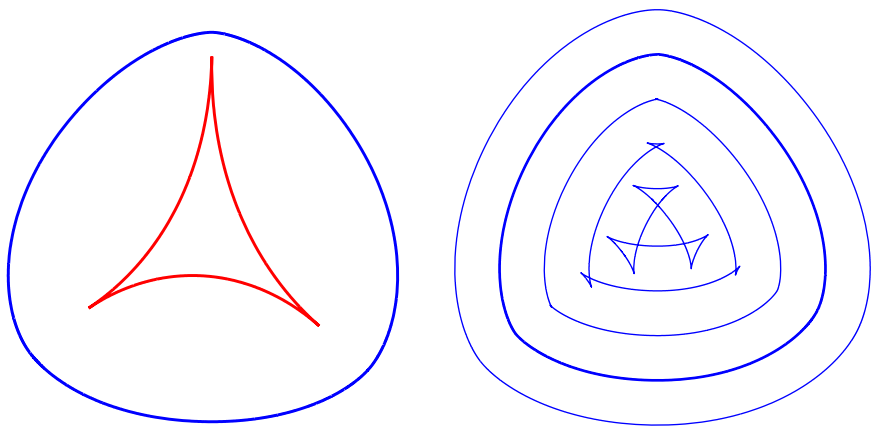

Fig. 1.11 - *T-quartic oval of constant width and its offsets.*

General case : k is an odd number – This case is a direct generalization of the previous algorithm for the construction of rational rosettes of constant width (see [5] for a detailed construction).

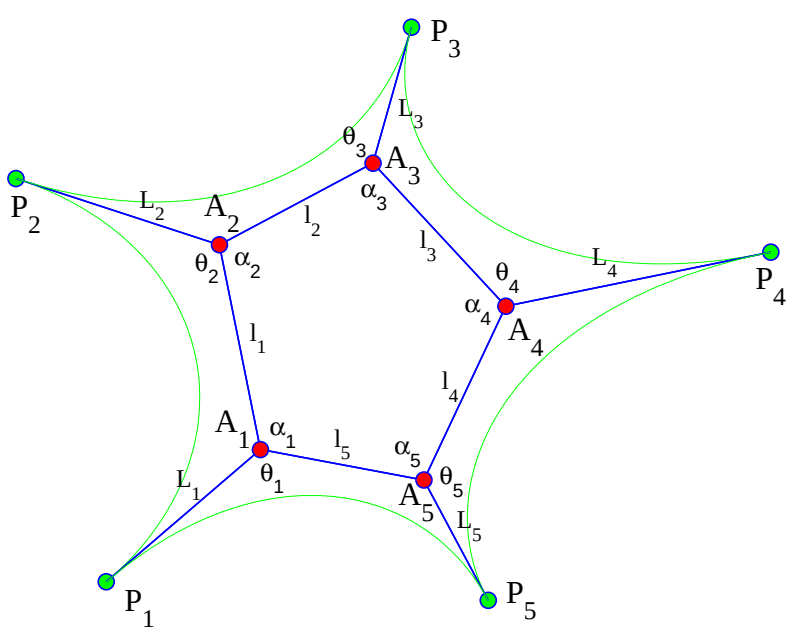

Fig. 1.12 - *Construction of the family* $T[A_1A_2...A_5]$.

1. There exists a unique piecewise T-cubic curve (see Fig. 1.12) associated with any polygon $(A_1A_2...A_{2n+1})$, $n \in I\!N^*$, with unoriented interior angles α_i satisfying the relations
$$\sum_{j=k}^{k+2n} (-1)^{j-k}\alpha_j > 0 \quad \text{for} \quad k = 1, 2, ..., 2n+1. \tag{1.8}$$

2. The family of the tangent lines to this piecewise T-cubic curve is $(2n-1)$-simple.

3. Therefore, regular involutes of this piecewise T-cubic curve yield rosettes of constant width, which are composed of $2(2n+1)$ T-quartic segments (see Fig. 1.13).

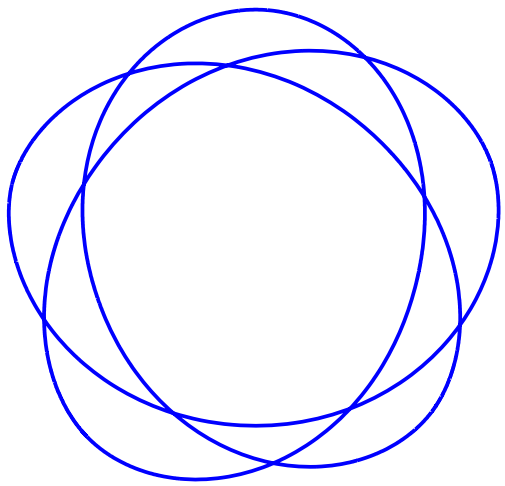

Fig. 1.13 - *T-quartic rosette of constant width.*

It is clear that this construction of rosettes of constant width will remain true for a large class of "appropriate" non-regular polygons.

• **Dual construction of rational ovals of constant width**.

The dual Bézier representation reveals a remarkably simple construction of ovals of constant width. A crucial element for this construction is the fact that the interior offset of an oval Γ of constant width D at the distance D is the curve Γ itself. Thus, using the fact that the dual control structure of the offset of a rational PH curve can be obtained by appropriate translations (which depend on the distance of the corresponding original dual control structure of the circular arc from its midpoint) we developed two slightly different constructions based on a piecewise rational dual representation of a given circle $\mathcal{C}$ of diameter D.

As these constructions are somewhat technical, we just outline the main ideas of the general algorithm (see [5] for details).

1. We first define a piecewise rational dual parametrization of the circle $\mathcal{C}$ composed of segments C_k, $k = 1, ..., 2n$, the segment C_j being the interior offset at the distance D of the segment C_{n+j} for $j = 1, ..., n$ (see Fig. 1.14).
   The constructions consist then in performing appropriate parallel translations of the Bézier and Farin lines of C_j and C_{n+j}.

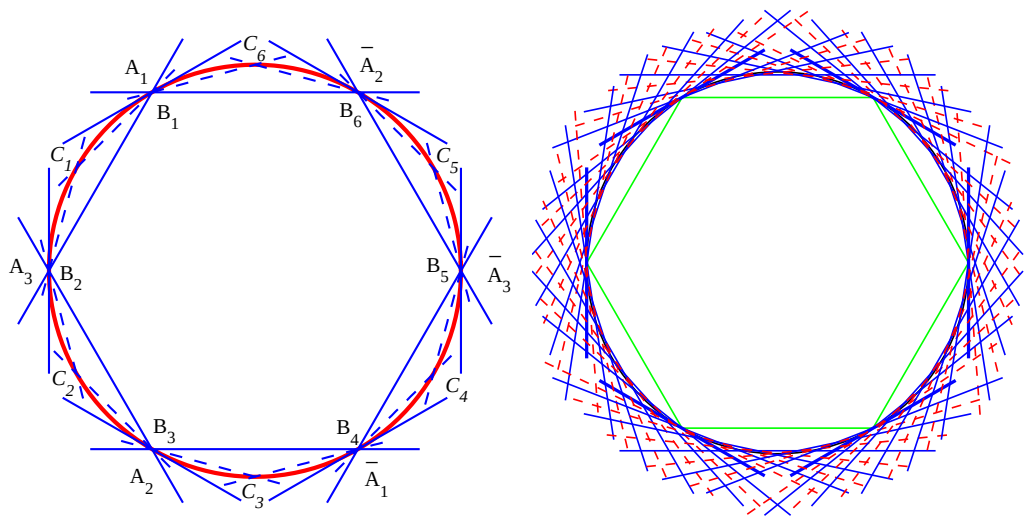

Fig. 1.14 - *Dual control structure of a circle in class* 2 *and* 6.

2. The main construction allows to interpolate general curvature elements "close" to the given circle $\mathcal{C}$ (see Fig. 1.15 and Fig. 1.16) by PH segments of class m, $m \geq 5$.

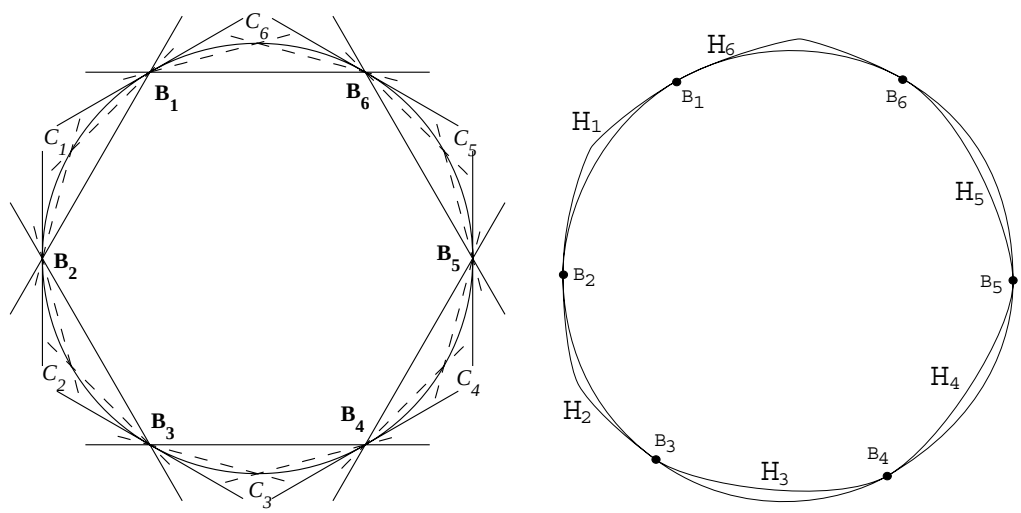

Fig. 1.15 - *Interpolating oval of constant width.*

Left : initial piecewise dual control structure of the circle $\mathcal{C}$*, with* $n = 3$*. Right : each PH curve* H_i *has a* G^2 *contact with the circle* $\mathcal{C}$ *at points* B_i *and* B_{i+1}*. Furthermore, each PH curve* H_{j+3} *is the interior offset at the distance* D *of the PH curve* H_j*.*

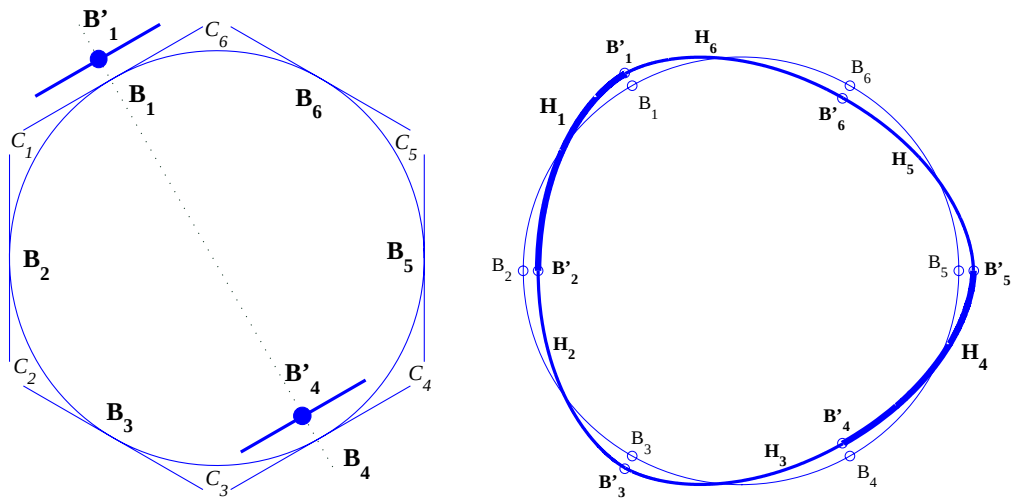

Fig. 1.16 - *Oval of constant width of class 6.*

Left : piecewise dual control structure of the circle $\mathcal{C}$, with $n = 3$, where only the first and last Bézier lines (tangent lines) are represented. We can proceed in the following way. First, we perform arbitrary parallel translations to the 3 first Bézier lines of the segment C_1. Second, in order to get a G^2 contact in B'_1, we perform parallel translations to the 3 last Bézier lines of the segment C_6 according to lemma 1 of [5]. The associated Farin lines are then translated accordingly. Finally, we translate the corresponding Bézier and Farin lines of the segments C_3 and C_4 so that the resulting PH curves H_3 and H_4 are the interior offsets at the distance D of the segments H_6 and H_1.
Right : each PH curve H_i has a G^2 contact with the PH curves H_{i-1} (at point B'_i) and H_{i+1} (at point B'_{i+1}). Furthermore, each PH curve H_{j+3} is the interior offset at the distance D of the PH curve H_j.

• **Concluding remarks**.

These two approaches provide ovals and rosettes of constant width with rational PH-parameterizations. The last construction allows us to interpolate curvature elements "close" to a given circle and thus can be used for the inverse problem concerning the construction of cams with respect to a given periodic longitudinal alternative motion $X(t)$. Precisely, some characteristic curvature elements of the cam could be estimated from the motion $X(t)$ providing data for the approximation.

Furthermore, notice that such an approach of construction will lead, in a straightforward way, to ovals of constant width in the Minkowski plane in which the analogue of PH curves are the Minkowski isoperimetric-hodograph curves as defined in (Ait-Haddou et al. [4]) (see also Section 1.4).

1.4 Minkowski IH curves

General offset curves (see Fig. 1.17) are treated in the context of Minkowski geometry, the geometry of the two-dimensional plane, stemming from the consideration of a strictly

convex, centrally symmetric given curve as its unit circle. Minkowski geometry permits us to move beyond classical confines and provides us with a framework in which to generalize the notion of Pythagorean-hodograph curves in the case of rational general offsets, namely, Minkowski isoperimetric-hodograph curves. Differential geometric topics in the Minkowski plane, including the notion of normality, Frenet frame, Serret Frenet equations, involutes and evolutes are introduced. These lead to an elegant process from which an explicit parametric representation of the general offset curves is derived. Using the duality between indicatrix and isoperimetrix, and between involutes and evolutes, rational curves with rational general offsets are characterized. The dual Bézier notion is invoked to characterize the control structure of Minkowski isoperimetric-hodograph curves. This characterization empowers the constructive process of freeform curve design involving offsetting techniques.

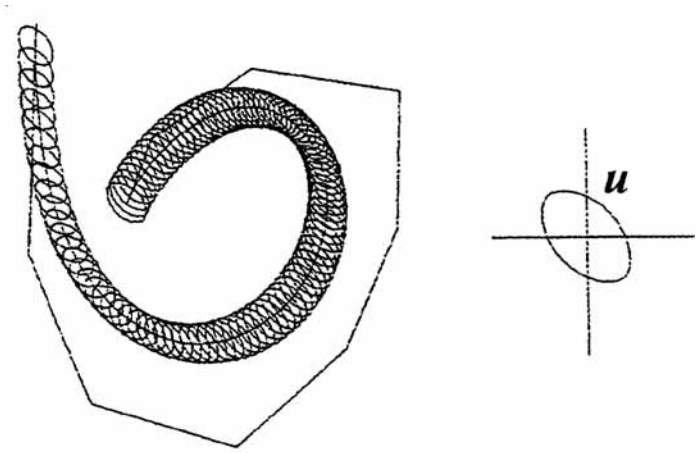

Fig. 1.17 - *General offset curves as the envelope of a family of copies of an indicatrix* $\mathcal{U}$

• **The Minkowski plane**.

We associate a norm with any centrally symmetric, closed, strictly convex plane curve $\mathcal{U}$ with its center O at the origin, such that this curve becomes the unit circle with respect to this norm. The plane endowed with such a norm is called the Minkowski plane. This norm allows us to define a notion of normality between two lines, which is analogous to orthogonality in the Euclidean plane. However, the Minkowski notion of normality is not reciprocal and requires the introduction of a dual geometry through which the reciprocity issue is resolved.

Precisely, we associate the curve $\mathcal{U}$ with the Minkowski metric $m(x,y)$ and the Minkowski norm $||x||_{\mathcal{U}}$ defined by

$$m(x,y) = \frac{2\,e(x,y)}{e(x',y')}\,, \quad \text{and} \quad ||x||_{\mathcal{U}} = \frac{||x||_2}{||x^\star||_2},$$

where points x' and y' of $\mathcal{U}$ define the diameter $[x',y']$ of the indicatrix parallel to the Euclidean line (xy) and with $e(x,y)$ the Euclidean distance (see Fig. 1.18).
The plane with this new metric shall be referred to as the *Minkowski plane* $\mathcal{M}$ with $\mathcal{U}$ being its *indicatrix* which can be viewed as the unit circle in the Minkowski plane.

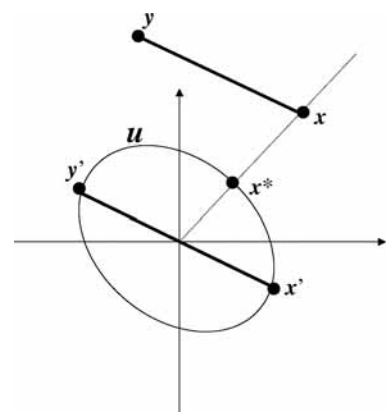

Fig. 1.18 - *Indicatrix $\mathcal{U}$ of the Minkowski plane.*

In all cases (Busemann [11]) wherein the indicatrix is not an ellipse, the norm does not stem from a scalar product, thereby requiring us to move beyond the confines of Euclidean geometry. The study of these cases is rendered possible in the context of Minkowski geometry.

In the Euclidean plane, of all closed, simple curves of equal perimeter, the circle is the one enclosing the greatest area. In the Minkowski plane, however, this extremal curve is not a homothetic copy of the Minkowski unit circle, i.e., the indicatrix $\mathcal{U}$ as one could expect by direct analogy. In fact, this extremal curve is the core of the dual geometry and consists of a curve which is homothetic to the *isoperimetrix* $\mathcal{U}^0$ of the Minkowski plane (Busemann [11]).

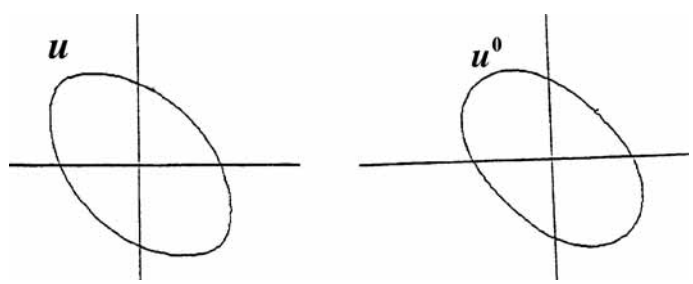

Fig. 1.19 - *Isoperimetrix $\mathcal{U}^0$ of the Minkowski plane.*

Precisely, the isoperimetrix $\mathcal{U}^0$ of a Minkowski plane with indicatrix $\mathcal{U}$ is the polar reciprocal of $\mathcal{U}$ with respect to the Euclidean unit circle, rotated by an angle $-\pi/2$. The isoperimetrix $\mathcal{U}^0$ can be considered as the indicatrix of a Minkowski plane $\mathcal{M}^0$. Then, we have $(\mathcal{M}^0)^0 = \mathcal{M}$ revealing the duality between the two Minkowski planes. Furthermore the parameterization $u(t)$ of the indicatrix $\mathcal{U}$ is related to the corresponding parameterization $u^0(t)$ of the isoperimetrix $\mathcal{U}^0$ by the identity $\det(u^0(t), u(t)) \equiv 1$.

This norm allows to define a notion of *normality* between two lines (and then between vectors). Precisely, a line $\bar{g}$ is $\mathcal{U}$-normal to a line g if and only if there exists a homothety and a translation that transforms the indicatrix $\mathcal{U}$ to a closed curve which has its center on the line $\bar{g}$ and is tangent to the line g at the point of intersection of the two lines (see Fig. 1.20).

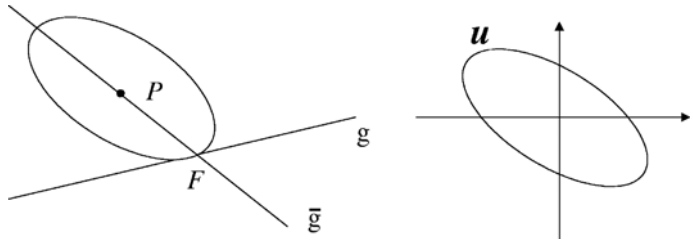

Fig. 1.20 - *Normality.*

Notice that the Minkowski notion of normality is not reciprocal since a line g_1 is $\mathcal{U}$-normal to a line g_2 if and only if the line g_2 is $\mathcal{U}^0$-normal to the line g_1.

• **Differential Geometry in the Minkowski plane**.

We then consider some material concerning differential geometry of plane curves in the Minkowski plane. By associating any plane curve with its Frenet frame, we establish the generalized Serret-Frenet equations. From this, we establish generalized notions of the involute and evolute, as well as their analytic and geometric properties. As this material is somewhat technical, we refer to (Ait-Haddou et al. [4]) and just outline the main ideas.

In the Minkowski plane (see Fig. 1.21), the *$\mathcal{U}$-tangent vector* $\mathbf{t}_{\mathcal{U}}(t)$ of the curve possesses the same direction as in the Euclidean case, being subject only to a normalization with respect to the new norm. To define the *$\mathcal{U}$-normal vector* $\mathbf{n}_{\mathcal{U}}(t)$, however, we consider the generalized notion of normality described above.
Thus, the vector $\mathbf{t}_{\mathcal{U}}(t)$ is $\mathcal{U}$-normal to the vector $\mathbf{n}_{\mathcal{U}}(t)$, and the vector $\mathbf{n}_{\mathcal{U}}(t)$ is $\mathcal{U}^0$-normal to the vector $\mathbf{t}_{\mathcal{U}}(t)$. Furthermore, $\mathbf{t}_{\mathcal{U}}(t)$ is a parameterization of a segment of the indicatrix whereas $\mathbf{n}_{\mathcal{U}}(t)$ is a parameterization of a segment of the isoperimetrix.

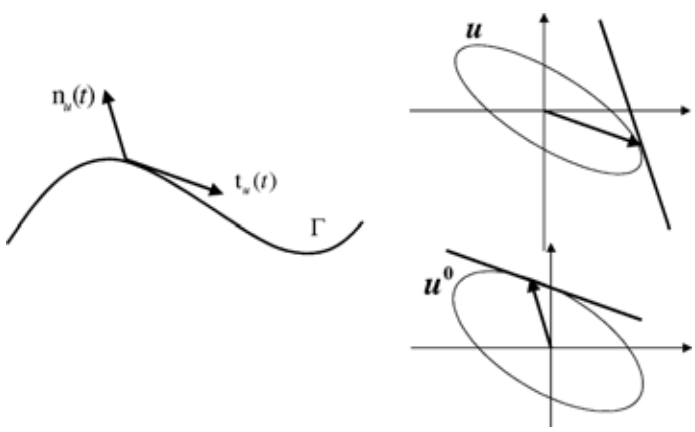

Fig. 1.21 - *Serret-Frenet frame in the Minkowski plane.*

Then, introducing the notions of *$\mathcal{U}$-arclength*, *$\mathcal{U}$-Minkowski curvature* and *$\mathcal{U}$-circular curvature* of a curve in the Minkowski plane, we generalize the Serret-Frenet equations (relating the $\mathcal{U}$-normal and $\mathcal{U}$-tangent vectors to their rate of change along the curve) and then the notions of *involute* and *evolute* (see Fig. 1.22) in the Minkowski plane, as well as their analytic and geometric properties (Ait-Haddou et al. [4]).

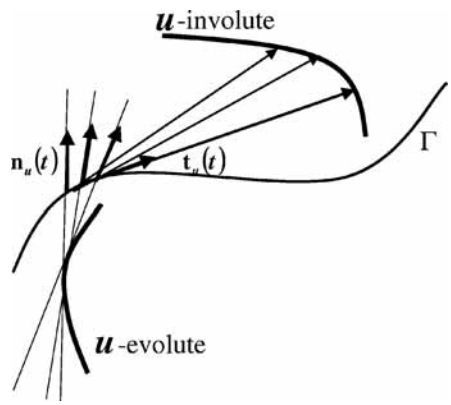

Fig. 1.22 - *Involute and evolute of a curve in the Minkowski plane.*

• **General offset curves**.

The notion of general offset curves is introduced as the envelope of a homothetic copy of $\mathcal{U}$ (see Fig. 1.17), translated, with no change in size, along a given curve. Such an $\mathcal{U}$-offset curve of a C^2, regular parametric curve $F(t)$ at a signed distance d is the curve defined by the parametric equation

$$F_d(t) = F(t) + d\,\mathbf{n}_{\mathcal{U}^0}(t).$$

Note that if the indicatrix of the geometry is the Euclidean unit circle, then the isoperimetrix is also the Euclidean unit circle and we recover the expression of the standard offset curve. Note also that the general offset curve can be viewed as the boundary of the Minkowski sum of the curve and the homothetic copy of the indicatrix, in the case where the general offset curve possesses no singularities (Kaul and Farouki [36], Lee et al. [39]). In a seismological context, a given curve can be viewed as an exploding interface/reflector separating two anisotropic-homogeneous media. The indicatrix $\mathcal{U}$ corresponds to an elementary wavefront generated at point sources along the reflector, while the general offset curve illustrates the total wavefront consisting of the envelope stemming from all point sources exploding along the interface (Arnold [6]). The concept of an exploding reflector is commonly used in modeling seismic data. The standard Euclidean approach corresponds to isotropic homogeneous media, while the Minkowski-plane approach conveniently and rigorously extends the exploding-reflector method to include anisotropic-homogeneous media (see Chapter 5).

• **Minkowski IH curves**.

We assume now that the indicatrix $\mathcal{U}$ is a rational curve. Then, given a rational curve $F(t)$, we show that *the $\mathcal{U}$-offset parametrization $F_d(t)$ is rational if and only if the function $||F'(t)||_{\mathcal{U}^0}$ is rational.* Such a curve is said to be a *Minkowski Isoperimetric-hodograph (Minkowski IH) curve*, or a $\mathcal{U}$-IH curve for simplicity.

We then consider the geometric characterization of $\mathcal{U}$-IH curve. Fiorot and Gensane [30] and, independently, Pottmann [42], provided a geometric characterization of the sets of rational Pythagorean-hodograph curves, namely, the involutes of rational curves with rational arclength. We provide a generalization of this characterization by means of Minkowski IH curves (Ait-Haddou et al. [3, 4]). Let $\mathcal{D}$ be the set of rational parametric

curves with support in a line and $\mathcal{C}$ be the set of rational parametric curves with support in the indicatrix.

The set of rational curves with rational U-offsets (i.e., Minkowski IH curves) is equal to the union of the set of the $\mathcal{U}$-involutes of rational curves with rational $\mathcal{U}$-arclength with the set $\mathcal{D}$ and $\mathcal{C}$.

• **Dual representation of Minkowski IH curves**.

Rational Pythagorean-hodograph curves, manipulated by their dual-Bézier control structure, have been elegantly incorporated into freeform design (Pottmann [42, 43]). We are now concerned by generalizing this feature to Minkowski IH curves where the indicatrix of the geometry is a rational curve.

We show (Ait-Haddou et al. [3, 4]) that the Bézier control structure of an IH curve in the Minkowski plane may be obtained by merely substituting the indicatrix of the Minkowski plane for the Euclidean unit circle in the Pottmann construction. Surprisingly, the isoperimetrix does not manifest itself in the final algorithmic construction despite the fact that it is indispensable in deriving this result. This fact is not obvious in the case of the Euclidean plane since the isoperimetrix of the Euclidean unit circle is the circle itself.

The dual control structure of a rational Minkowski IH curve is characterized by the property that each of its Bézier and Farin lines is parallel to its corresponding line in the control structure of the dual representation of a segment of the indicatrix (see Fig. 1.23).

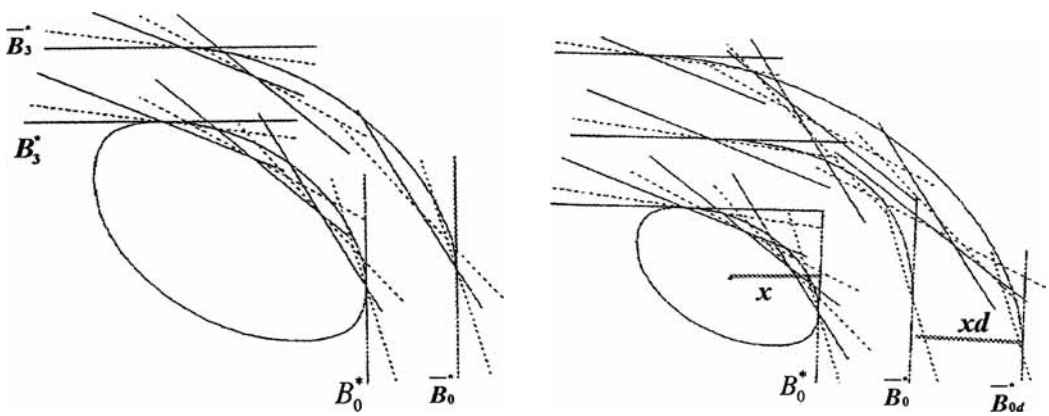

Fig. 1.23 - *Left : dual Bézier representation of an $\mathcal{U}$-IH curve. Right : dual Bézier construction of the $\mathcal{U}$-offset curve.*

• **Concluding remarks**.

The introduction of Minkowski geometry allows to establish a comprehensive mathematical framework for the study of Pythagorean-hodograph curves to the case of general offset curves. The geometric and dual Bézier characterizations of the set of rational curves with rational general offsets (Minkowski IH curves) empower the constructive process of freeform curve design involving offsetting techniques. Further research is aimed at the inverse-theory applications for determining the shape and position of a deep, seismic reflector beneath an anisotropic-homogeneous medium.

1.5 Future works

The works and results presented in Sections 1.2, 1.3 & 1.4 where only concerned with *planar* Pythagorean-hodograph curves in the Euclidean and Minkowski plane.

We took advantage of these planar offsetting techniques in Chapter 5 for industrial applications in a seismological context. In this context, the standard Euclidean approach corresponds to isotropic homogeneous media, while the Minkowski-plane approach conveniently and rigorously extends the exploding-reflector method to include anisotropic-homogeneous media. The indicatrix $\mathcal{U}$ corresponds to an elementary wavefront generated at point sources along the reflector, while the general offset curve illustrates the total wavefront consisting of the envelope stemming from all point sources exploding along the interface.

Pythagorean-hodograph (PH) *space* curves have been introduced by Farouki and Sakkalis [24]. Pythagorean-hodograph (PH) space curves are polynomial parametric curves $\mathbf{r}(t) = (x(t), y(t), z(t))$ with the distinguishing property that their derivatives or hodographs $\mathbf{r}'(t) = (x'(t), y'(t), z'(t))$ satisfy the Pythagorean condition

$$x'^2(t) + y'^2(t) + z'^2(t) = \sigma^2(t), \tag{1.9}$$

where $\sigma(t)$ is a polynomial. This feature ensures that PH space curves admit exact measurement of arc length, a fact that is especially advantageous in the formulation of real-time interpolators to drive multi-axis CNC machines along curved paths at fixed or variable feedrates [26, 27, 46].

Spatial PH curves were first investigated in [24], using the form

$$\begin{aligned} x'(t) &= u^2(t) - v^2(t) - w^2(t), \\ y'(t) &= 2u(t)v(t), \\ z'(t) &= 2u(t)w(t), \\ \sigma(t) &= u^2(t) + v^2(t) + w^2(t), \end{aligned} \tag{1.10}$$

in terms of three polynomials $u(t), v(t), w(t)$ as a sufficient condition for the satisfaction of (1.9). However, the form (1.10) has a fundamental defect - it is not invariant under arbitrary 3-dimensional rotations. A sufficient-and-necessary condition for satisfaction of (1.9) was identified by Dietz et al. [17] - namely, the hodograph components must be expressible in terms of four polynomials $u(t), v(t), p(t), q(t)$ in the form

$$\begin{aligned} x(t) &= u^2(t) + v^2(t) - p^2(t) - q^2(t), \\ y(t) &= 2[u(t)q(t) + v(t)p(t)], \\ z(t) &= 2[v(t)q(t) - u(t)p(t)], \\ \sigma(t) &= u^2(t) + v^2(t) + p^2(t) + q^2(t). \end{aligned} \tag{1.11}$$

Subsequently, Choi et al. [13] gave an elegant characterization of this form in terms of quaternions. This interpretation is invaluable in demonstrating [28] the rotation-invariance of (1.11).

More recently, a new special family of spatial PH curves, namely the RRMF curves, has been introduced by Choi and Han [14, 34] for motion control purposes. The first non

trivial examples of such curves have then been exhibited by Farouki et al. [29]. In motion planning, computer animation, geometric design, and robotics, it is often necessary to specify the variation of an orthonormal frame $(\mathbf{f}_1, \mathbf{f}_2, \mathbf{f}_3)$ along a given space curve $\mathbf{r}(t)$, that describes the orientation of a rigid body along the given path. The so so-called *adapted* frames on space curves, in which the unit curve tangent $\mathbf{t}$ is chosen as the frame vector $\mathbf{f}_1$ are commonly invoked in such contexts. Klok [37] identified the rotation-minimizing frames (RMFs) as the best suited to swept surface constructions.

The variation of any adapted frame $(\mathbf{f}_1, \mathbf{f}_2, \mathbf{f}_3)$ with $\mathbf{f}_1 = \mathbf{t}$ along a curve $\mathbf{r}(t)$ is specified in terms of its vector *angular velocity* $\omega(t)$, through the differential relations

$$\mathbf{f}_1' = \omega \times \mathbf{f}_1 \,, \quad \mathbf{f}_2' = \omega \times \mathbf{f}_2 \,, \quad \mathbf{f}_3' = \omega \times \mathbf{f}_3 \,.$$

The characteristic property of a *rotation–minimizing* adapted frame on $\mathbf{r}(t)$ is that its angular velocity has no component along $\mathbf{f}_1 = \mathbf{t}$. This implies that $\mathbf{f}_2$, $\mathbf{f}_3$ have no instantaneous rotation about $\mathbf{f}_1 = \mathbf{t}$ — they vary only because $\mathbf{t}$ is varying along $\mathbf{r}(t)$, and they are compelled to remain orthogonal to it (and each other).

Polynomial and rational space curves do not ordinarily admit exact rational RMF representation. Nevertheless, recently, greater interest in constructing polynomial curves that possess exact *rational rotation–minimizing frames* (or RMMF curves) has emerged. Such curves are necessarily PH curves since only the PH curves have rational unit tangents.

Thus, a collaboration with Rida Farouki (UC Davis) is currently in progress concerning spatial PH curves and RRMF curves. The fact that the Darboux frame is rotation–minimizing along the lines of curvature of a smooth surface is invoked to construct rational surface patches with given boundary curves as lines of curvature. The patch boundaries are specified as quintic RRMF curves — i.e., spatial Pythagorean–hodograph (PH) curves that possess rational rotation–minimizing frames.

Some other topics are also of interest. – Identification and characterization of family of polynomial surfaces with PH curves as isoparametrics. – Geometric design of rational PH cams for optimum performance in high–speed applications (in addition to direct geometric constructions).

Bibliography Chapter 1

[1] Ait-Haddou, R. and L. Biard, Curve design with T-quartics, *Research Report RR 946 M, Université Joseph Fourier, March 1995.*

[2] Ait-Haddou, R. and L. Biard, G^2approximation of an offset curve by Tschirnhausen quartics, *in Mathematical Methods in CAGD III, M. Daehlen, T. Lyche, and L. L. Schumaker (eds.), Vanderbilt University Press, pp. 1-10, 1995.*

[3] Ait-Haddou Rachid, PhD Thesis,
Courbes à hodographe pythagorien en géométrie de Minkowski et modélisation géométrique, *Applied Mathematics, University Joseph Fourier, Laboratory LMC-IMAG, 6 septembre 1996.*

[4] Ait-Haddou, R., L. Biard and M. A. Slawinski, Minkowski isoperimetric-hodograph curves, *in Computer Aided Geom. Design, vol 17, issue 9, October 2000, pp 835-861.*

[5] Ait-Haddou Rachid, Walter Herzog and Luc Biard, Pythagorean-hodograph ovals of constant width, *Computer Aided Geometric Design, Volume 25, 4-5, pp. 258–273, May 2008.*

[6] Arnold, V.I., Mathematical Methods of Classical Mechanics, *Springer Verlag, 1978.*

[7] Boehm, W., Rational Geometric Splines, *Computer Aided Geom. Design 4, (1987), 66–77.*

[8] Bonnesen, T. and W. Fenchel, Theorie der konvexen Körper (Berlin 1934).

[9] Brechner, E., Envelope and tool paths for three-axis end milling, *PhD Thesis, Renssealaer Polythechnic Institute, Troy, NY, 1990.*

[10] Brechner, E., General offset curves, *in: Barnhill, R.E., ed., Geometry Processing for Design and Manufacturing, SIAM, Philadelphia, 1992, 101–121.*

[11] Busemann, H., *The foundation of Minkowskian geometry Annali di Mat. Pura ed Appl. 69, 1965, 305–370.*

[12] Busemann, H., *Metric methods in Finsler spaces and in the foundations of the geometry, Annals of Mathematics Studies, 8, 1965.*

[13] Choi H.I., D.S. Lee and H.P. Moon, Clifford algebra, spin representation, and rational parameterization of curves and surfaces, *Adv. Comput. Math., 17 (2002), 5-48.*

[14] Choi H. I. and C. Y. Han, Euler–Rodrigues frames on spatial Pythagorean–hodograph curves, *Computer Aided Geom. Design 19, 2002, 603–620.*

[15] Cieślak, W. and W. Mozgawa, On rosettes and almost rosettes, *Geom. Dedicata 24, (1987), 221–228.*

[16] Cieślak, W. and J. Zajac, The rosettes, *Math. Scand. 58, (1986), 114–118.*

[17] Dietz R., J. Hoschek and B. Jüttler, An algebraic approach to curves and surfaces on the sphere and on other quadrics, *Computer Aided Geom. Design 10 (1993) 211229.*

[18] Eric Drexler, K., Nanosystems, Molecular Machinery, Manufacturing, and Computation *Wiley-Interscience Publication, (1992).*

[19] Farin, G., Curvature continuity and offset of piecewise conics, *ACM Trans. Graphics, 8, (1989), 89–99.*

[20] Farin, G. and A. Worsey, Reparameterization and Degree Elevation for Rational Bézier Curves, in *G. Farin (ed.), NURBS for Curve and Surface Design, SIAM, Philadelphia 1991, pp. 47–58.*

[21] Farouki, R. T., Pythagorean-hodograph curves in practical use, *in Geometry Processing for Design and manufacturing, R. E. Barnhill (ed.), SIAM, Philadelphia, 1992, 3–33.*

[22] Farouki, R. T. and T. Sakkalis, Pythagorean hodographs, *IBM J. Res. Develop. 34, (1990), 736–752.*

[23] Farouki R.T., The conformal map $z \to z^2$ of the hodograph plane, *Computer Aided Geom. Design 11 (1994) 363390.*

[24] Farouki R.T. and T. Sakkalis, Pythagorean-hodograph space curves, *Adv. Comput. Math. 2 (1994) 4166.*

[25] Farouki, R. T. and H. Pottmann, Polynomial and rational Pythagorean-hodograph curves reconciled, *in The Mathematics of Surfaces VI (G. Mullineux, ed), pp. 355–378, Oxford University Press, 1996.*

[26] Farouki R.T. and S. Shah, Real-time CNC interpolators for Pythagorean-hodograph curves, *Computer Aided Geom. Design 13 (1996) 583600.*

[27] Farouki R.T., J. Manjunathaiah, D. Nicholas, G.-F. Yuan and S. Jee, Variable feedrate CNC interpolators for constant material removal rates along Pythagorean-hodograph curves, *Computer Aided Design 30 (1998) 631640.*

[28] Farouki R.T. , M. al-Kandari and T. Sakkalis, Structural invariance of spatial Pythagorean hodographs, *Computer Aided Geom. Design 19, (2002) 395–407.*

[29] Farouki R. T., C. Giannelli, C. Manni, and A. Sestini, Quintic space curves with rational rotation–minimizing frames, *Computer Aided Geom. Design 26, 2009, 580–592.*

[30] Fiorot, J. C. and Th. Gensane, Characterization of the set of rational parametric curves with rational offsets, *in curves and Surfaces in Geometric Design, P. J. Laurent, A. Le Méhauté, and L. L. Schumaker (eds.), AK Peters, Wellesley, (1994), 153–160.*

[31] Guggenheimer H. W., Differential Geometry, *McGraw-Hill Book Company, Inc, 1963.*

[32] Hammer, P. C. and A. Sobczyk, Planar line families, II, *Proc. Amer. Math. Soc. 4 (1953).*

[33] Hammer, P. C., Constant breadth curves in the plane, *Proc. Amer. Math. Soc. 6, (1955).*

[34] Han C. Y., Nonexistence of rational rotation–minimizing frames on cubic curves, *Computer Aided Geometric Design 25, 2008, 298–304.*

[35] Hoschek, J., Dual Bézier curves and surfaces, *in : R.E. Barnhill and W. Boehm, eds., Surfaces in Computer Aided Geometric Design, North Holland, (1983), 147–156.*

[36] Kaul, A. and Farouki, R.T., Computing Minkowski sums of plane curves, *Int. J. Computational Geometry and Applications 5, 413–432.*

[37] Klok F., Two moving coordinate frames for sweeping along a 3D trajectory, *Computer Aided Geometric Design 3, 1986, 217–229.*

[38] Kubota, K. K., Pythagorean triples in unique factorization domains, *Amer. Math. Monthly 79, (1972), 503–505.*

[39] Lee, I.K., Kim, M.S. and Elber, G., Polynomial and rational approximation of Minkowski sum boundary curves, *Graphical Models and Image Processing, 60, 1998, 136–165.*

[40] Moon, H.P., Minkowski Pythagorean hodographs, *Computer Aided Geometric Design 16, 1999, 739–753.*

[41] Paternell, M. and Pottmann, H., A Laguerre geometric approach to rational offsets, *Computer Aided Geometric Design 15, 1998, 223–249.*

[42] Pottmann, H., Rational curves and surfaces with rational offsets, *Computer Aided Geom. Design 12, (1995), 175–192.*

[43] Pottmann, H., Curve design with rational Pythagorean-hodograph curves, *Advances in Computational Mathematics, Vol. 3, pp.147–170, 1995.*

[44] Pottmann, H., General offset surfaces, *Neural, Parallel and Scientific Computations, Vol. 5, Issue 1-2, 55–80, 1997.*

[45] Strubecker, K., Differentialgeometrie, *Bd. 1, Sammlung Göschen, Berlin 1964, pp. 120–124.*

[46] Tsai Y-F., R.T. Farouki and B. Feldman, Performance analysis of CNC interpolators for time–dependent feedrates along PH curves, *Compututer Aided Geom. Design 18 (2001) 245265*.

[47] Wegner, B., Some global properties and constructions for closed curves in the plane, *Geom. Dedicata 29, (1989), 317–326*.

Chapter 2

Computing Geodesics on subdivision surfaces

Computation of shortest paths is a well known problem in Computational Geometry. Geodesic curves play an important role in many areas of science, engineering and computer graphics, such as robot motion planning, surface parameterization, terrain navigation, geographical information systems, re-meshing, front propagation over surfaces... The increasing development of discrete surface models as well as linear approximations of smooth surfaces require the definition of geodesics, sometimes called discrete geodesics, on surfaces represented by triangular meshes.

Considering smooth surfaces, analytical approaches using differential equations are pretty complex. Maekawa [13], consider the problem of computing the shortest path between two points and between a point and a curve on a free-form parametric surface by solving a two point boundary value problem, thanks a relaxation method relying on finite difference discretization. Hotz & Hagen [7], introduced a geometric method for the construction of geodesics on any smooth surface. They construct locally the geodesic by orthogonal projection relative to the tangent plane. This approach is computationally less intensive and has been used for visualizing geodesic nets. New approaches emerged for efficient computation of geodesic distances on triangular meshes. Polthier and Schmies [20] introduced the notion of discrete geodesic curvature of curves and defined straightest geodesics on polyhedral surfaces. This approach gives information about how a geodesic should pass through a vertex but does not take into account the polyhedral surface normals while computing the straightest geodesics. This allows a unique solution of the initial value problem for geodesics. Ravi Kumar et al. [21], consider the computation of discrete geodesics on the tessellated surface of a NURBS by taking into account the tessellation normal.

Some other different formulations for this problem are the following. The *single source* shortest path problem, in which we wish to find a shortest path between a source point and any other point on the surface. And the more complex formulation is to find a shortest path between any pair of points in the surface. Most of the algorithms use front propagation or some other kind of Dijkstra's-like algorithm. Many authors, Kimmel et al. [10], Kimmel & Sethian [11], Novotni & Klein [17], Zigelman et al. [25], approximate geodesic distances on triangulated domains by considering wavefront propagation algorithms. The

central idea is to advance a front to produce new distance values at the vertices of the mesh. These informations allow then to get an approximation of the geodesic path. Following these ideas, Martinez et al. [14], compute a locally shortest geodesic joining two points over a triangulated surface. Their method uses an iterative process to obtain discrete geodesic approximation, both on convex and non-convex surfaces.

The Ph.D thesis of Valérie Pham-Trong [19], co-directed with N. Szafran, is related to the computation of shortest and geodesic paths on any continuous surface. As already mentioned, geodesic paths on smooth surfaces can be evaluated by solving differential equations. Nevertheless, due to the use of linear elements, whole real objects are often modeled by surfaces which are not even C^1, and for many applications in computer graphics, smooth surfaces are just a limit of a subdivision process. So that, computer geometric design often operates with triangle elements. Thus, considering the computing of geodesic paths, we are concerned with the need of a purely geometric algorithm.

So, we consider in Section 2.1 of this chapter a geometric method for the computation of a geodesic (or shortest) path between two given points on any three-dimensional subdivision surface or triangular mesh. Notice that this method also works for the computation of geodesic curves originated from a point in a given direction. The implementation is based on finding the shortest path on the successive control nets of the surface. The convergence property of the control nets to the surface provides then the required shortest path or geodesic path (Pham-Trong et al. [18, 19]), or an approximation of this geodesic path according any desired accuracy. In a second part, in Section 2.3, we present an algorithm for determining geodesic loops on surfaces. This work has been initiated for a specific application to the geometric modeling of myocardium (Mourad et al. [15]). The aim of this project, involving research groups from Grenoble (TIMC, LMC, CHU, L3S) was to check a conjecture according to which myocardial fibres are geodesic curves running on some surfaces (Streeter [22]). Finally, in Section 2.4, future works are outlined.

2.1 Geodesic path on a polyhedron

Characterization and properties of geodesic curves on smooth surfaces are considered in Chapter 3. We assume in this section that all surfaces are polyhedron composed of triangular faces, so that we are essentially concerned with geodesic curves running on piecewise continuous planar surfaces. On a planar surface, a *geodesic curve* is a straight line and is thus the shortest path between two any of its points. On a general surface, a shortest path is always a geodesic curve whereas a geodesic curve is not necessarily a shortest path (see Fig. 2.1 : the red curve is a geodesic path but not the shortest path between the two vertices of the left face). A geodesic curve is defined as a *locally shortest path*, which means that any local deformation of the curve between two close points of the curve lengthen the path.

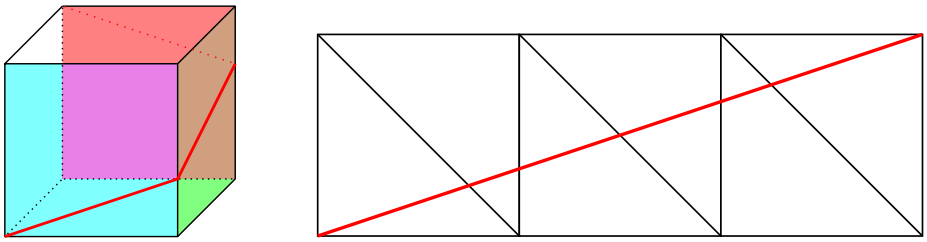

Fig. 2.1 - *Flattening of a cube and geodesic path.*

Consider a simplicial polyhedron $\mathcal{P}$ (so that all faces are triangles) and a sequence $\mathcal{F}_1, \mathcal{F}_2, ..., \mathcal{F}_n$ of *adjacent triangular faces* of $\mathcal{P}$ such that $\mathcal{F}_i$ and $\mathcal{F}_{i+1}$ $(i = 1, ..., n-1)$ share a common non trivial edge $\mathcal{A}_i$ with $\mathcal{A}_i \neq \mathcal{A}_{i+1}$ for all i. The flattening of this sequence consists in performing successive rotations around the common edges (without overlap between two adjacent faces) in order that these triangular faces lie in a same plane. We thus obtain a new sequence $F_1, F_2, ..., F_n$ of adjacent faces lying in a plane Π with edges A_i. Each face F_i is isometric to the corresponding face $\mathcal{F}_i$. Notice that the flattening of a sequence can produce some global overlap.

A *linear path* on a simplicial polyhedron is a continuous curve running on the polyhedron, linear on each triangular face. A linear path is thus associated with a sequence of adjacent faces $\mathcal{F}_1, \mathcal{F}_2, ..., \mathcal{F}_n$ and is characterized by a sequence of points $\big[X_0,\ a_1, a_2,\ ..., a_{n-1},\ X_1\big]$, with $a_i \in \mathcal{A}_i$ and where $X_0 \in \mathcal{F}_1$, $X_1 \in \mathcal{F}_n$ are the starting and arrival points. The flattening of the sequence $(\mathcal{F}_i)$ transform the path $\Gamma = \big[X_0,\ a_1,\ a_2,\ ...,\ a_{n-1},\ X_1\big]$ into the path $\gamma = \big[x_0,\ \alpha_1,\ \alpha_2,\ ...,\ \alpha_{n-1},\ x_1\big]$ included in the planar sequence of faces $F_1,\ F_2,\ ...,\ F_n$ such that *the two paths* Γ *and* γ *have the same length.*

Polthier and Schmies [20] introduced *straightest geodesics* inspired by the characterization of smooth geodesics. They defined *discrete geodesic curvature* as a generalization of the well-known concept of geodesic curvature and straightest geodesics as polygonal curves over the polyhedron $\mathcal{P}$ with zero geodesic curvature everywhere. If we call θ the sum of incident angles at a vertex P of a curve over $\mathcal{P}$ and θ_r and θ_l the respective sum of right and left angles, a straightest geodesic verify in particular $\theta_r = \theta_l$ at every point. A vertex P is said to be *parabolic or euclidean* if $\theta = 2\pi$, *elliptic* if $\theta < 2\pi$ and *hyperbolic* if $\theta > 2\pi$. The following results (Polthier & Schmies [20]) explores the differences between straightest and shortest geodesics (a shortest geodesic being a local shortest geodesic curve as mentioned above).

(1) A straightest geodesic through an elliptic vertex is not locally shortest.

(2) A geodesic containing no surface vertex is both shortest and straightest.

(3) There exist a family of shortest geodesics through a hyperbolic vertex. Exactly one of them is a straightest geodesic.

However, since our main purpose is to compute shortest paths, we shall consider local shortest geodesics (i.e., geodesic curves) instead of straightest geodesics. The following remarks will be useful for our strategy.

(a) A geodesic curve can not go through an elliptic vertex.

(b) If γ lie on a straight line going through the sequence of faces (F_i), then Γ is a geodesic curve on the polyhedron $\mathcal{P}$.

(c) The converse is not true in general. A geodesic curve Γ on the polyhedron $\mathcal{P}$ can be associated with a path γ admitting some deviation in the flattened sequence of adjacent

faces (F_i). Such deviations can only occur at vertices associated with hyperbolic vertices (such vertices will be called *critical–vertices*).

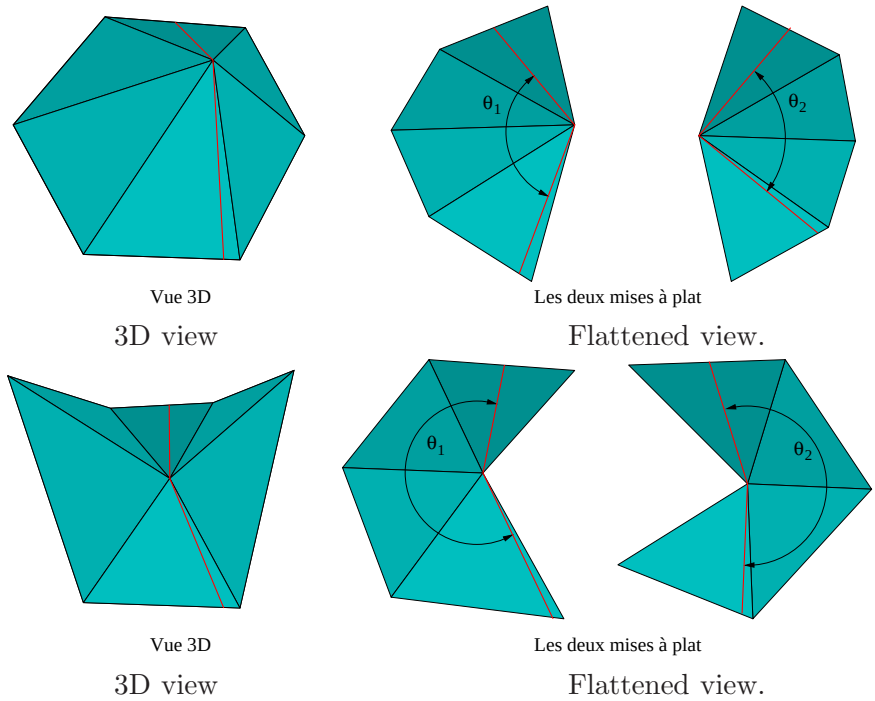

Fig. 2.2 - *Path going through an elliptic and an hyperbolic vertex.*

• **Strategy**.

The determination of a geodesic path joining two given points on a simplicial polyhedron consists essentially in determining the appropriate sequence of adjacent faces on which lies this path. Then, the flattening of this sequence permits to explicit this geodesic curve. So, given two points X_0 and X_1 of the polyhedron $\mathcal{P}$ lying on two faces $\mathcal{F}$ and $\mathcal{F}'$, the algorithm is the following.

1. Choose an initial sequence of adjacent faces $\mathcal{F} = \mathcal{F}_1$, $\mathcal{F}_2$, ..., $\mathcal{F}_n = \mathcal{F}'$ joining faces $\mathcal{F}$ and $\mathcal{F}'$.

2. Determine the shortest path γ between x_0 et x_1 inside the flattened sequence $F_1, ..., F_n$. This path γ can possess some deviations at some vertices (called *pivot–vertices*).

3. For each pivot–vertex, update the sequence of adjacent faces by minimizing the deviation. At the end of this process, the (eventual) remaining pivot–vertices are critical–vertices and the final updated curve γ provides the shortest path Γ.

• **Choice of the initial sequence**.

If the simplicial polyhedron is an approximation of a parameterized surface, the initial sequence is evaluated in the parameter domain. In that case, since each face of the

polyhedron is associated with a triangular face in the parameter domain, we consider the sequence of faces of the parameter domain meeting the segment $[\hat{x_0}, \hat{x_1}]$, where $\hat{x_0}$ and $\hat{x_1}$ are the parameter points associated with the two points X_0 and X_1 of the polyhedron $\mathcal{P}$.

For a more general simplicial polyhedron or subdivision surface, the initial sequence can be obtained by an appropriate projection of the segment $[X_0, X_1]$ on the surface. This point has not been treated since we only consider Bézier and NURBS surfaces.

• **Shortest path in a flattened sequence**.

The problem of finding a shortest path between two points x_0 and x_1 inside a flattened sequence $F_1, ..., F_n$ has been studied by many authors : Chazelle [1], Lee & Preparata [12]. Such a shortest path exists and is unique. It consists in a polygonal line $[x_0,\ y_1,\ ...,\ y_p,\ x_1]$, whose vertices y_j are a subset of the vertices involved in the flattened sequence. As already mentioned, these vertices are the pivot–vertices.

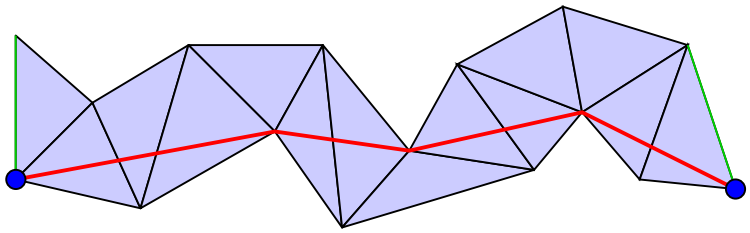

Fig. 2.3 - *Shortest path in a flattened sequence.*

A linear algorithm (with respect to the number of faces) has been developed independently by Chazelle [1] and Lee & Preparata [12] for computing the shortest path in a flattened sequence.

• **Update of the sequence of adjacent faces**.

The update is performed with respect to pivot–vertices. Let y be a pivot–vertex of the flattened sequence, Y the associated vertex of the polyhedron and $F_k, F_{k+1}, ..., F_{k+r}$ the faces of the flattened sequence which contain the pivot–vertex y. Thus, in this flattened sequence, the shortest path goes through the face F_k, the vertex y and the face F_{k+r} (see Fig. 2.4).

Denote then by $\mathcal{F}_k$, $\mathcal{F}_{k+1}$, ..., $\mathcal{F}_{k+r}$, $\mathcal{F}_{k+r+1}$, ..., $\mathcal{F}_{k+s}$, $(\mathcal{F}_{k+s+1} = \mathcal{F}_k)$ the ordered set of all faces of the polyhedron containing the vertex Y. The update of the flattened sequence with respect to the vertex y consists in considering the complementary faces, i.e., the faces $\mathcal{F}_k, \mathcal{F}_{k+s}, \mathcal{F}_{k+s-1}, ..., \mathcal{F}_{k+r}$.

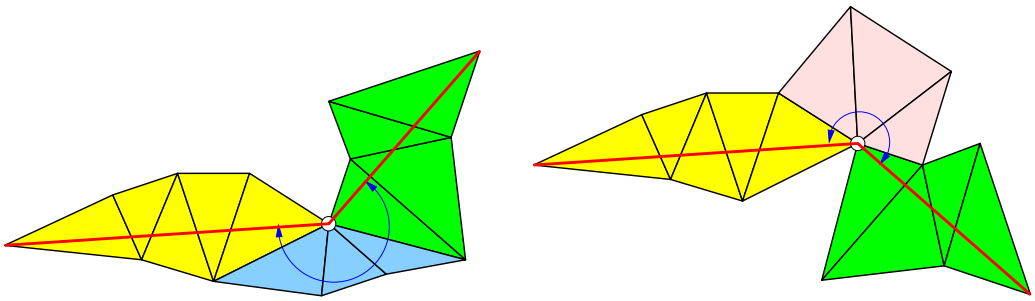

Fig. 2.4 - *Update with respect to a critical–vertex.*

Then, two situations can occur.
◇ Generally, the pivot–vertex disappears in the new flattened sequence, which means that the shortest path in the new flattened sequence does not go anymore through vertex y .
◇ However, the vertex y can remain as a pivot–vertex in the new flattened sequence. Such a pivot–vertex has a deviation angle strictly greater than π whatever the flattening, and is potentially a critical–vertex. The notion of critical–vertex is global. Indeed, the update of the flattened sequence with respect to other pivot–vertices can lead to the disappearance of some "potentially" critical–vertex.

Thus, *critical–vertices* are the residual pivot–vertices at the end of the process.

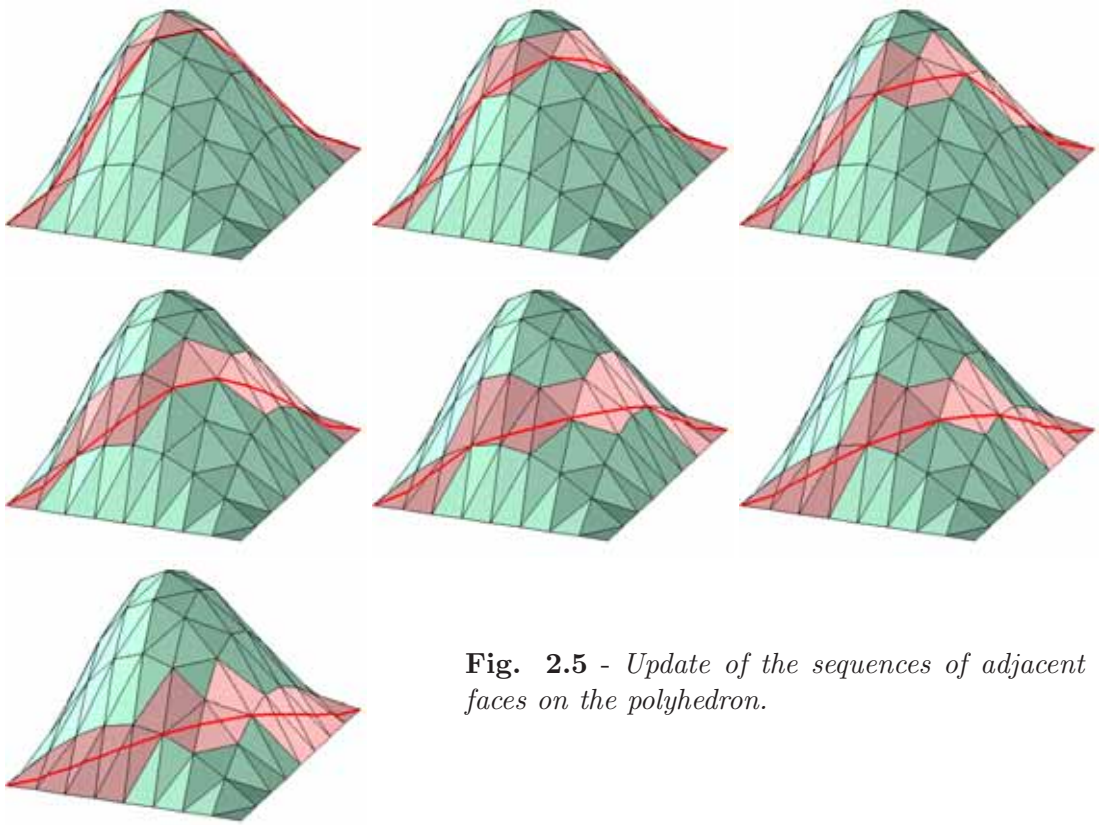

Fig. 2.5 - *Update of the sequences of adjacent faces on the polyhedron.*

Fig. 2.5 exhibits the different updates of the sequence of adjacent faces for the computation of the shortest path (or a geodesic path) between two opposite corners of the surface. It can be seen that the geodesic path on this polyhedron contains two critical–vertices at hyperbolic vertices.

• **ALGORITHM** :

$F \leftarrow$ initial list of triangles joining X_0 and X_1
$C \leftarrow$ shortest path in F
$L \leftarrow$ list of pivot–vertices of C in F
$L' \leftarrow$ empty
while $L \neq L'$ **do**
  $L' \leftarrow L$
  update F around each vertex of L
  $C \leftarrow$ shortest path in F
  $L \leftarrow$ list of pivot–vertices of C
end–while
$G \leftarrow C$
(L list of critical–vertices)

2.2 Geodesic paths on a subdivision surface

The previous algorithm will now allow us to compute geodesic paths on any subdivision surface but appears to be more efficient on subdivision surfaces associated with a parametrization such as Bézier or NURBS surfaces (Pham-Trong et al. [18, 19]). Such a surface $\mathcal{S}$ is associated with an initial control polyhedron $\mathcal{P}_0$, a parameter domain D and a subdivision process. The sequence of subdivided polyhedron $\mathcal{P}_k$ converges towards the surface.

The method consists at each step in using the geodesic curve Γ_k evaluated on the polyhedron $\mathcal{P}_k$ to initialize, by projection, the computation of the geodesic curve Γ_{k+1} on the subdivided polyhedron $\mathcal{P}_{k+1}$. The projection of Γ_k is performed in the parameter domain D.

Precisely, the main ideas for our strategy are the following.

- ◇ Each triangular face of a polyhedron $\mathcal{P}_k$ is associated with a unique triangular face in the parameter domain.
- ◇ Each geodesic curve Γ_k on the polyhedron $\mathcal{P}_k$ is associated with a unique curve $\hat{\Gamma}_k$ in the domain parameter.
- ◇ Each shortest (or geodesic) path Γ_k on a polyhedron $\mathcal{P}_k$ is computed from an initial path $\Gamma_{k,0}$ on $\mathcal{P}_k$.

Thus, the algorithm can be summarized as follows.

- ◇ Consider two points $\hat{x_0}$ and $\hat{x_1}$ in the parameter domain D. These two points are uniquely associated with two points X_0^k and X_1^k on each subdivided polyhedron $\mathcal{P}_k$, defining two points X_0 and X_1 on the limit surface $\mathcal{S}$.
- ◇ $\hat{\Gamma}_{0,0}$ is the linear segment $[\hat{x_0}, \hat{x_1}]$ from which we deduce an initial sequence of faces for the evaluation of the shortest path Γ_0 between the two points X_0^0 and X_1^0 on the initial polyhedron $\mathcal{P}_0$.

◇ $\hat{\Gamma}_{k+1,0}$ is the projection of $\hat{\Gamma}_k$ on the associated faces of the polyhedron $\mathcal{P}_{k+1}$ in the parameter domain D. The path $\hat{\Gamma}_{k+1,0}$ provides an initial sequence of faces for the evaluation of the shortest path Γ_{k+1} between the two points X_0^{k+1} and X_1^{k+1} on the polyhedron $\mathcal{P}_{k+1}$.

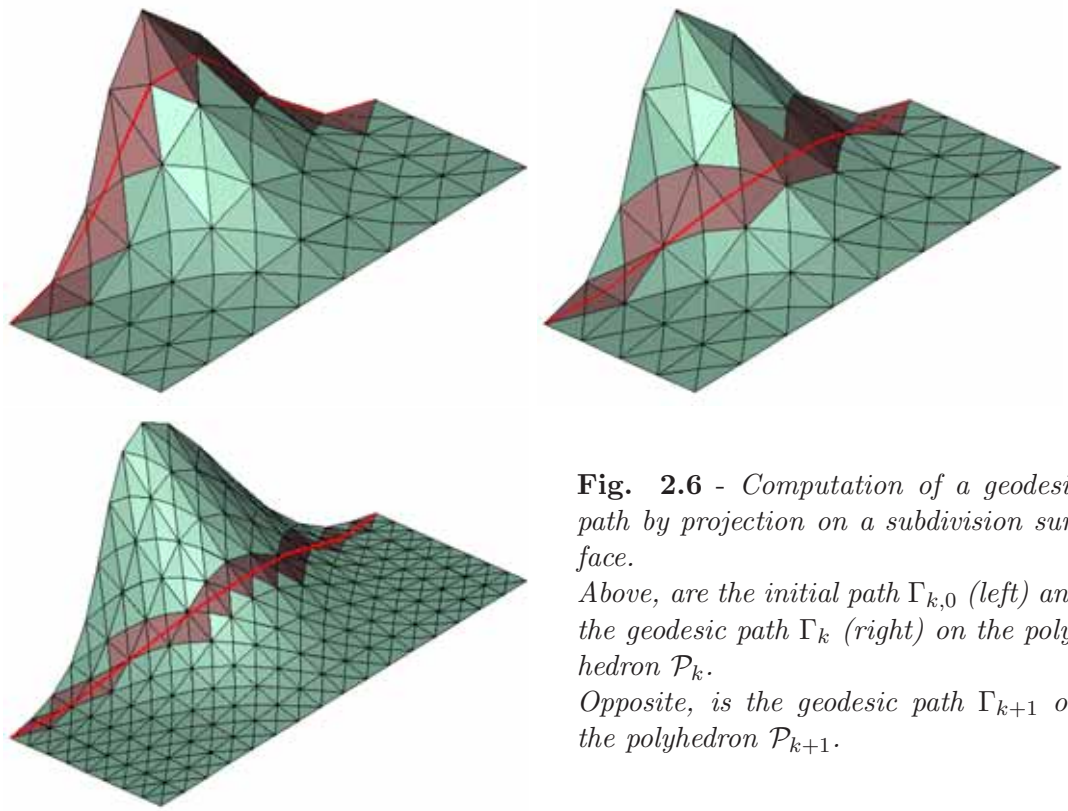

Fig. 2.6 - *Computation of a geodesic path by projection on a subdivision surface.*
Above, are the initial path $\Gamma_{k,0}$ (left) and the geodesic path Γ_k (right) on the polyhedron $\mathcal{P}_k$.
Opposite, is the geodesic path Γ_{k+1} on the polyhedron $\mathcal{P}_{k+1}$.

Notice that the projected path $\hat{\Gamma}_{k+1,0}$ is generally close from the associated geodesic path $\hat{\Gamma}_{k+1}$.
Fig. 2.7 exhibits an example with four computed geodesic curves on a Bézier surface.

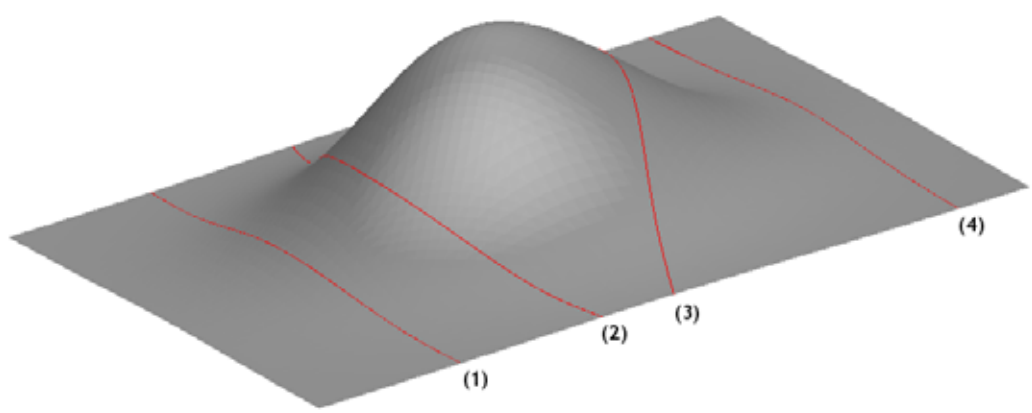

Fig. 2.7 - *Four geodesic curves on a subdivision surface.*

2.3 Myocardium and geodesic loops

In this section, we present an algorithm for determining geodesic loops on surfaces. This work has been initiated for a specific application to the geometric modeling of myocardium (Mourad et al. [15]). The aim of this project, involving research groups from Grenoble (TIMC, LMC, CHU, L3S) and directed by A. Raoult and D. Caillerie was to check a conjecture according to which myocardial fibres are geodesic curves running on some surfaces (Streeter [22]). This conjecture was first stated and experimentally checked by Streeter (1979) for the equatorial part of the left free wall. Quantitative polarized light microscopy provides measurements on fibre orientation that could lead to evidence that the conjecture remains true for the whole of the left ventricle (Jouk et al. [8, 9]).

• **Left ventricle**.

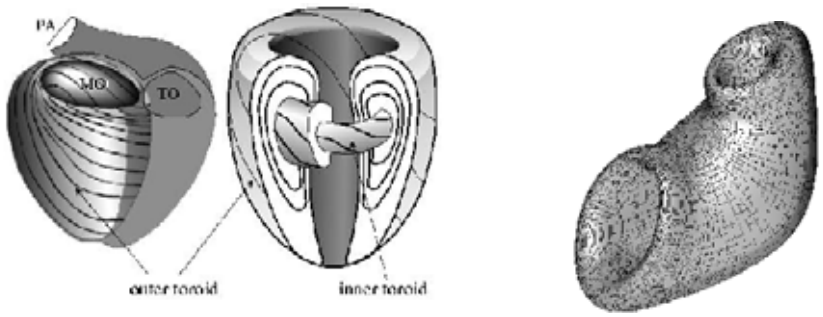

Fig. 2.8 - *Simplified geometric models for left and right ventricle.*

This conjecture has been studied in the PhD thesis of A. Mourad [16] for the left ventricle which can be modeled as a "stack" of included revolution surfaces. On such revolution surfaces, the computation of geodesic curves is performed by using the invariance of the *Clairaut constant* along geodesics [3]. This approach provided geodesic loops on this 3D simple model compatible with the experimental anatomic data [9, 15, 16].

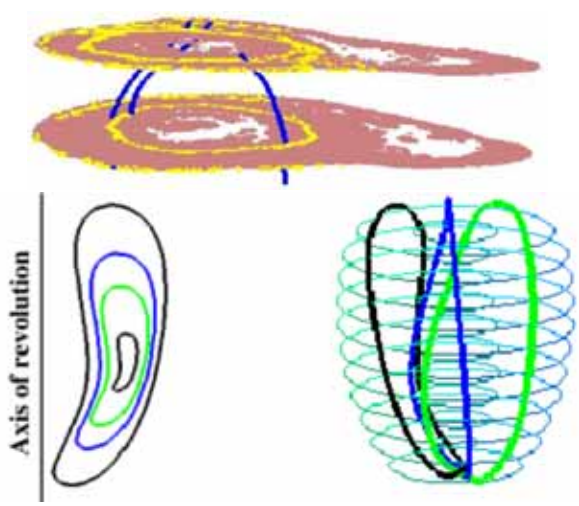

Fig. 2.9 - *Anatomic data and reconstruction of myocardial fibres paths in order to verify Streeter hypothesis on the left ventricle – Mourad et al. [15].*

• **Geodesic loops on toroidal surfaces**.

The right ventricle possesses a more intricate geometry and is modeled by a toroidal surface (see Fig. 2.8 – Right). There is no easy way for computing geodesics or geodesic loops on such a surface. Our contribution was essentially to develop an algorithm for computing geodesic loops on such toroidal surfaces (assumed to be modeled by a subdivision process).

For this purpose, we consider the previous algorithm, developed in Sections 2.2 and 2.1 and any initial closed curve on the surface by taking $X_0 = X_1$. We associate this initial loop with the periodic sequence of adjacent faces (see Fig. 2.10)

$$..., \mathcal{F}_1, \mathcal{F}_2, ..., \mathcal{F}_{n-1}, \mathcal{F}_n = \mathcal{F}_1, ...$$

where $X_0 = X_1 \in \mathcal{F}_1 = \mathcal{F}_n$.

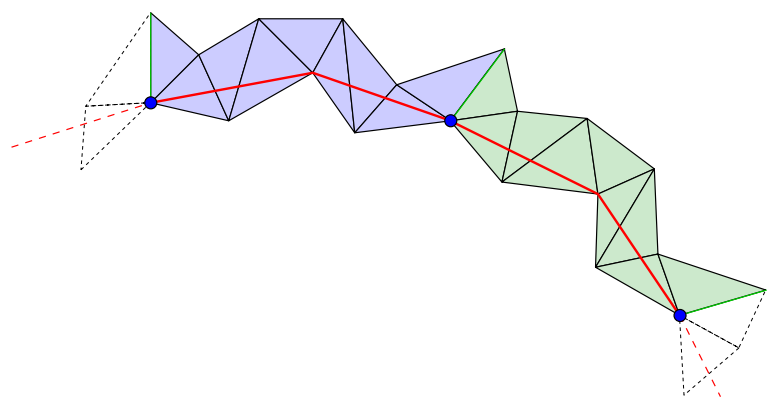

Fig. 2.10 - *Flattened periodic sequence for a geodesic loop.*

In fact, as point $X_0 = X_1$ will generally disappear in the shortening process, this point is chosen as a vertex of the subdivided surface. Formally we should not consider any more starting and ending points, even if such an extremity vertex is useful in practice.

◇ If the extremity vertex is a pivot–vertex of the shortest path in the flattened periodic sequence, the update is performed around all pivot–vertices.
◇ If not, any other pivot–vertex is chosen as the extremity vertex and the update is performed as above.
◇ If there are no more pivot–vertices in the shortest path, it is then possible to shorten the path inside the same flattened sequence, providing so a new vertex as extremity (Szafran et al. [23]).

• **Results**.

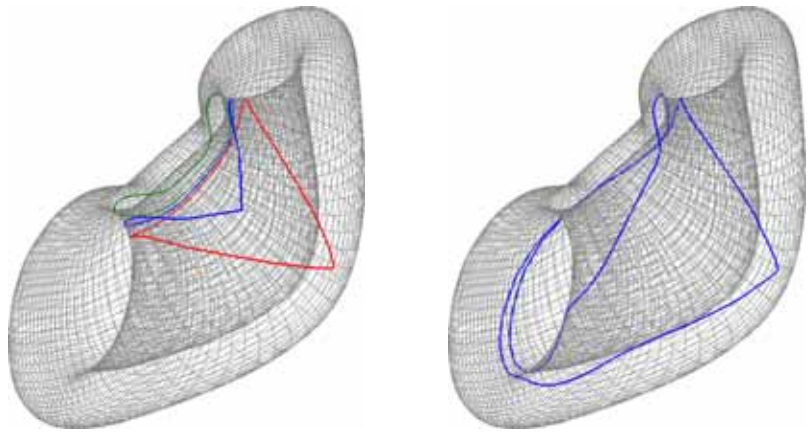

Fig. 2.11 - *Geodesic loops on a model of the right ventricle. Initial and geodesic loop are drawn on the same view.*

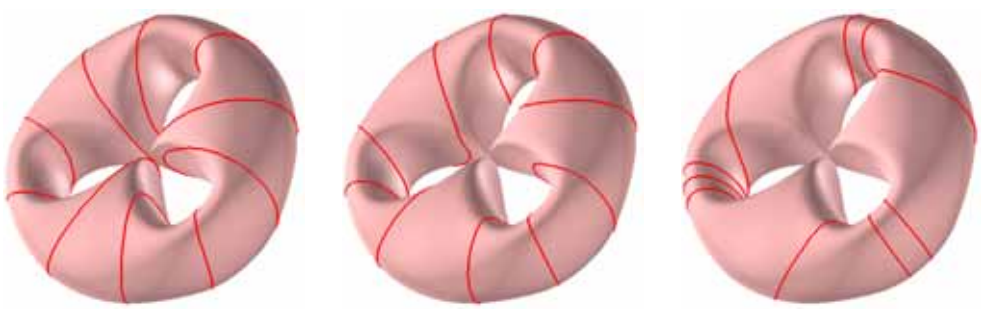

Fig. 2.12 - *Geodesic loop on a toroidal surface : initialization (Left) and final result (Right).*

• **Concluding remarks**.

For smooth subdivision surfaces the algorithm produces, as expected, a smooth geodesic loop. Indeed, the process is essentially to tighten an initial closed curve (a loop) running on the surface.

The following problem arises in the verification of the hypothesis of Streeter for the right ventricle. Given a point P and a direction T on a toroidal surface, does it exist a geodesic loop running on this surface through point P in the direction T ?
Nevertheless, we did not obtain a satisfactory result relating to this problem.

2.4 Conlusion and future works

The computation of a geodesic curve joining two points on any subdivision surface (i.e., without a parameterization) is quite similar. For this purpose, the *projection step* must be defined. That is, the projection of the geodesic Γ_k (evaluated on the polyhedron $\mathcal{P}_k$) on the subdivided polyhedron $\mathcal{P}_{k+1}$ (for the initialization step). Each face of the subdivided

polyhedron $\mathcal{P}_{k+1}$ is related to few faces of the polyhedron $\mathcal{P}_k$ by a local scheme, so that a local projection can be defined.

Then, following the idea of Ravi Kumar et al. [21], we are now considering, with N. Szafran, an other approach for computing geodesic curves on triangular surfaces by taking into account the normal at each vertex. Our purpose is to consider local properties of the surface for the approximation of the geodesics. Our first experiments, shows that exact geodesic curves can be evaluated on non regular triangular approximations of a smooth surface (See Fig. 2.13).

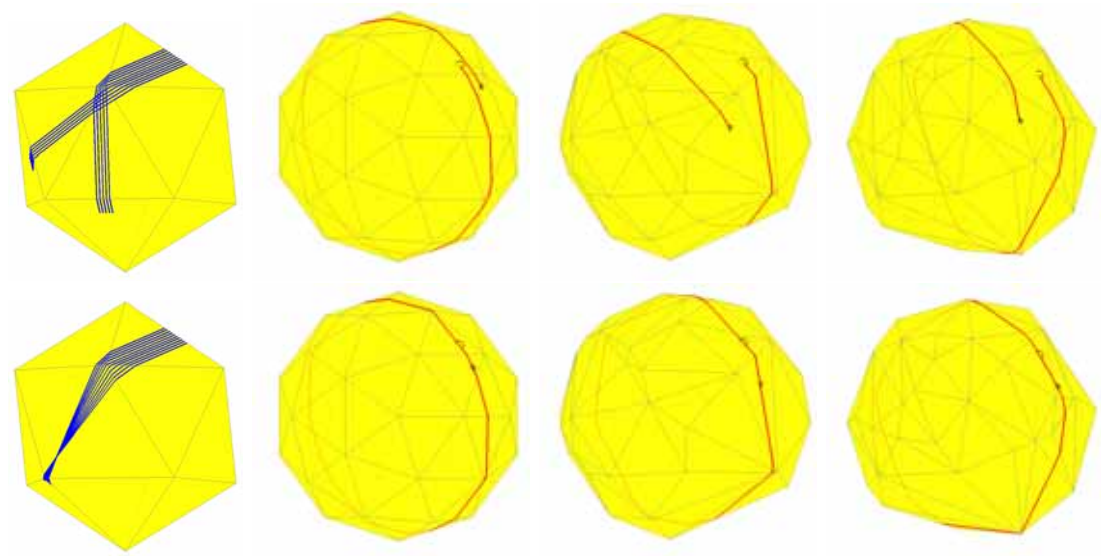

Fig. 2.13 - *Some examples computed by N. Szafran. Geodesic paths of the first row are evaluated with the classical flattening method whereas geodesic paths of the second row are computed by taking into account the normal at each vertex. In these examples, we consider geodesic paths starting from a point, in a given direction. It can be noticed, that even with a symmetric regular triangulation of the sphere such a geodesic is not closed by using the classical method.*

The results concerning geodesic loops have just been published in the proceeding of a national conference [23]. The question of the regularity of the evaluated geodesic loops on a smooth surface should be studied precisely... Furthermore, the existence of a geodesic loop running on a surface through a given point and in a assigned direction appears intricate. It involves both the local differential properties (for the geodesic definition) and the global behavior of the surface (for the existence of a regular loop).

Bibliography Chapter 2

[1] Chazelle B., A theorem on polygon cutting with applications, *Proc. 23rd IEEE Symposium on Foundations of Computer Science, Chicago, November 1982, pp. 339–349.*

[2] Colin de Verdière E., Lazarus F., Optimal System of Loops on an Orientable Surface, *Proceedings of the 43rd IEEE Symposium on Foundations of Computer Science (FOCS'02), november 2002, pp. 627–636.*

[3] Do Carmo M.P., *Differential geometry of curves and surfaces, Prentice-Hall, 1976.*

[4] Duflos C., P. Meheut, and J. C. Weill, Calcul de géodésiques par une méthode de projection, *R.R. Inria-Roquencourt, no 0907, 1988.*

[5] Euler L., On the shortest line on an arbitrary surface connecting any two points whatsoever, *Commentary of the Imperial Academy of St. Petersburg, 1728.*

[6] Farin G., Curves and Surfaces for CAGD, *Fifth Edition, Academic Press, 2002.*

[7] Hotz, I., Hagen, H., Visualizing geodesics, *In: Proceedings IEEE Visualization, Salt Lake City, UT, 2000 ,pp. 311-318.*

[8] Jouk P.S., Usson Y., Michalowicz G., and Parazza F., Mapping of the orientation of myocardial cells by means of polarized light and confocal scanning laser microscopy, *Microsc. Res. Tech., Vol. 30, pp. 480-490, 1995.*

[9] Jouk P.S., Usson Y., Michalowicz G., and Grossi L., Three-dimensional cartography of the pattern of the myofibres in the second trimester fetal human heart, *Anat. Embryol., Vol. 202, pp. 103-118, 2000.*

[10] Kimmel R., A. Amir, and A. M. Bruckstein, Finding shortest paths on surfaces, *in Curves and Surfaces in Geometric Design, P.-J. Laurent, A. LeMéhauté, and L. L. Schumaker (eds), A. K. Peters, Wellesley MA, 1994, 259–268.*

[11] Kimmel R. and J. A. Sethian, Computing geodesic paths on manifolds, *Proc. Natl. Acad. Sci. USA, Vol. 95, pp. 8431-8435, July 1998 Applied Mathematics.*

[12] Lee D.T. and Preparata F.P., Euclidean shortest paths in the presence of rectilinear barriers, *Networks, Vol. 14, No. 3, pp. 393–410, 1984.*

[13] Maekawa T., Computation of shortest paths on free-form parametric surfaces, *J. of Mechanical Design 118, 1996, 499–508.*

[14] Martinez Dimas, Luiz Velho, Paulo C. Carvalho, Computing geodesics on triangular meshes, *Computers & Graphics 29 (2005) 667-675.*

[15] Mourad A., L. Biard, D. Caillerie, P.-S. Jouk, A. Raoult, N. Szafran and Y. Usson, Geometrical modelling of the fibre organization in the human left ventricle, *In Katila, Magnin, Clarysse, et Montagnat, editors, Functional Imaging and Modeling of the Heart, vol. 2230 of Lecture Notes in Computer Sciences, pp 32–38, Helsinki, Nov. 2001. Springer.*

[16] Mourad Aiman, Description topologique de l'architecture fibreuse et modélisation mécanique du myocarde, *PhD thesis, Institut National Polytechnique, Grenoble, 2003.*

[17] Novotni Marcin, Reinhard Klein, Computing geodesic distances on triangular meshes, *In Proc. of WSCG2002 (2002), pp. 341-347. In The 10-th International Conference in Central Europe on Computer Graphics, Visualization and Computer Vision (WSCG).*

[18] Pham-Trong V., N. Szafran and L. Biard, Pseudo-geodesics on three-dimensional surfaces and pseudo-geodesic meshes, *Numerical Algorithms © Kluwer Academic Publishers, Volume 26, Issue 4, pp. 305-315, April 2001.*

[19] Pham-Trong Valérie, PhD Thesis,
Détermination géométrique de chemins géodésiques sur des surfaces de subdivision, *Applied Mathematics, University Joseph Fourier, Laboratory LMC-IMAG, 28 septembre 2001.*

[20] Polthier, K., M. Schmies, Straightest Geodesics On Polyhedral Surfaces, *In: Hege, H.C., Polthier, H.K. (Eds.), in Mathematical Visualization. Springer-Verlag, Berlin, 1998.*

[21] Ravi Kumar G.V.V., Prabha Srinivasan, V. Devaraja Holla, K.G. Shastry, B.G. Prakash, Geodesics curve computations on surfaces, *Computer Aided Geometric Design, Vol. 20, pp. 119–133, 2003.*

[22] Streeter D., Gross morphology and fiber geometry of the heart, *Handbook of Physiology. The cardiovascular system, Berne R.M., Sperelakis N., Geiger S.R. eds, Am. Phys. Soc., Williams & Wilkins, Baltimore, 1979.*

[23] Szafran N., V. Pham-Trong, L. Biard, Boucles et chemins géodésiques, *in proceeding of "Journées du GTMG03", 19-20 mars 2003, Aix-en-Provence.*

[24] Wang Charlie C.L., Kai Tang, Benjamin M.L. Yeung, Freeform surface flattening based on fitting a woven mesh model, *Computer-Aided Design, Vol. 37, pp. 799–814, 2005.*

[25] Zigelman G., R. Kimmel, N. Kiryati, Texture Mapping Using Surface Flattening via Multidimensional Scaling, *IEEE Transactions on Visualization and Computer Graphics archive Volume 8, Issue 2 (April 2002), pp 198–207*

Chapter 3

Surface reconstruction via geodesic interpolation and micro-sensors

We are concerned here with the reconstruction of physical surfaces from curves running on the surface. The Coons methods [4, 3, 16, 7] allow one to construct interpolating surfaces from some given curves on the surface by "filling" processes. See also [21, 25, 26] for construction processes of smooth surfaces from given boundary curve data. The shape of the surface is thus essentially modeled by these initial spatial curves. Considering a *physical surface*, we are first concerned with the question of acquiring such curves from the surface. Then, in order to develop a reliable construction process, these curves must represent intrinsic features of the surface. That can be achieved by employing a ribbon of embedded micro-sensors providing geodesic curves running on the surface (see below). The construction of surfaces that incorporate one or two given space curves as geodesics has been considered by several authors [1, 20, 24, 33, 34], in the context of applications such as distortion–free mapping of textures onto free–form surfaces; specifying fabric shapes for garment and shoe design; and in the layout of fibers in composite material structures. However, the problem of constructing rectangular or triangular surface patches, when all four prescribed boundary curves are required to be geodesics of the resulting surface, does not appear to have been previously studied.

The activity presented in this chapter was initiated by a collaboration with D. David from the team of *Micro-systèmes et Objets Communicants* of the laboratory CEA/LETI (CEA is a French government-funded technological research organization) in Grenoble. We are here concerned with the reverse engineering problem of re–constructing 2D and 3D shapes from tangential data. These tangential data are provided by embedded sensors (micro–accelerometers and micro–magnetometers) along a curve represented by a ribbon. This problem is not a *dual* interpolation or approximation problem (Hoschek [18]) as the tangential data are not localized in space. In her PhD thesis [29] (co-directed with B. Lacolle), Nathalie Sprynski developed methods for the reconstruction of planar and spatial curves, by using appropriate geometric tools. These results have been validated by a real-time demonstrator : the *Morphosense* ribbon–like device (see Fig. 3.1 & 3.4) equipped with 32 micro–sensors (Sprynski & CEA, [27]).

Different strategies [29] have then been developed for the problem of reconstructing a surface from spatial curves running on it, obtained with the *Morphosense* ribbon. Precisely, by placing the Morphosense on a physical surface at regular intervals along different directions, the surface is divided into a system of rectangular and triangular patches, which can then be filled by Coons processes [3, 4]. However, in practice some difficulties appear due to numerical imprecisions of the reconstructed spatial curves. The network of reconstructed 3D curves does not always cross as expected, so that corrections are necessary. In addition, since the distances between sensors are physically imposed on the ribbon, another major difficulty is to reconstruct the network of spatial curves fulfilling the length constraints. Methods for solving these constraints are proposed in the PhD thesis of N. Sprynski [29].

Then, remarking that the *Morphosense* ribbon assumes the shape of a geodesic when laid on a smooth physical surface (see [31] for a proof), we developed specific methods for the re–construction of surfaces interpolating boundary geodesic curves (Sprynski et al. [31] – Farouki et al. [13, 14, 15]). In particular, considering the motivation of constructing computer representations of free–form surfaces, we first considered the problem of constructing a C^2 surface patch $\mathbf{R}(u, v)$ interpolating two given spatial curves in such a way that these two boundary curves correspond to geodesics of the surface (Sprynski et al. [31]).

Then, given two pairs of regular space curves $\mathbf{r}_1(u)$, $\mathbf{r}_3(u)$ and $\mathbf{r}_2(v)$, $\mathbf{r}_4(v)$ that define a curvilinear rectangle, we considered the problem of constructing a C^2 surface patch $\mathbf{R}(u, v)$ for which these four boundary curves correspond to geodesics of the surface (Farouki et al. [13]). The possibility of constructing such a surface patch has been shown to depend on the given boundary curves satisfying two types of consistency constraints. The first constraint is global in nature, and is concerned with compatibility of the variation of the principal normals along the four curves with the normal to an oriented surface. The second constraint is a local differential condition, relating the curvatures and torsions of the curves meeting at each of the four patch corners to the angle between those curves. For curves satisfying these constraints, the surface patch is constructed using a bicubically–blended Coons interpolation process. We then considered the similar problem of constructing a C^2 triangular surface patch $\mathbf{R}(u_1, u_2, u_3)$, in terms of barycentric coordinates, bounded by three curves in such a way that they are geodesics of the constructed surface (Farouki et al. [15]).

Finally, the motivation to constructing surfaces represented as polynomial or rational Bézier surface patches, compatible with modern CAD systems, leads us to develop a rational geodesic–interpolating method for four boundary curves (Farouki et al. [14]), by modifying the bicubically–blended Coons interpolation process. However, a difficulty arises when considering the whole reconstruction method of a physical surface by using the ribbon, due to numerical imprecisions. The surface reconstruction methodology is as follows. First, a network of geodesics on the physical surface is constructed from the *Morphosense* measurements by the method described in (Sprynski [29]). Due to the numerical imprecisions, this step provides Bézier curves that do not exactly satisfy the geodesic crossing constraints, but it does allow us to determine the surface tangent plane at each corner, and the osculating planes and curvatures of the boundaries at each corner. Then, we determine a set of four Bézier boundary curves satisfying the conditions required for surface geodesics, as described in Section 5 of (Farouki et al. [14]). Finally,

the construction of a tensor–product Bézier patch interpolating these curves as boundary geodesics is performed [14].

Notice that all these re–construction methods generate a family of interpolating surfaces depending on free parameters. So we benefit from these free parameters to perform some smoothing of the surface. Our experiments shows that the thin–plate spline energy usually provides good results.

The remainder of this chapter is organized as follows. The Morphosense ribbon and the micro–sensors are presented in Section 3.1. The reconstruction process for planar and space curves, together with some insight about the strategy for surface reconstruction, are outlined in Section 3.2. We discuss the geodesic acquisition property of the ribbon in Section 3.3. In Section 3.4, the construction of a surface interpolating two curves as geodesics on the surface is discussed. In Section 3.5 are identified the constraints on the boundary curves, whose satisfaction constitutes a sufficient–and–necessary condition for the *existence* of analytic surfaces that interpolate those curves as geodesics. The construction of surface patches interpolating a curvilinear rectangle (or triangle) as geodesics (knowing *a priori* that these curves satisfy the above constraints) is presented in Section 3.6. The Section 3.7 is devoted to the problem of constructing polynomial or rational tensor–product Bézier patches interpolating four polynomial or rational given curves as geodesics. Finally, in Section 3.8 future works are outlined.

3.1 The Morphosense ribbon

The laboratory CEA/LETI has developed micro–sensors (micro–accelerometers or micro–magnetometers) able to give some information about their own orientation. The objective of CEA/LETI is to introduce new kinds of instrumented devices such as plastic or textile ribbons or surfaces, equipped with arrays of sensors. The alliance between instrumented materials and mathematical algorithms will allow materials to access some knowledge about their own shape, introducing what we could call proprioceptive materials (Sprynski [29]).

Micro–accelerometers are able to provide the angle between the sensor and the vertical, whereas micro–magnetometers are able to provide angular information with the earth magnetic field. The combination of these sensors in a biaxial or a triaxial way, allows to get the angular orientation of a solid body. The laboratory CEA/LETI developed two different implementations of such devices on ribbons.

The first one uses only 1D micro–accelerometers (2g MEMS accelerometers by Analog Device, Tronic's) which are mounted on a flexible PCB ribbon. The distance between the sensors is nearly 25 mm. In order to keep robustness and flexibility at a good level, the sensors are read using the I2C serial bus, which allows limiting the numbers of connections. The serial bus is connected to a micro–controller which in turn sends the data to the host computer. Using only 1D micro–accelerometers restricts the variability of recognized shapes inside a *vertical plane*.

A second generation ribbon has been developed which overcomes all limitations of the first system. The ribbon is now equipped with a set of 3D micro–accelerometers, alternating with a set of 2D micro–magnetometers (AMR type sensors from Honeywell or similar). Such arrangement of the sensors allows gaining complete tangential information

(not exactly at each sensor location, but for a set of two adjacent sensors). Fig. 3.1 shows sensors on the ribbon.

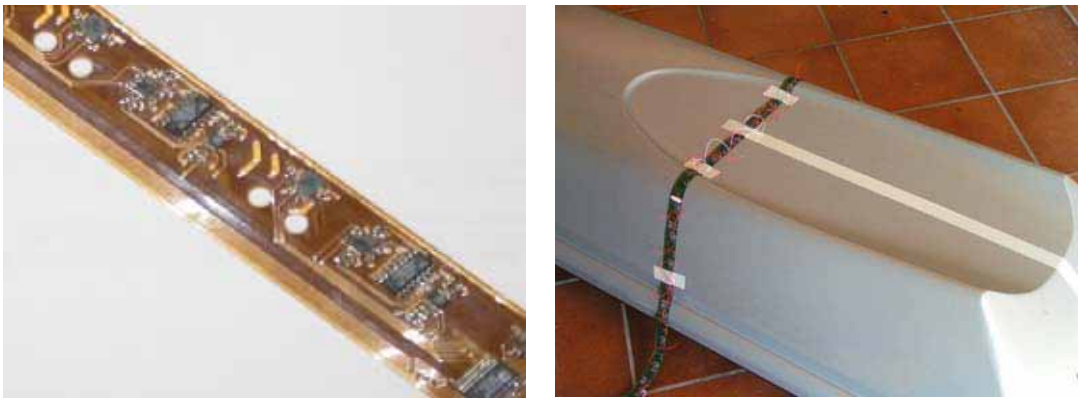

Fig. 3.1 - From [29] - *The Morphosense ribbon alone or laying on a physical surface.*

Size and cost reductions of microelectronics and micro–sensors make today possible the integration of such electronic functions in numerous manufacturing areas. Applications of such materials are countless in medical domain (e.g. determining shape and curvature of the spinal column), in aerodynamic domain (acquiring the shape and deformation of a wing)...

3.2 Curve reconstruction

We present a method for reconstructing curves relying on tangential data which are provided by embedded sensors (Sprynski et al. [28]). The reconstruction process is based on the knowledge of the distribution of the sensors along the curve, represented by a ribbon, and on the associated tangential orientation measurements without any information about their positioning in space, so that this problem is not an envelope problem (see Fig. 3.2). We present the methods for planar and spatial curves and discuss some physical interpretation. The results have been validated by the real-time demonstrator *Morphosense* (Sprynski & CEA, [27]) (see Fig. 3.4).

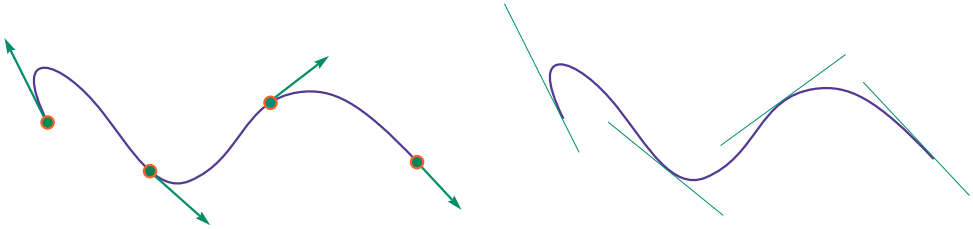

(1) Hermite interpolation (2) Dual interpolation

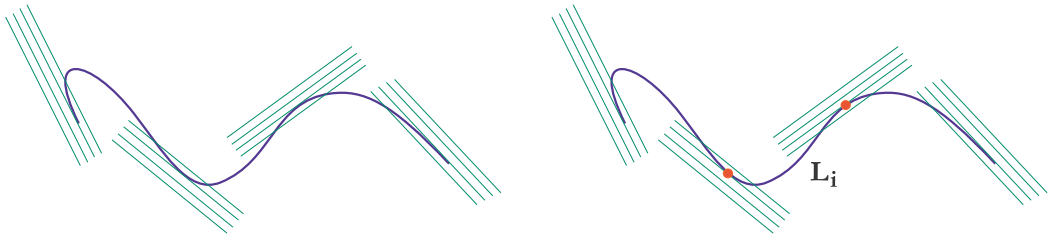

(3a) Tangent directions (3b) Prescribed lengths between contacts

(3) Sensors interpolation

Fig. 3.2 - *Reconstruction from sensors data.*

As shown in Fig. 3.2, the reconstruction from sensors data differs from the Hermite and dual interpolation. The dual interpolation (involved in the envelope theory) assumes that some tangent lines to a planar curve are given, the contact point being unknown. In our context, the embedded sensors only provide the tangent directions. Furthermore, the distances between two consecutive contact points must satisfy the prescribed distances between sensors on the ribbon.

• **Planar curves**.

Considering the planar curve described by arc-length parameterization $C(s) = (x(s),y(s))$, its derivative can be written as a function of the angle $\alpha(s)$, i.e., $C'(s) = (\cos(\alpha(s)), \sin(\alpha(s))$ where $\alpha(s)$ is the angle between the tangent line to the curve and the horizontal axis. As a consequence, the data from sensors are sampled values of the angle function $\alpha(s)$ for prescribed arc-length values. Then, we can simply deduce the resolution method from this model (Sprynski et al. [28]).

◇ First, we reconstruct the angle function $\alpha(s)$ by interpolation/approximation with respect to the arc-length parameter (see Fig. 3.3 – right).

◇ Then, the integration of the two coordinates provides a reconstructed curve (see Fig. 3.3 – left).

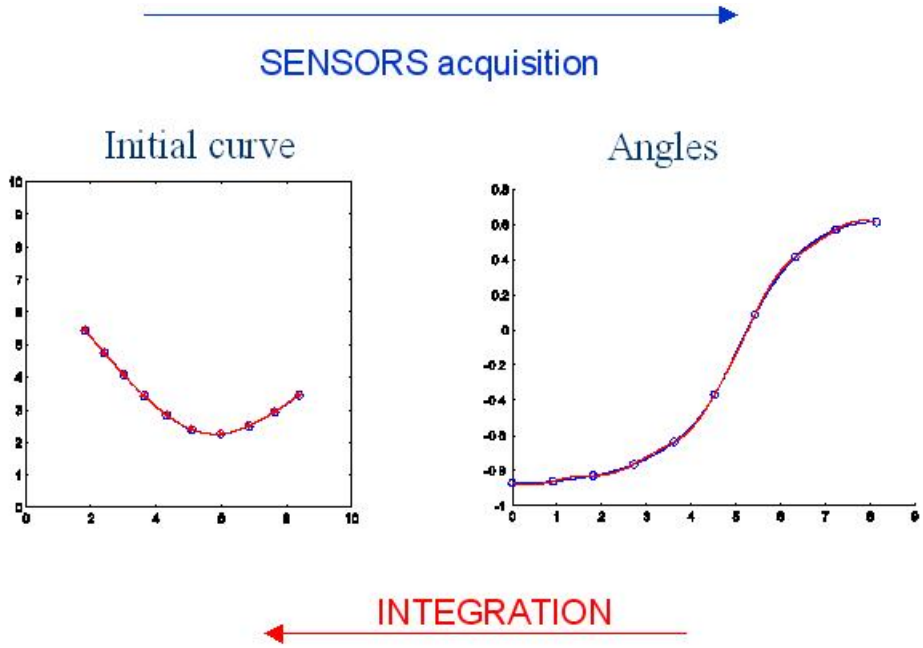

Fig. 3.3 - From [29] - *Planar curve reconstruction. The initial and reconstructed curves are both represented on the left figure.*

We thus obtain a curve satisfying the *length* and *tangency* constraints. Moreover, it is shown in (Sprynski [29]) that this scheme is *invariant under rotation* of the data and that the curve solution converges towards the initial curve when the number of sensors increases. As we consider arc-length parameterization, the choice of natural cubic spline for the reconstruction of the angle function $\alpha(s)$ leads to minimize the variations of the curvature, which is satisfactory, considering the physical behavior of the ribbon.

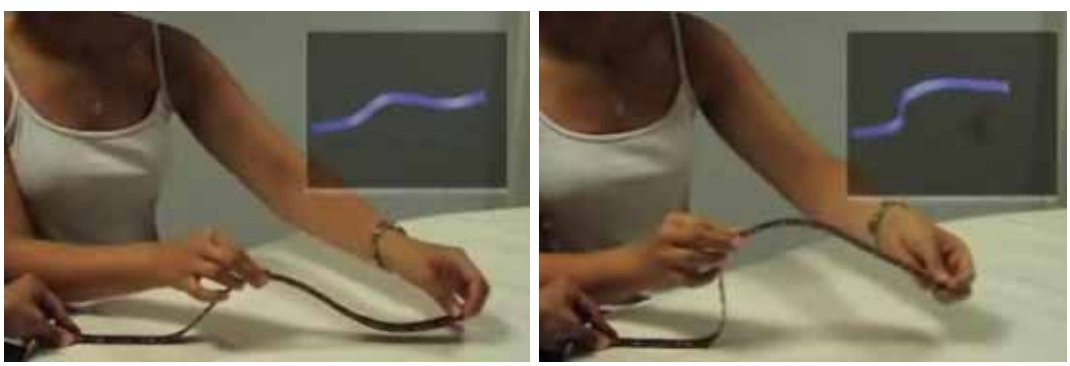

Fig. 3.4 - From [29] - *The real-time demonstrator "Morphosense".*

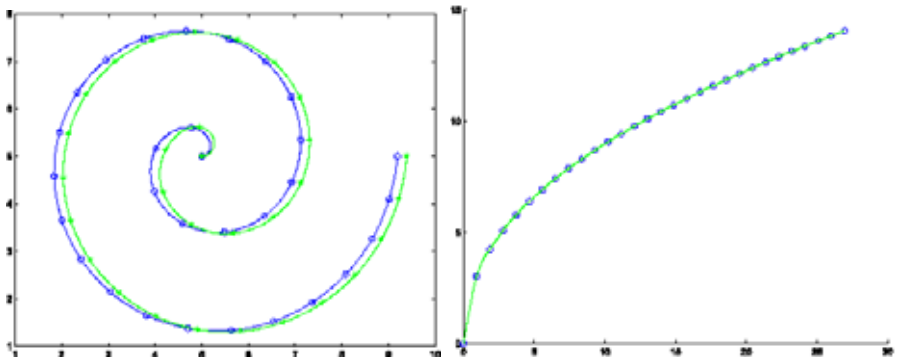

Fig. 3.5 - From [29] - *Planar curve reconstruction : another example.*
Left are shown the original (blue) and reconstructed (green) curves. Right are data values from sensors together with the reconstructed angle function.

• **Spatial curves**.

We now extend the previous method for the reconstruction of spatial curves. For a spatial curve $C(s) = (x(s), y(s), z(s))$ parameterized by arc-length, the derivative is a unit vector, and can thus be interpreted as a curve running on the unit sphere. In the same way, the data from sensors can be viewed as points on the unit sphere. The methodology is thus quite similar to the planar case (Sprynski et al. [28]).

◇ First, we interpolate the data by using cubic splines on the unit sphere (Nielson [19]) (see Fig. 3.6 – right).

◇ Then, we integrate the three coordinates to obtain the reconstructed curve (see Fig. 3.6 – left).

Cubic splines on the unit sphere are an extension of the classical B-splines in the euclidian space. Notice that linear interpolation has to be replaced by spherical interpolation. See (Nielson [19]) or (Sprynski [29]) for details.

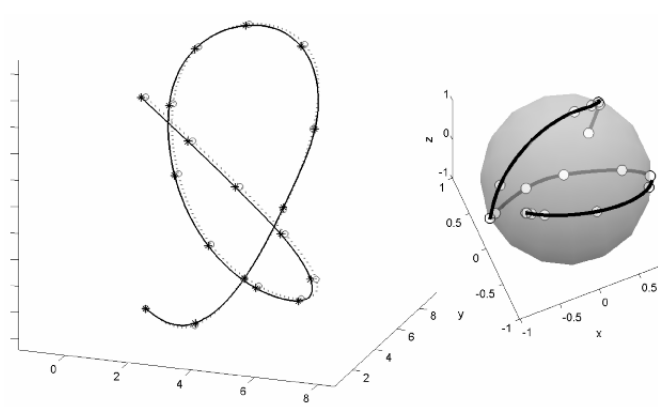

Fig. 3.6 - From [29] - *Spatial curve reconstruction.*
Left : the original curve (thin) and the reconstructed one (bold). Right : the derivative reconstructed on the sphere with data values from sensors.

It is shown in (Sprynski [29]) that this scheme is *invariant under rotation* of the data, and that the method minimizes a combination of the curvature, the torsion and the curvature variations of the curve.

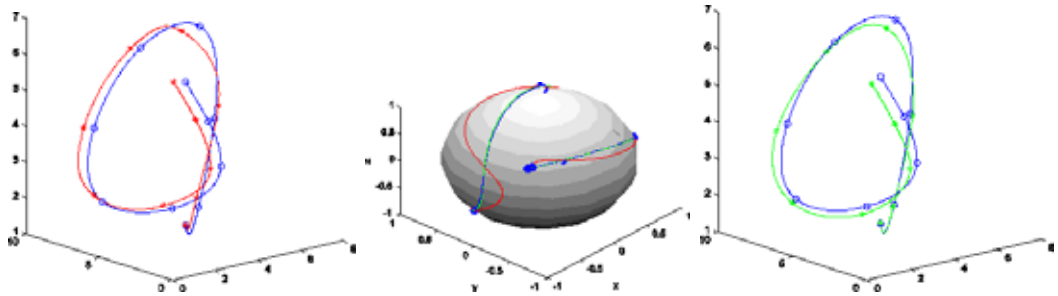

Fig. 3.7 - From [29] - *Spatial curve reconstruction : another example. The original curve is in blue, as well on the left as on the right. The red curve (left) is reconstructed by using spherical coordinates whereas the green curve (right) is reconstructed by using cubic splines on the sphere. Middle : the original and reconstructed derivatives on the sphere with data values from sensors.*

• **Surface reconstruction...**

By placing the Morphosense on a physical surface at regular intervals along different directions, the surface is divided into a system of rectangular (or triangular) patches, which can then be filled by Coons processes [3, 4]. In practice, difficulties appear due to numerical imprecisions of the reconstructed spatial curves. The network of reconstructed 3D curves does not always cross as expected, so that corrections are necessary. In addition, since the distances between sensors are physically imposed on the ribbon, another major difficulty is to reconstruct the network of spatial curves fulfilling the length constraints.

As mentioned in the introduction of this chapter, different strategies and methods for solving these constraints are proposed in the PhD thesis of N. Sprynski (2007) [29]. However, none of these methods take into account any specific geometric feature of these curves, as surprisingly, we did not bring to light at that time the *geodesic acquisition property* of the ribbon.

The remainder of this chapter focus on that point.

3.3 The Morphosense ribbon and geodesic curves

Remarking that the *Morphosense* ribbon assumes the shape of a geodesic when laid on a smooth physical surface, we developed specific methods (Sprynski et al. [31], Farouki et al. [13, 14, 15]) for the re–construction of surfaces interpolating boundary geodesic curves.

For this purpose, we first review in this section some elementary backgrounds concerning geodesic curves. Then, we discuss the geodesic acquisition property of the ribbon. The surface reconstruction via geodesic interpolation of two curves is deferred to Section 3.4.

• **Background on geometry**.

In the following, all curves and surfaces are considered to be *regular* and "sufficiently smooth" and all surfaces are considered to be *oriented*. The variable s is employed to denote arc length along a space curve. Note that the arc–length parameterization $\mathbf{r} : s \mapsto \mathbf{r}(s)$ of a curve satisfies $||\mathbf{r}'(s)|| = 1$ and $\mathbf{r}'(s) \perp \mathbf{r}''(s)$ for all s. However, a general parameterization $\mathbf{r} : t \mapsto \mathbf{r}(t)$ is often used in the surface construction problem. The parameters of functions may sometimes be omitted when no confusion can arise.

◇ With each point $\mathbf{r}(s)$ of a curve satisfying $\mathbf{r}''(s) \neq 0$, we associate the *Serret–Frenet frame* $(\mathbf{e}(s), \mathbf{n}(s), \mathbf{b}(s))$ where $\mathbf{e}(s) = \mathbf{r}'(s)$, $\mathbf{n}(s) = \mathbf{r}''(s)/||\mathbf{r}''(s)||$, and $\mathbf{b}(s) = \mathbf{e}(s) \times \mathbf{n}(s)$ are, respectively, the unit *tangent*, *principal normal*, and *binormal* vectors of the curve at the point $\mathbf{r}(s)$. The arc–length derivative of the Serret–Frenet frame is governed by the relations

$$\frac{\mathrm{d}}{\mathrm{d}s}\begin{bmatrix} \mathbf{e}(s) \\ \mathbf{n}(s) \\ \mathbf{b}(s) \end{bmatrix} = \begin{bmatrix} 0 & k(s) & 0 \\ -k(s) & 0 & \tau(s) \\ 0 & -\tau(s) & 0 \end{bmatrix} \begin{bmatrix} \mathbf{e}(s) \\ \mathbf{n}(s) \\ \mathbf{b}(s) \end{bmatrix}, \tag{3.1}$$

where the *curvature* $k(s)$ and *torsion* $\tau(s)$ of the curve $\mathbf{r}(s)$ are defined by

$$k(s) = ||\mathbf{r}''(s)|| \quad \text{and} \quad \tau(s) = \frac{\det(\mathbf{r}'(s), \mathbf{r}''(s), \mathbf{r}'''(s))}{||\mathbf{r}''(s)||^2}. \tag{3.2}$$

The osculating plane at each curve point $\mathbf{r}(s)$ is spanned by the two vectors $\mathbf{e}(s)$, $\mathbf{n}(s)$ and does not depend on the curve parameterization. If $k(s) = 0$ for some s, then $\mathbf{r}''(s) = 0$ and the normal vector $\mathbf{n}(s)$ and osculating plane are undefined at that point. This condition identifies an *inflection* of the curve.

◇ On a regular oriented surface $(u, v) \mapsto \mathbf{R}(u, v)$, the unit normal is defined at each point in terms of the partial derivatives $\mathbf{R}_u = \partial\mathbf{R}/\partial u$, $\mathbf{R}_v = \partial\mathbf{R}/\partial v$ by

$$\mathbf{N}(u, v) = \frac{\mathbf{R}_u(u, v) \times \mathbf{R}_v(u, v)}{||\,\mathbf{R}_u(u, v) \times \mathbf{R}_v(u, v)\,||}. \tag{3.3}$$

◇ Consider a curve $\mathbf{r}(s) = \mathbf{R}(u(s), v(s))$ on a surface $\mathbf{R}(u, v)$, where s denotes arc length for the space curve $\mathbf{r}(s)$, but not necessarily for the plane curve defined by $s \mapsto (u(s), v(s))$. With each point $\mathbf{r}(s)$, we associate the *Darboux frame* $(\mathbf{e}(s), \mathbf{h}(s), \mathbf{N}(s))$ — where $\mathbf{e}(s)$ is the unit tangent vector of the curve, $\mathbf{N}(s)$ is the unit normal vector of the surface at the point $\mathbf{R}(u(s), v(s)) = \mathbf{r}(s)$, and $\mathbf{h}(s) = \mathbf{N}(s) \times \mathbf{e}(s)$. The arc–length derivative of the Darboux frame is given by the relations

$$\frac{\mathrm{d}}{\mathrm{d}s}\begin{bmatrix} \mathbf{e}(s) \\ \mathbf{h}(s) \\ \mathbf{N}(s) \end{bmatrix} = \begin{bmatrix} 0 & k_g(s) & k_n(s) \\ -k_g(s) & 0 & -\tau_g(s) \\ -k_n(s) & \tau_g(s) & 0 \end{bmatrix} \begin{bmatrix} \mathbf{e}(s) \\ \mathbf{h}(s) \\ \mathbf{N}(s) \end{bmatrix}, \tag{3.4}$$

which define the *normal curvature* $k_n(s)$, the *geodesic curvature* $k_g(s)$, and the *geodesic torsion* $\tau_g(s)$ at each point of the curve $\mathbf{r}(s)$ as

$$k_n = \langle \frac{\mathrm{d}\mathbf{e}}{\mathrm{d}s}, \mathbf{N} \rangle, \qquad k_g = \langle \frac{\mathrm{d}\mathbf{e}}{\mathrm{d}s}, \mathbf{h} \rangle, \qquad \tau_g = \langle \frac{\mathrm{d}\mathbf{N}}{\mathrm{d}s}, \mathbf{h} \rangle. \tag{3.5}$$

◇ A regular curve $\mathbf{r}(t)$ on a surface $\mathbf{R}(u, v)$ is called a *geodesic* of the surface if its geodesic curvature is identically zero. From (3.1) and (3.4), this is equivalent to requiring that

$$\mathbf{N}(s) = \pm\,\mathbf{n}(s), \qquad \mathbf{h}(s) = \mp\,\mathbf{b}(s) \tag{3.6}$$

— i.e., the Frenet and Darboux frames agree modulo signs. Hence, we have the following useful characterizations of geodesic curves.

A regular curve $t \mapsto \mathbf{r}(t)$ is a geodesic on the surface $\mathbf{R}(u, v)$ if and only if

(D1) *the geodesic curvature of $\mathbf{r}(t)$ is identically zero*;

(D2) *the principal normal at each non–inflection point of $\mathbf{r}(t)$ is orthogonal to the surface tangent plane at the point $\mathbf{R}(u(t), v(t)) = \mathbf{r}(t)$*;

(D3) *the osculating plane at each non–inflection point of $\mathbf{r}(t)$ is orthogonal to the surface tangent plane at the point $\mathbf{R}(u(t), v(t)) = \mathbf{r}(t)$.*

• **Geodesic acquisition property of the ribbon**.

A developable surface D is isometric to a plane, so that any geodesic curve γ on D can be associated with a straight line on a plane. Then, considering any regular surface F, if we assume that the two surfaces D and F have a G^1 contact along a common curve γ and that this common curve γ is a geodesic curve on D, we can verify that γ is then a geodesic curve on the surface F (Sprynski et al. [31]). In practice, to ensure this G^1 contact we consider a ribbon D_ϵ on the surface D, of width 2ϵ, centered on the curve γ. Obviously, even with a thin ribbon, the contact is theoretical on hyperbolic points of the surface F.

Fig. 3.8 - *The "Morphosense" ribbon follows geodesic curves on a surface.*

Precisely, let $(\mathbf{e}(s), \mathbf{h}(s), \mathbf{N}(s))$ be the Darboux frame of the curve $\gamma(s)$ on the developable surface D_ϵ. When installing the ribbon on the surface F, this one is deformed in an isometric way which only authorize local rotations around the vectors $\mathbf{e}(s)$ and $\mathbf{h}(s)$ along the curve γ. The idea is that geodesics have to go straight, so that local rotations around the vector $\mathbf{N}(s)$ are forbidden. Such a curve γ on the ribbon D_ϵ (and on the surface F) is to be said to be $\mathbf{N}$-*rigid*. More generally, we can verify that *a regular curve γ running on a surface F is $\mathbf{N}$-rigid if and only if γ is a geodesic curve on F*. Finally, the following result leads to the wanted result (Sprynski et al. [31]).

Proposition 3. *Consider two regular oriented surfaces F_1 and F_2 with a G^1 contact along a common curve γ. Then, if γ is a geodesic curve on one surface, it is a geodesic curve on the other surface.*

From these results we are now able to verify that the Morphosense ribbon actually follows geodesic curves on the surface F. The ribbon is inextensible and not "flexible". It has the same behavior as a thin strip of paper, i.e., as a developable surface. Thus, Proposition 3 provides a direct proof of the wanted result. Furthermore, results concerning $\mathbf{N}$-rigid curves connect the mechanical properties of the ribbon to its geometric behavior.

3.4 Geodesic interpolation of two curves

From the ribbon we get tangential informations from which we reconstruct geodesic curves running on the surface. Thus, considering two regular 3D-curves $\mathbf{f}_0(t)$ and $\mathbf{f}_1(t)$, assumed to be geodesics on a physical surface, our purpose is to construct a numerical surface $\mathbf{F}$ which interpolates these two curves as geodesics on the surface. The algorithm involves Hermite interpolation and is quite classical [20, 24, 33, 34]. However, the method proposed

here assumes further numerical developments by providing free parameters for smoothing and for the whole piecewise reconstruction process.

• **The method**.

The algorithm can be outlined in the following way (Sprynski et al. [31]) – (see also Fig. 3.9).

◇ For each curve $\mathbf{f}_i$, the geodesic property determines (at each non-inflection point) the osculating plane and then the tangent plane of the desired surface $\mathbf{F}$.

◇ A unit starting vector $\mathbf{T}_0(u)$ in the tangent plane at point $\mathbf{F}(u,0) = \mathbf{f}_0(u)$ and a unit ending vector $\mathbf{T}_1(u)$ in the tangent plane at point $\mathbf{F}(u,1) = \mathbf{f}_1(u)$ are defined as follows.

$$\mathbf{T}_i(u) = \cos[\alpha_i(u)]\,\mathbf{b}_i(u) + \sin[\alpha_i(u)]\,\mathbf{e}_i(u), \qquad i = 0, 1.$$

◇ The surface $\mathbf{F}(u,v)$ is then defined by Hermite interpolation.

$$\mathbf{F}(u,v) = [H_0(v),\, H_1(v),\, H_2(v),\, H_3(v)] \begin{bmatrix} \mathbf{f}_0(u) \\ \lambda_0(u)\,\mathbf{T}_0(u) \\ \lambda_1(u)\,\mathbf{T}_1(u) \\ \mathbf{f}_1(u) \end{bmatrix}$$

with the classical Hermite functions H_i.

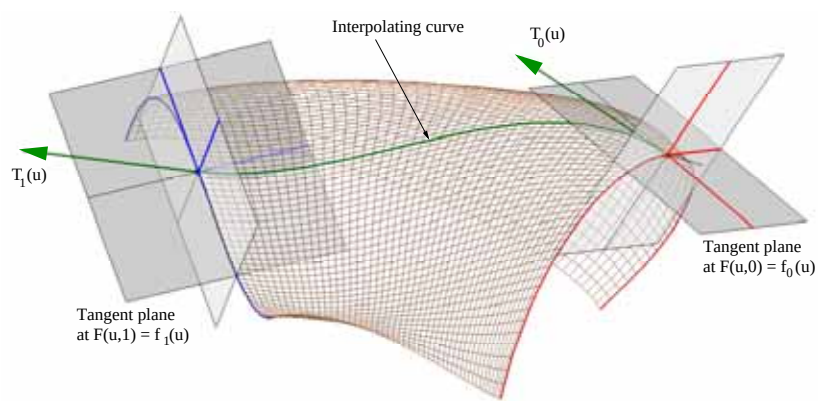

Fig. 3.9 - *Geodesic interpolation of two spatial curves* $\mathbf{f}_0(u)$ *and* $\mathbf{f}_1(u)$.

The angle functions $\alpha_i(u)$ and the magnitude functions $\lambda_i(u)$ are free functions of the parameter u. The following examples give some insight into the influence of these functions.

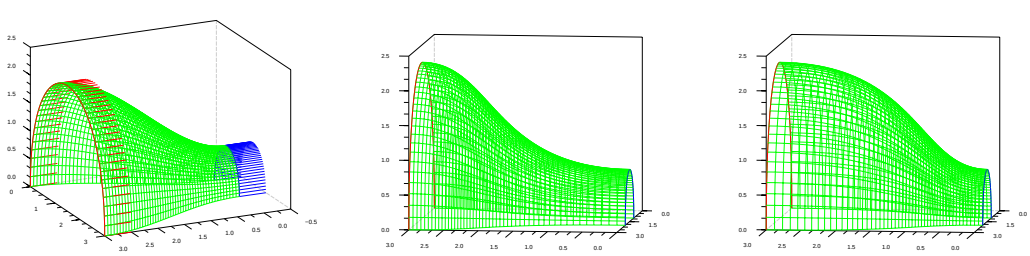

$(\lambda_0, \lambda_1) \equiv (1,1)$ $\qquad$ $(\lambda_0, \lambda_1) \equiv (1,2)$ $\qquad$ $(\lambda_0, \lambda_1) \equiv (2,1)$

Fig. 3.10 - *Influence of functions* $\lambda_i(u)$ *with* $\alpha_i(u) \equiv 0$ *in each case.*

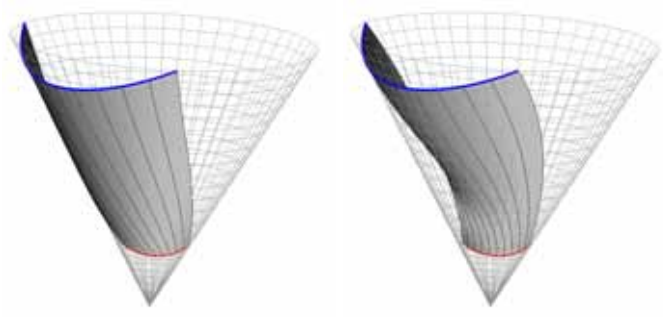

Fig. 3.11 - *Influence of the angle functions $\alpha_i(u)$ for the geodesic interpolation of two geodesics on a cone.*

• **Smoothing**.

Smoothing of the interpolating surface **F** can be performed by using the free parameter functions $\alpha_i(u)$ and $\lambda_i(u)$. Several criteria have been tested and of course the final interpolating surface depends strongly on the initial geodesic curves. Three local criteria and a global criterion are presented in (Sprynski et al. [31]).

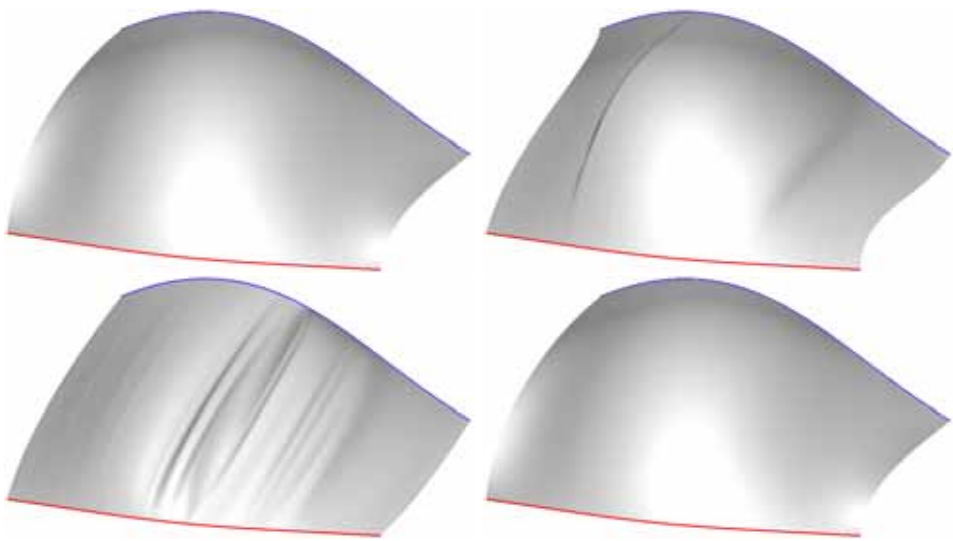

Fig. 3.12 - *Interpolating surfaces obtained according four different criteria, with the same initial data.*

Using the three local criteria, interpolating curves are optimized independently, which can generate oscillations, especially here in Fig. 3.12 with criterion 3. The last global criterion produces the best interpolating surface for these data.

Furthermore, notice that the initial geodesic curves considered in Fig. 3.12 have been evaluated on a Bézier surface by employing the algorithm developed in (Pham-Trong [23]) – (see also Chapter 2). Thus, only numerical data are available concerning these geodesic curves, and the surface reconstruction is carried out by means of a numerical evaluation of the first and the second derivatives, which requires the smoothing of the binormal vectors. See (Sprynski et al. [31] – Fig. 12 & Fig. 13) for a complete analysis.

• **Surface reconstruction with the ribbon**.

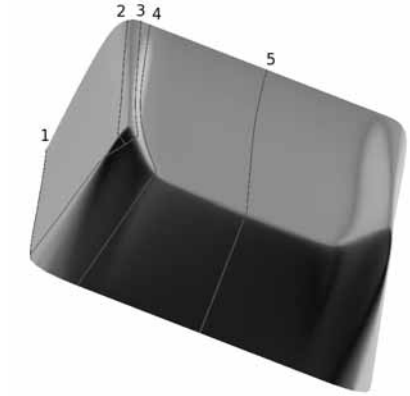

Fig. 3.13 - *Numerical model on which five geodesic curves, numbered from 1 to 5, have been computed.*

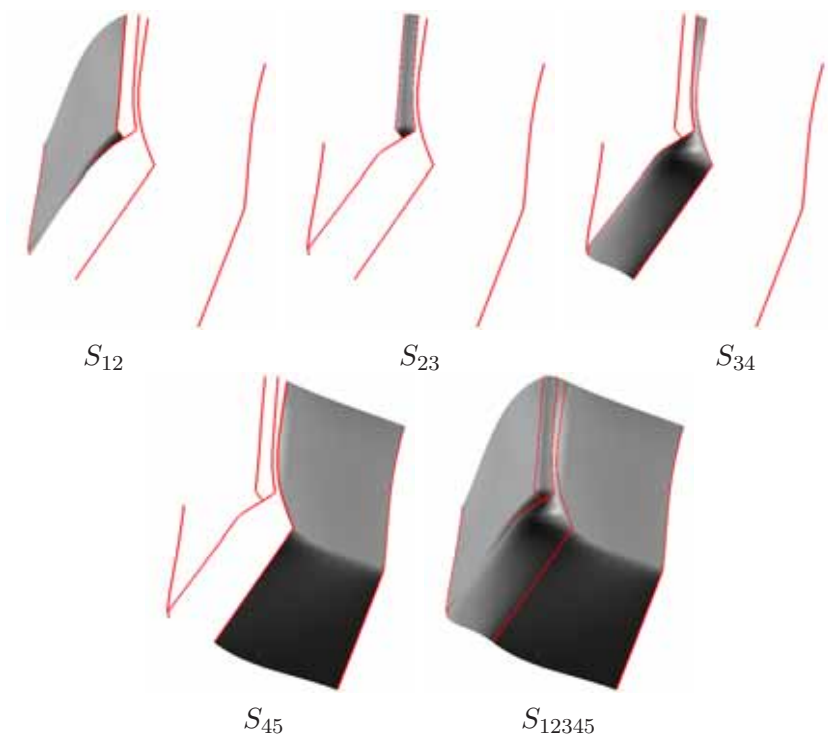

Fig. 3.14 - *Reconstruction via geodesic interpolation. Each surface S_{ij} is the interpolating surface between geodesics i and j and S_{12345} is the whole reconstructed surface.*

Fig. 3.15 - *Reconstruction of a part of a physical surface from ribbon's data representing transversal geodesic curves.*

3.5 Existence conditions for patches interpolating geodesic boundary curves

As a generalization of Section 3.4, we now consider the problem of constructing C^2 triangular and rectangular surface patches for which the boundary curves correspond to geodesics of the surface (Farouki et al. [13, 15]).

The possibility of constructing such surface patches is shown to depend on the given boundary curves satisfying two types of consistency constraints. The first constraint is global in nature, and is concerned with compatibility of the variation of the principal normals along the curves with the normal to an oriented surface. The second constraint is a local differential condition, relating the curvatures and torsions of the curves meeting at each of the patch corners to the angle between those curves.

In this section, we are concerned with identifying constraints on the boundary curves, whose satisfaction constitutes a sufficient–and–necessary condition for the *existence* of analytic surfaces that interpolate those curves as geodesics. Then, for curves satisfying these constraints, constructive methods are developed in Section 3.6.

• **The geodesic crossing property**.

We consider notations of Section 3.3 and refer to (Farouki et al. [13]) for details. For subsequent use, we consider Proposition 4, which identifies a necessary condition for two intersecting space curves to be geodesics on a regular surface (see [13]).

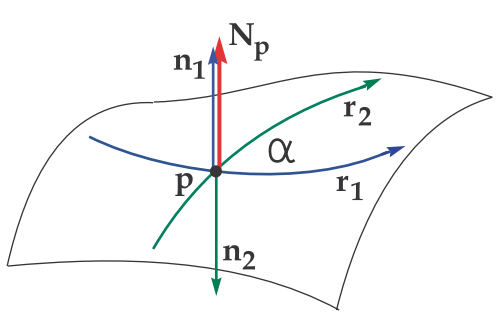

Fig. 3.16 - *Crossing geodesic curves.*

Proposition 4. *Consider two geodesics* $\mathbf{r}_1(s)$ *and* $\mathbf{r}_2(s)$ *parameterized by arc length on the surface* $\mathbf{R}(u,v)$*, with principal normal* $\mathbf{n}_1(s)$ *and* $\mathbf{n}_2(s)$*, crossing at the point* $\mathbf{p} = \mathbf{r}_1(s_1) = \mathbf{r}_2(s_2)$*. Assuming that* $\mathbf{p}$ *is not an inflection on either of the curves* $\mathbf{r}_1(s)$ *and* $\mathbf{r}_2(s)$*, let* $\alpha = (\mathbf{r}_1'(s_1), \mathbf{r}_2'(s_2))_{\mathbf{N_p}}$ *be the oriented angle between them at* $\mathbf{p}$*, in the sense of the surface normal* $\mathbf{N_p}$ *at that point. Also, let* $k_i(s)$ *and* $\tau_i(s)$ *be the curvature and torsion of* $\mathbf{r}_i(s)$ *for* $i = 1, 2$*. Then, for the values* $\sigma_1, \sigma_2 \in \{-1, +1\}$ *such that* $\mathbf{N_p} = \sigma_1\, \mathbf{n}_1(s_1) = \sigma_2\, \mathbf{n}_2(s_2)$*, we have*

$$[\,\tau_1(s_1) + \tau_2(s_2)\,]\,\sin\alpha \;=\; [\,\sigma_2\, k_2(s_2) - \sigma_1\, k_1(s_1)\,]\,\cos\alpha\,. \tag{3.7}$$

As a simple example, one can easily check that this relation is satisfied by great–circle geodesics crossing on a sphere.

Corollary 1. *If two space curves intersecting at a point* $\mathbf{p}$ *do not satisfy the relation* (3.7)*, no regular* C^2 *oriented surface can interpolate these curves in such a manner that they are geodesics of the surface.*

• **Consistency constraints on boundary curves**.

We are now concerned with identifying constraints on the boundary curves, whose satisfaction constitutes a sufficient–and–necessary condition for the *existence* of analytic surfaces that interpolate those curves as geodesics. As these consistency constraints are quite similar for a curvilinear rectangle and a curvilinear triangle, we shall establish these existence–conditions only for a curvilinear rectangle.

Consider, as illustrated in Fig. 3.17, four regular space curves $\mathbf{r}_1(u)$, $\mathbf{r}_3(u)$ and $\mathbf{r}_2(v)$, $\mathbf{r}_4(v)$ meeting at corners $\mathbf{p}_{ij}$ with a non–zero angle of intersection. At each corner $\mathbf{p}_{ij}$, the tangent plane $\Pi_{\mathbf{p}_{ij}}$ of the interpolating surface $\mathbf{R}(u,v)$ is thus well defined.

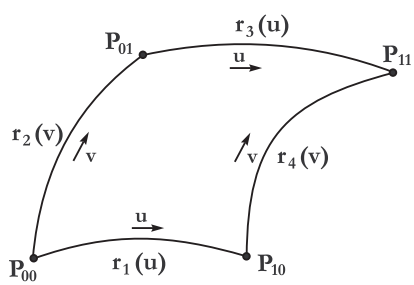

Fig. 3.17 - *Surface patch boundary curves.*

◇ Condition **(C1)**: *Osculating constraints at corners.* –

From the geodesic definitions in Section 3.3 we see that, at each corner $\mathbf{p}_{ij}$, the principal normals of the boundary curves that meet there must agree modulo sign. These conditions imply that, at each corner $\mathbf{p}_{ij}$, the boundary curves meeting there have osculating planes orthogonal to the surface tangent plane Π_{ij}.

◇ Condition **(C2)**: *Global normal orientation constraint.* –

Let $\mathbf{r}(t)$ for $t \in [\,0,4\,]$ denote the "concatenation" of the four boundary curves $\mathbf{r}_2(t)$, $\mathbf{r}_3(t)$, $\mathbf{r}_4(t)$, $\mathbf{r}_1(t)$, defined as follows:

$$\begin{array}{rclll} \mathbf{r}(t) & = & \mathbf{r}_2(t), & t \in [\,0,1\,], & \mathbf{r}(t) = \mathbf{r}_3(t-1), \quad t \in [\,1,2\,], \\ \mathbf{r}(t) & = & \mathbf{r}_4(3-t), & t \in [\,2,3\,], & \mathbf{r}(t) = \mathbf{r}_1(4-t), \quad t \in [\,3,4\,]. \end{array} \tag{3.8}$$

The principal normal $\mathbf{n}(t)$ of the concatenated curve $\mathbf{r}(t)$ is simply the concatenation of the principal normals $\mathbf{n}_i(t)$ of the four boundary curves $\mathbf{r}_i(t)$, according to the parameterization (3.8) used for the definition of $\mathbf{r}(t)$. *The existence of a regular oriented surface* $\mathbf{R}(u,v)$ *that interpolates the concatenated boundary* $\mathbf{r}(t)$*, with the four individual curves* $\mathbf{r}_i(t)$ *as geodesics, is contingent on the existence of a continuous unit vector function* $\mathbf{N}(t)$ *such that* $\mathbf{N}(t) = \pm\,\mathbf{n}(t)$ *for all* $t \in \mathbb{R}$*. Specifically, a regular oriented interpolating surface (with unit normal vector* $\mathbf{N}(t)$*) can exist only if the unit vector function* $\mathbf{n}(t)$ *exhibits an even number of reversals on the interval* $t \in [\,0,4\,)$*.*

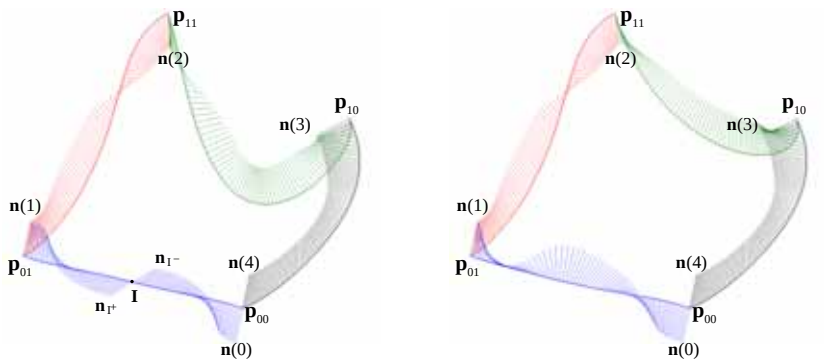

Fig. 3.18 - *Left: patch boundaries that satisfy the global normal orientation constraint. Right: a curvilinear rectangle that is inconsistent with the global normal orientation constraint since there is only one reversal at corner* $\mathbf{p}_{00}$*.*

◇ Condition **(C3)**: *Geodesic crossing constraints at corners.* –

By Corollary (1), the boundary curves $\mathbf{r}_i(t)$ must satisfy the geodesic crossing constraint (3.7) at each corner $\mathbf{p}_{ij}$.

• **Existence of an interpolating surface**.

Proposition 5. (Farouki et al. [13, 15]). – *Given a curvilinear rectangle or triangle, satisfying the consistency constraints* **(C1-C3)***, there exists a regular oriented surface* $\mathbf{R}$ *interpolating these curves in such a way that these curves are geodesics of the surface. Conversely, if any of the conditions* **(C1-C3)** *is not satisfied, such an interpolating surface can not be constructed.*

For curvilinear rectangles or triangles satisfying these consistency constraints, constructive methods are developed in Section 3.6.

3.6 Geodesic interpolation of curvilinear rectangles and triangles

We now consider the construction of surface patches with given geodesic boundary curves, knowing *a priori* that these curves satisfy the above constraints described in Section 3.5.

This stipulation can be met by, for example, selecting the boundary curves as known geodesics on simple analytic surfaces. For general free–form boundary curves, their construction so as to satisfy the system of constraints — or the modification of initial boundary curves so as to satisfy them — is a substantive problem in its own right, which shall be addressed separately in the next section 3.7.

For such curves satisfying the consistency constraints, a constructive method is proposed using a modified bicubically–blended Coons interpolation process in case of curvilinear rectangle, or using a modified cubically–blended triangular Coons interpolation scheme together with barycentric coordinates in case of a curvilinear triangular.

• **Geodesic interpolation of a curvilinear rectangle**.

Given four parametric space curves $\mathbf{r}_1(u)$, $\mathbf{r}_3(u)$ and $\mathbf{r}_2(v)$, $\mathbf{r}_4(v)$ specifying a curvilinear rectangle, the Coons interpolation procedure [3, 4, 7, 16] defines a surface patch $\mathbf{R}(u,v)$ bounded by these four curves. In addition to the four boundary curves, the bicubically–blended Coons patch requires transverse derivative data along them — i.e., the four vector functions $\mathbf{R}_v(u,0)$, $\mathbf{R}_v(u,1)$ and $\mathbf{R}_u(0,v)$, $\mathbf{R}_u(1,v)$ must also be specified.

The desired interpolating surface is defined as a combination of three surfaces (see Fig. 3.19).

$$\mathbf{R}(u,v) \;=\; \mathbf{R}_{13}(u,v) \;+\; \mathbf{R}_{24}(u,v) \;-\; \mathbf{R}_0(u,v)\,.$$

The Coons patch is modified in (Farouki et al. [13]) to admit these curves as *geodesics* on the constructed surface. Precisely, fields of transverse derivatives are first specified in a similar way as in Section 3.4.

◇ For each curve $\mathbf{r}_i$, the geodesic property determines (at each non-inflection point) the osculating plane and then the tangent plane of the desired surface $\mathbf{R}$.

◇ For each curve $\mathbf{r}_i$, a field $\mathbf{T}_i$ of unit vectors in the tangent plane is defined as in Section 3.4.

However, the method involves some supplementary constraints for the consistency of the bicubically–blended Coons process.

◇ – *Interpolating property of vector fields at corners.* The four vector fields must interpolate the derivatives of the given curves at corners.

◇ – *Geodesic crossing property and twist vectors.* The definition of twist vectors must be consistent with the specification of vector fields.

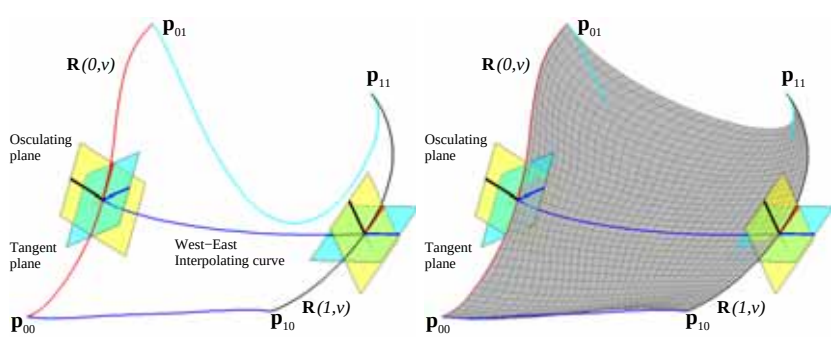

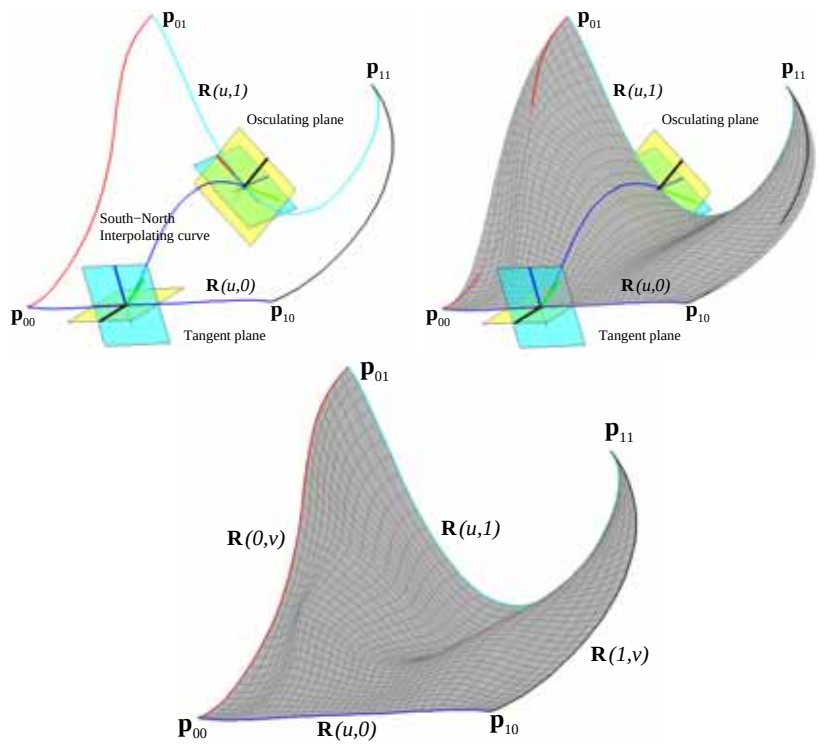

Fig. 3.19 - *Coons interpolation of four geodesic boundary curves.*

As the method is rather technical, we refer to (Farouki et al. [13]) for details. Precisely, consider corner $\mathbf{p}_{00}$. In order to satisfy all the constraints and be able to define the twist vector at that corner, we must find parameters α_{11}, d_{11}, α_{21}, d_{21} such that the three following relations are satisfied:

$$\begin{cases} -d_{1L}\,\alpha_{11}\dfrac{1}{\sin A_{00}} \;=\; d_{21} - d_{2L}\,\alpha_{21}\dfrac{\cos A_{00}}{\sin A_{00}}\,, \\ d_{11} + d_{1L}\,\alpha_{11}\dfrac{\cos A_{00}}{\sin A_{00}} \;=\; d_{2L}\,\alpha_{21}\dfrac{1}{\sin A_{00}}\,, \\ (\cos A_{00})\,\sigma_{1L}\;\; k_1(0) + (\sin A_{00})\,\tau_1(0) \\ \qquad\qquad = \;(\cos A_{00})\,\sigma_{2L}\;\; k_2(0) - (\sin A_{00})\,\tau_2(0)\,, \end{cases}$$

where d_{1L}, d_{2L} are coefficients previously evaluated and where A_{00} is the crossing angle of curves meeting at corner $\mathbf{p}_{00}$.

The third equation is the *geodesic crossing property* (3.7), and is satisfied through the assumption that the boundary curves obey the *consistency constraints*. The two first equations form a linear system. This linear system admits solutions and provides two free parameters at each corner which are then used for the smoothing of the interpolating surfaces.

Smoothing.

Some criteria have been proposed to find optimal parameters d_{ij} and α_{ij} in order to get smooth interpolating surfaces.

Criterion 1: *minimization of the parametric speed variation along isoparametric curves.*

$$\min_{d_{ij}} \left[\int_0^1 \int_0^1 \left(\frac{\mathrm{d}}{\mathrm{d}v} ||\mathbf{R}_v(\bar{u}, v)|| \right)^2 \mathrm{d}v \, \mathrm{d}\bar{u} \; + \int_0^1 \int_0^1 \left(\frac{\mathrm{d}}{\mathrm{d}u} ||\mathbf{R}_u(u, \bar{v})|| \right)^2 \mathrm{d}u \, \mathrm{d}\bar{v} \right] .$$

Criterion 2: *minimization of the Dirichlet energy.*

$$\min_{d_{ij}} \left[\int_0^1 \int_0^1 \left(||\mathbf{R}_u(u, v)||^2 + ||\mathbf{R}_v(u, v)||^2 \right) \mathrm{d}u \, \mathrm{d}v \right] .$$

Criterion 3: *minimization of the thin plate spline energy.*

$$\min_{d_{ij}} \left[\int_0^1 \int_0^1 \left(||\mathbf{R}_{uu}(u, v)||^2 + 2\, ||\mathbf{R}_{uv}(u, v)||^2 + ||\mathbf{R}_{vv}(u, v)||^2 \right) \mathrm{d}u \, \mathrm{d}v \right] .$$

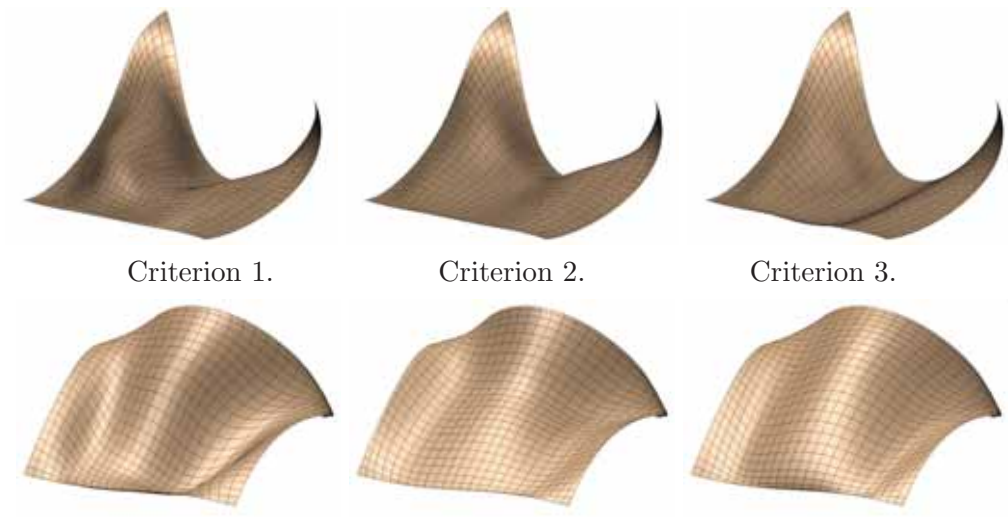

Fig. 3.20 - *Coons patches interpolating the curvilinear rectangle shown in Fig. 3.18 - left, smoothed according to the criteria 1, 2, and 3 (two different views of each smoothed surface are presented).*

• **Geodesic interpolation of a curvilinear triangle**.

The previous methods have been extended to the case of geodesic–bounded triangular surface patches, parameterized in terms of barycentric coordinates, in the submitted paper (Farouki et al. [15]). Precisely, given three regular space curves $\mathbf{r}_1(t)$, $\mathbf{r}_2(t)$, $\mathbf{r}_3(t)$, that define a curvilinear triangle, we consider the problem of constructing a C^2 triangular surface patch $\mathbf{R}(u_1, u_2, u_3)$ bounded by these three curves, such that they are geodesics of the constructed surface.

Consistency constraints on the given curves for the existence of such geodesic–bounded triangular surface patches are identified as above. For curves satisfying these conditions, the patch is constructed by means of a cubically–blended triangular Coons interpolation scheme (Gregory et al. [17]). The properties of the constructed surface patches are then discussed, in the context of the Gauss–Bonnet theorem. A formulation of thin–plate spline

energy in terms of barycentric coordinates with respect to a general domain triangle is also derived, and used to optimize the smoothness of the geodesic–bounded triangular surface patches.

As the process is technical due to barycentric coordinates, we refer to the submitted paper [15] for details. We just present here some numerical results.

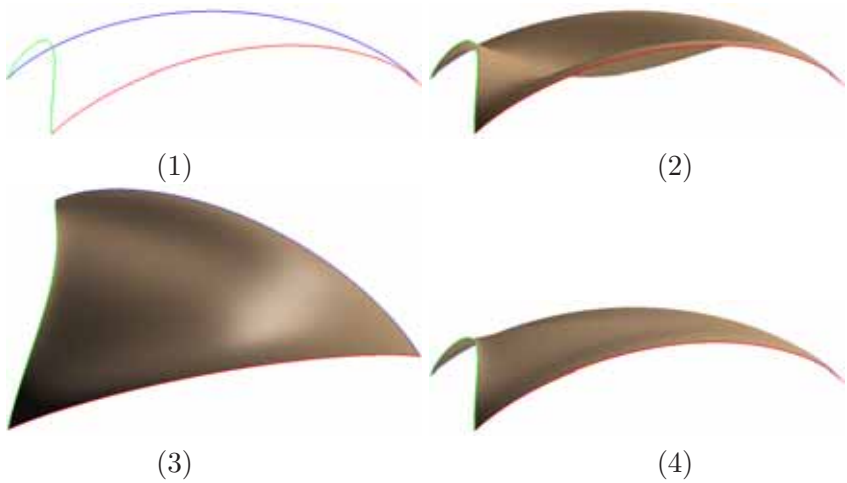

Fig. 3.21 - *(1) the three boundary curves satisfying consistency conditions, and for which the corner angles sum to 2π; (2) the initial reconstructed surface with free parameters equal to zero; (3) and (4) two different views of the reconstructed surface after smoothing according the thin–plate spline energy criterion.*

As a conclusion, consider the following remark. The well–known *Gauss–Bonnet theorem* [5, 32] relates the integral of Gaussian curvature over a region of a surface to the integral of the geodesic curvature along the boundary of that region. This theorem is of particular relevance to the geodesic–bounded surface patches constructed herein. Precisely, if we construct a triangular surface patch so that its boundary curves are geodesics, the Gaussian curvature K of this surface must satisfy

$$\iint_{\mathbf{R}} K \, \mathrm{d}\sigma \, = \, 2\pi \, - \, \sum_{i=1}^{3} A_i \, , \tag{3.9}$$

where A_1, A_2, A_3 are the corner angles at the vertices. Thus, given three regular space curves satisfying consistency conditions (**C1**)–(**C3**), such that $\sum_{i=1}^{3} A_i = 2\pi$, any interpolating surface must satisfy

$$\iint_{\mathbf{R}} K \, \mathrm{d}\sigma \, = \, 0 \, , \tag{3.10}$$

which indicates that the interpolating surface must contain both elliptic and hyperbolic points (where $K > 0$ and $K < 0$) — see Fig. 3.21.

3.7 Geodesic Bézier interpolation

Given four polynomial or rational Bézier curves defining a curvilinear rectangle, we consider the problem of constructing polynomial or rational tensor–product Bézier patches

bounded by these curves, such that they are geodesics of the constructed surface. The existence conditions and interpolation scheme, developed in a general context previously, are adapted herein to ensure that the geodesic–bounded surface patches are compatible with the usual polynomial/rational representation schemes of CAD systems. Precise conditions for four Bézier curves to constitute geodesic boundaries of a polynomial or rational surface patch are identified, and an interpolation scheme for the construction of such surfaces is presented when these conditions are satisfied (Farouki et al. [14]).

• **Geodesic Bézier interpolation**.

In general, the interpolation scheme presented in Section 3.6 does not generate a polynomial/rational surface patch, even when the given boundaries are polynomial/rational curves. Hence, it is desirable to modify it to produce patches that are compatible with the standard Bézier representation of CAD systems, starting from boundaries specified as Bézier curves consistent with conditions (**C1**)–(**C3**).

Precisely, fields of polynomial or rational transverse derivatives $\mathbf{T}_i$ are specified in the tangent plane, along each boundary curve $\mathbf{r}_i$, in the following way (Farouki et al. [14]).

$$\mathbf{T}_i(t) \;=\; x_i(t)\,\mathbf{r}_i'(t) \;+\; y_i(t)\,\mathbf{r}_i{}'(t) \times \mathbf{r}_i{}''(t)\,, \tag{3.11}$$

where $x_i(t)$, $y_i(t)$ are polynomial functions. As in Section 3.6, the method involves supplementary constraints for the consistency of the bicubically–blended Coons process. Finally, the method produces two free parameters at each corner.

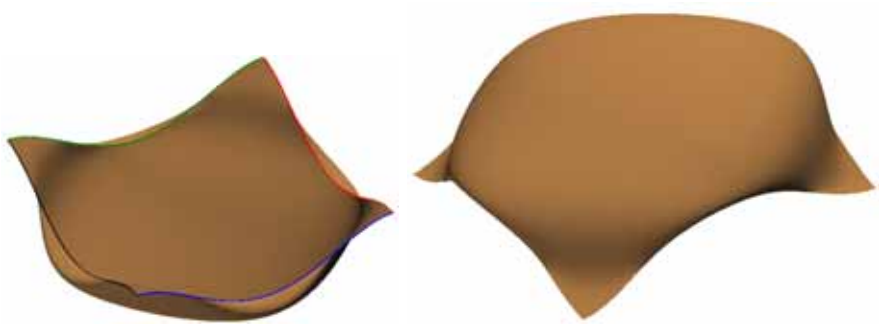

Fig. 3.22 - *Surface interpolating four planar symmetric boundary curves of degree 4, each with two inflections, as geodesics.*

• **Geodesic Bézier curvilinear rectangle**.

Precise conditions for four Bézier curves to constitute geodesic boundaries of a polynomial or rational surface patch are identified and a constructive process is described.

The *Morphosense* measurements provides Bézier curves that do not precisely satisfy the geodesic conditions (**C1**)–(**C3**), but it does allow us to determine the surface tangent plane at each corner, and the osculating planes and curvatures of the boundaries at each corner. Thus, using Hermite approximation scheme, we consider the construction of curvilinear rectangles, composed of four Bézier curves, that satisfy the sufficient–and–necessary conditions (**C1**)–(**C3**) for the existence of a surface patch with these curves as geodesic boundaries.

Polynomial boundary curves of degree 7.

When polynomial Bézier curves of degree 7 are chosen as the patch boundaries, we may freely choose the corner points, the surface tangent planes at those points, and the osculating planes and (non–zero) curvatures at the end points of each Bézier curve, in a manner compatible with the conditions (**C1**)–(**C3**).

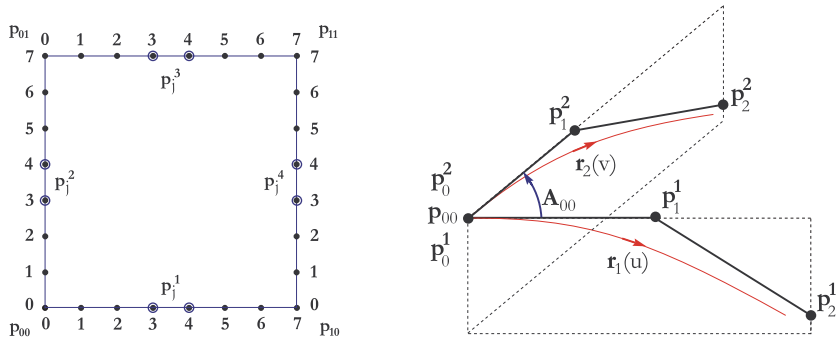

Fig. 3.23 - *Left: control points of the four degree 7 polynomial boundary curves. Right: the tangent plane and osculating planes at the corner* $\mathbf{p}_{00}$.

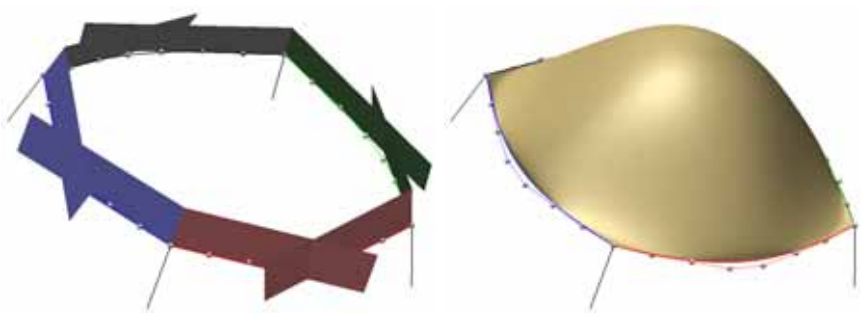

Fig. 3.24 - *Left: the osculating half–planes at each corner. Right: the constructed boundary Bézier curves together with the Bézier patch interpolating these boundary curves as geodesics.*

Rational boundary curves of degree 5.

We now propose a geometric construction using four rational Bézier curves of degree 5. This construction allows one to freely choose the four patch corners and corresponding surface tangent planes, and the osculating planes at the Bézier curve end points, in accordance with conditions (**C1**) and (**C2**), and also the end–point curvatures of the Bézier curves.

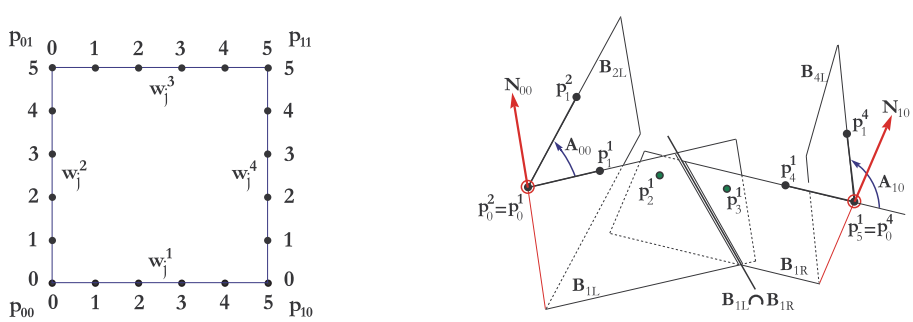

Fig. 3.25 - *Left: four rational Bézier curves of degree 5. Right: osculating planes at corners* $\mathbf{p}_{00}$ *and* $\mathbf{p}_{10}$.

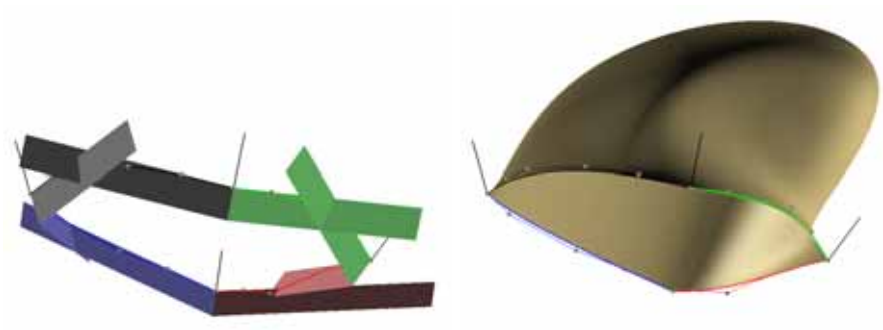

Fig. 3.26 - *Left: osculating half–planes at each corner point. Right: the constructed rational Bézier curves together with the constructed interpolating Bézier patch.*

3.8 Future works

A new collaboration with CEA/LETI is currently in progress. Our goal is to extend the previous surface re–construction methods for animated surfaces. Based on this idea, a real–time demonstrator, the *Morphosense* ribbon, has already been built.

The problem of generating computer models of surfaces from physical measurements obtained with the *Morphosense*, leads to re–construct surfaces whose boundary curves are constrained to have a fixed length. A remarkable property of the spatial PH quintic C^1 Hermite interpolation algorithm (Farouki et al. [12]) is that the solutions depend on two free parameters — which essentially control the *length* and *shape* of the interpolants. The ability to construct curves of given length, with fixed end points/tangents, is very useful in reconstructing surfaces from physically measured data.

A collaboration with Rida Farouki (UC Davis) is currently in progress concerning such an approach. As a first step, we propose to develop algorithms to construct spatial PH curves under arc length constraints, for surface reconstruction applications. A key requirement is to solve the inverse problem of identifying interpolants that match a prescribed arc length.

Bibliography Chapter 3

[1] Bennis, C., Vézien, J.–M., Iglésias, G., Piecewise surface flattening for non–distorted texture mapping, *Computer Graphics 25 (4), pp. 237–246, 1991.*

[2] Boehm, W., Rational Geometric Splines, *Computer Aided Geom. Design 4, (1987), 66–77.*

[3] Coons S., Surfaces for computer aided design, *Technical Report, M.I.T.,1964. Available as AD 663 504 from the National Technical Information service, Springfield, VA 22161.*

[4] Coons S., Surface patches and B-spline curves, *In R. Barnhill and R. Riesenfeld editors, Computer Aided Geometric Design, Academic Press, 1974.*

[5] Do Carmo M.P., *Differential geometry of curves and surfaces, Prentice-Hall, 1976.*

[6] Farin, G., Triangular Bernstein–Bézier patches, *Computer Aided Geometric Design 3, 83–127, 1986.*

[7] Farin G., Curves and Surfaces for CAGD, *Fifth Edition, Academic Press, 2002.*

[8] Farouki R.T. and T. Sakkalis, Pythagorean-hodograph space curves, *Adv. Comput. Math. 2 (1994) 4166.*

[9] Farouki R. T. and H. Pottmann, Polynomial and rational Pythagorean-hodograph curves reconciled, *in The Mathematics of Surfaces VI (G. Mullineux, ed), pp. 355–378, Oxford University Press, 1996.*

[10] Farouki R.T. and S. Shah, Real-time CNC interpolators for Pythagorean-hodograph curves, *Computer Aided Geom. Design 13 (1996) 583600.*

[11] Farouki R.T., J. Manjunathaiah, D. Nicholas, G.-F. Yuan and S. Jee, Variable feedrate CNC interpolators for constant material removal rates along Pythagorean-hodograph curves, *Computer Aided Design 30 (1998) 631640.*

[12] Farouki R. T., M. al–Kandari, and T. Sakkalis, Hermite interpolation by rotation–invariant spatial Pythagorean–hodograph curves, *Adv. Comp. Math. 17, 2002, 369–383.*

[13] Farouki R. T., N. Szafran, L. Biard, Existence conditions for Coons patches interpolating geodesic boundary curves, *Computer Aided Geometric Design, Volume 26, Issue 5, pp. 599-614, June 2009.*

[14] Farouki R. T., N. Szafran, L. Biard, Construction of Bézier surface patches with Bézier curves as geodesic boundaries, *to appear in Computer-Aided Design, doi:10.1016/j.cad.2009.02.019, 2009.*

[15] Farouki R. T., N. Szafran, L. Biard, Construction and smoothing of triangular Coons patches with geodesic boundary curves, *SUBMITTED to CAGD, June 2009.*

[16] Gordon W., An operator calculus for surface and volume modeling, *IEEE Computer Graphics and Applications 3, pp. 18–22, 1983.*

[17] Gregory J. A., P. Charrot, A C^1 triangular interpolation patch for computer–aided geometric design, *Computer Graphics and Image Processing 13, 80–87, 1980.*

[18] Hoschek, J., Dual Bézier curves and surfaces, *in : R.E. Barnhill and W. Boehm, eds., Surfaces in Computer Aided Geometric Design, North Holland, (1983), 147–156.*

[19] Nielson G.M., ν-quaternion splines for the smooth interpolation of orientations, *in IEEE Transactions on visualization and computer graphics, 10(2), March 2004, pp. 224-229.*

[20] Paluszny M., Cubic polynomial patches through geodesics, *Computer Aided Design 40 (1), pp. 56–61, 2008.*

[21] Peters, J., Local smooth surface interpolation: A classification, *Computer Aided Geometric Design 7, 191-195; 1990.*

[22] Pham-Trong V., N. Szafran and L. Biard, Pseudo-geodesics on three-dimensional surfaces and pseudo-geodesic meshes, *Numerical Algorithms © Kluwer Academic Publishers, Volume 26, Issue 4, pp. 305-315, April 2001.*

[23] Pham-Trong Valérie, PhD Thesis,
Détermination géométrique de chemins géodésiques sur des surfaces de subdivision, *Applied Mathematics, University Joseph Fourier, Laboratory LMC-IMAG, 28 septembre 2001.*

[24] Sánchez–Reyes J., Dorado, R., Constrained design of polynomial surfaces from geodesic curves, *Computer Aided Design 40 (1), pp. 49–55, 2008.*

[25] Sarraga, R. F., $G1$ interpolation of generally unrestricted cubic Bézier curves, *Computer Aided Geometric Design 4, 23-39; 1987.*

[26] Shirman, L. A., Séquin, C. H., Local surface interpolation with Bézier patches, *Computer Aided Geometric Design 4, 279-295, 1987.*

[27] Sprynski N. et al (CEA/LETI), PATENT no WO/2006/095109,
Method and Device For Acquisition of a Geometric Shape, September 2006.

[28] Sprynski N., B. Lacolle, L. Biard, D. David, Curve and Surface Reconstruction via Tangential Information, *Curve and Surface Design : Avignon 2006, P. Chenin, T. Lyche, L. L. Schumaker (eds), Nashboro Press, pp. 254–263, 2007.*

[29] Sprynski Nathalie, PHD Thesis,
Reconstruction de courbes et surfaces à partir de données tangentielles, *Applied Mathematics, University Joseph Fourier / Laboratory LJK & CEA/LETI, 5 juillet 2007.*

[30] Sprynski N., B. Lacolle, D. David, and L. Biard, Curve Reconstruction via a Ribbon of Sensors, *In Proceeding of the 14th IEEE International Conference on Electronics, Circuits and Systems, ICECS - 2007, Marrakech, Maroc, December 2007.*

[31] Sprynski N., N. Szafran, B. Lacolle, L. Biard, Surface reconstruction via geodesic interpolation, *Computer-Aided Design, Volume 40, Issue 4, pp. 480-492, April 2008.*

[32] Struik, D. J., Lectures on Classical Differential Geometry, *Dover (reprint), 1988.*

[33] Tucker, C. L. III, Forming of advanced composites, *in Advanced Composites Manufacturing (Gutowski, T. G., ed.), pp. 297–372, Wiley, New York, 1997.*

[34] Wang G., Tang, K., Tai, C. H., Parametric representation of a surface pencil with a common spatial geodesic, *Computer Aided Design 36 (5), pp. 447–459, 2004.*

Chapter 4

Variation Diminishing Property of Bézier Curves

The variation diminishing property of Bézier curves states that the number of time any straight line L crosses a Bézier curve Γ, defined on a finite interval I, does not exceed the number of intersections of the line, L with the corresponding control polygon of the curve Γ over the interval I [3]. There have been several proofs of this variation diminishing property such as the proof using the Descarte's rule of signs [4], or the proof using the Karlin Theorem on totally positive matrices [5] or the proof using the concept of degree elevation of Bézier curves. The diminishing variation property ensures, to a certain extent, that the Bézier curve imitate the shape of the corresponding control polygon. For instance, it states that a convex control polygon is always associated with a convex Bézier curve. The converse is not true in general [1].

Using the notion of polar derivative introduced by Laguerre [6], we investigate generalizations of the variation diminishing property of Bézier curves to include statements on the number of intersections of a line with a Bézier curve as compared to the number of intersections of the line with a concatenation of sub-Bézier curves (Ait-Haddou et al. [2]).

Any refinement of the variation diminishing property for Bézier curves will improve on the applications of the classical variation diminishing property. For instance, localizing the real roots of a polynomial over an interval can be achieved by iterative subdivision of the control polygon and elimination of the sub-intervals in which the control polygon have the same sign. Therefore, the refinement above can lead to more efficient detection of sub-intervals free of real roots even if the control polygon change sign. Other applications of this refinement will be given subsequently.

4.1 Polar derivative

Let $F(t)$ be a polynomial of degree n ($n \geq 1$), and denote by $f(u_1, u_2, \ldots, u_n)$ its blossom. Considering the Bernstein basis $B_i^n(t)$ over the interval $[a, b]$, we can write $F(t) = \sum_{i=0}^{n} p_i B_i^n(t)$, with $p_i = f(a^{n-i}, b^i)$, where the notation x^k indicates that x is to be repeated k times. The *polar derivative* ([6], pp. 48-49) with respect to the pole ζ, of

the polynomial $F(t)$, is the polynomial $F_\zeta(t)$ of degree $n-1$, defined by

$$F_\zeta(t) = \sum_{i=0}^{n-1} f(a^{n-1-i}, b^i, \zeta)\, B_i^{n-1}(t)\,.$$

Therefore (see Fig. 4.1), for a polynomial with Bézier points $p_0, ...p_n$ on $[a,b]$, the polar derivative with respect to the pole ζ is the polynomial of degree $(n-1)$, with Bézier points

$$q_i = \frac{b-\zeta}{b-a}\, p_i + \frac{\zeta - a}{b-a}\, p_{i+1}, \quad i = 0, ..., n-1\,.$$

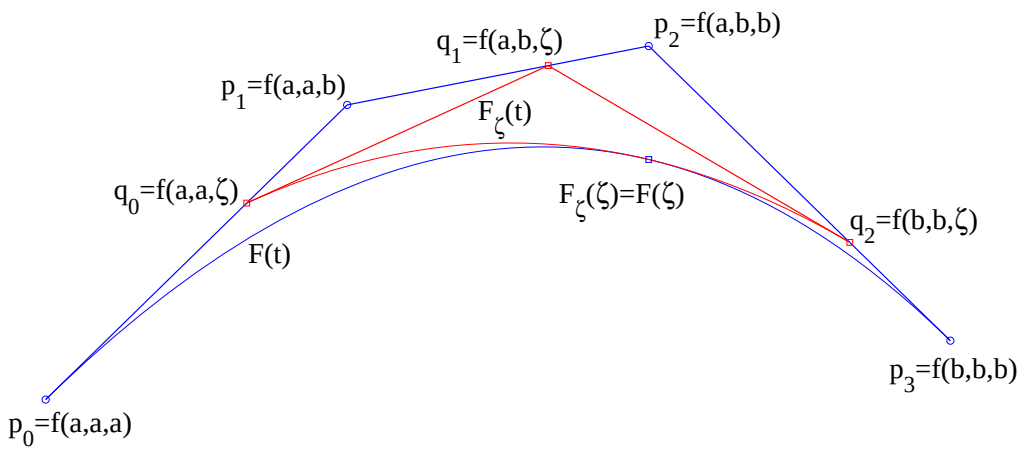

Fig. 4.1 - *Polar derivative of a parametric cubic polynomial curve expressed in the Bernstein basis over the interval* $[a,b]$.

• **A new expression of the polar derivative**.

Denoting by $\mathcal{P}_n$ the linear space of polynomials of degree less or equal to n, we consider the following two linear operators $d : \mathcal{P}_n \to \mathcal{P}_{n-1}$ and $\psi_{\zeta,n} : \mathcal{P}_n \to \mathcal{P}_n$ defined by

$$d(F(t)) = F'(t) \quad \text{and} \quad \psi_{\zeta,n}(F(t)) = (t-\zeta)^n\, F(\zeta + \frac{1}{t-\zeta})\,.$$

Introducing the map $\hat{\zeta} : t \mapsto \hat{\zeta}(t) = \zeta + 1/(t-\zeta)$ we have $\hat{\zeta} \circ \hat{\zeta}(t) = t$ for all $t \neq \zeta$, from which we deduce

$$\psi_{\zeta,n} \circ \psi_{\zeta,n} = I_d\,,$$

where I_d is the identity on $\mathcal{P}_n$.
The polar derivative of a polynomial $F(t)$ of degree n, with respect to a pole ζ, can be expressed in terms of the two operators d and $\psi_{\zeta,n}$.

$$\psi_{\zeta,n-1} \circ d \circ \psi_{\zeta,n}(F(t)) = n\, F_\zeta(t). \tag{4.1}$$

4.2 Diminishing variation property for univariate polynomials

For our purpose we need precise definitions.

1 *For a polynomial $F(t)$ of degree at most n, we define $Z^n_{[a,b]}(F(t))$ as follows. If $F(t)$ is identically zero, then $Z^n_{[a,b]}(F(t)) = n+1$. Otherwise $Z^n_{[a,b]}(F)$ denotes the number of real roots of $F(t)$ in the interval $[a,b]$, counting multiplicities.*

2 *For $s \geq 1$ and real numbers $r_1, ..., r_s$, let*

$$S(r_1, ..., r_s) = \big|i : 1 \leq i \leq s, r_i = 0\big| + \big|i : 1 \leq i \leq s-1, r_i r_{i+1} < 0\big|$$

be the number of sign changes in the ordered sequence $(r_1, ..., r_s)$ and

$$S_L(r_1, ..., r_s) = S(r_1, ..., r_s) - S(r_s),$$
$$S_R(r_1, ..., r_s) = S(r_1, ..., r_s) - S(r_1),$$

be the Left and Right number of sign changes in the sequence.

• **Main result (univariate case)**. *Let $F(t)$ be a polynomial of degree n. Then for every real number ζ in the interval $[a,b]$, $a < b$, we have*

$$Z^n_{[a,b]}\big(F(t)\big) \leq S_L(F(a), F_\zeta(a)) + Z^{n-1}_{[a,b]}\big(F_\zeta(t)\big) + S_R(F_\zeta(b), F(b))\,. \tag{4.2}$$

• **Corollary**. *Applying repeatedly inequality (4.2) with $\zeta = a$ or $\zeta = b$, leads to the following result.*

$$Z^n_{[a,b]}\Big(\sum_{i=0}^{n} p_i B^n_i(t)\Big) \leq S_L(p_0, ...p_k) + Z^{l-k}_{[a,b]}\Big(\sum_{i=k}^{l} p_i B^{l-k}_{i-k}(t)\Big) + S_R(p_l, ..., p_n)\,,$$

for any k, l with $0 \leq k \leq l \leq n$.
Notice that for $k = l$ the right hand simplifies as $S(p_0, ..., p_n)$ which provides the classical variation diminishing property.

• <u>Remark</u>. The polynomial $F(t)$ below (see Fig. 4.2) has two real roots in the interval $[0,1]$, while the two sub-polynomials $F_1(t) = \sum_{i=0}^{2} p_i B^2_i(t)$ and $F_2(t) = \sum_{i=0}^{3} p_{2+i} B^3_i(t)$ have no real roots in the interval $[0,1]$. Therefore, in this situation, we have

$$Z^5_{[0,1]}\Big(\sum_{i=0}^{5} p_i B^5_i(t)\Big) \;>\; Z^2_{[0,1]}\Big(\sum_{i=0}^{2} p_i B^2_i(t)\Big) + Z^3_{[0,1]}\Big(\sum_{i=0}^{3} p_{2+i} B^3_i(t)\Big)\,,$$

which shows that inequality (4.2) can not be generalized in a straightforward way.

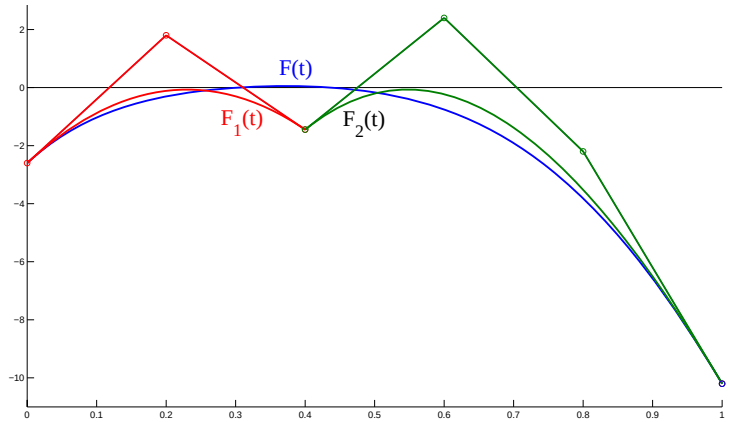

Fig. 4.2 - *Inequality (4.2) can not be generalized in a straightforward way.*

4.3 Variation diminishing property for parametric polynomials

In this section, we merely translate all the results of the last section to 2-dimensional parametric polynomial curves. Of course there are corresponding results for any d-dimensional space curve. Thus, consider a parametric polynomial curve $F(t) = (p(t), q(t))$ of degree n and a line Δ in the 2-dimensional space and denote by $Z^n_{\Delta,[a,b]}(F(t))$ the number of intersections of the line Δ with the curve $F([a,b])$ $(a < b)$ counting multiplicities. If the curve $F([a,b])$ is included in the line Δ, we shall consider that $Z^n_{\Delta,[a,b]}(F(t)) = n+1$.

Then, for $s \geq 1$ and points $M_1, \ldots, M_s$ in the 2-dimensional space, we consider the number of intersections $S_\Delta(M_1, \ldots, M_s)$ of the line Δ with the polygonal line $(M_1, \ldots, M_s)$ defined in a similar way as in the previous section. See also (Ait-Haddou et al. [2]).

By a standard method, in which statements about the number of roots of a univariate polynomial can be translated to statements about the number of intersections of a parametric curve with a given line, we obtain the following result.

• **Main result (parametric case)** . *Let $F(t) = \sum_{i=0}^n F_i B_i^n(t)$ be a parametric polynomial curve of degree n defined on an interval $[a,b]$, with $F_i = (p_i, q_i)$ for $i = 0, \ldots, n$. Let Δ be an affine line defined by $\alpha\, x + \beta\, y + \gamma = 0$. For any real number ζ in the interval $[a,b]$ we denote by $G_i = \frac{b-\zeta}{b-a} F_i + \frac{\zeta - a}{b-a} F_{i+1}$ for $i = 0, \ldots, n-1$. Then we have*

$$Z^n_{\Delta,[a,b]}\Big(\sum_{i=0}^n F_i B_i^n(t)\Big) \;\leq\; S_{\Delta,L}(F_0, G_0) + Z^{n-1}_{\Delta,[a,b]}\Big(\sum_{i=0}^{n-1} G_i B_i^{n-1}(t)\Big) + S_{\Delta,R}(G_{n-1}, F_n). \tag{4.3}$$

• **Corollary**. *Let $F(t) = \sum_{i=0}^n F_i B_i^n(t)$ be a parametric polynomial curve of degree n defined on an interval $[a,b]$. For any k, l with $0 \leq k \leq l \leq n$ we have*

$$Z^n_{\Delta,[a,b]}\Big(\sum_{i=0}^n F_i B_i^n(t)\Big) \leq S_{\Delta,L}(F_0, ...F_k) + Z^{l-k}_{\Delta,[a,b]}\Big(\sum_{i=k}^{l} F_i B_{i-k}^{l-k}(t)\Big) + S_{\Delta,R}(F_l, ..., F_n).$$

Notice again that for $k = l$ the right hand simplifies as $S_\Delta(F_0, ..., F_n)$ which provides the classical variation diminishing property of Bézier curves.

• Example 1.

More precisely (see Fig. 4.3), the number of intersections of any straight line Δ with a Bézier curve $P(t) = \sum_{i=0}^{n} P_i B_i^n(t)$ (in blue) does not exceed the number of intersections of the line with the red curve (in bold) composed of the polygon $(P_0, ..., P_k)$, the Bézier curve of degree $l - k$ associated with the control polygon $(P_k, ..., P_l)$ and the polygon $(P_l, ..., P_n)$, for any value of k, l with $0 \leq k \leq l \leq n$. In the case of Fig. 4.3, and since the Bézier curve with control points $(P_k, ..., P_l)$ has no intersection with the line Δ_2, the refinement of the variation diminishing property asserts that, no matter how we change the control points $(P_0, ..., P_{k-1})$ and $P_{l+1}, ..., P_n)$ the number of intersections of the blue curve with control points $(P_0, ..., P_n)$ and the line Δ_2 cannot exceed $n - l + k$.

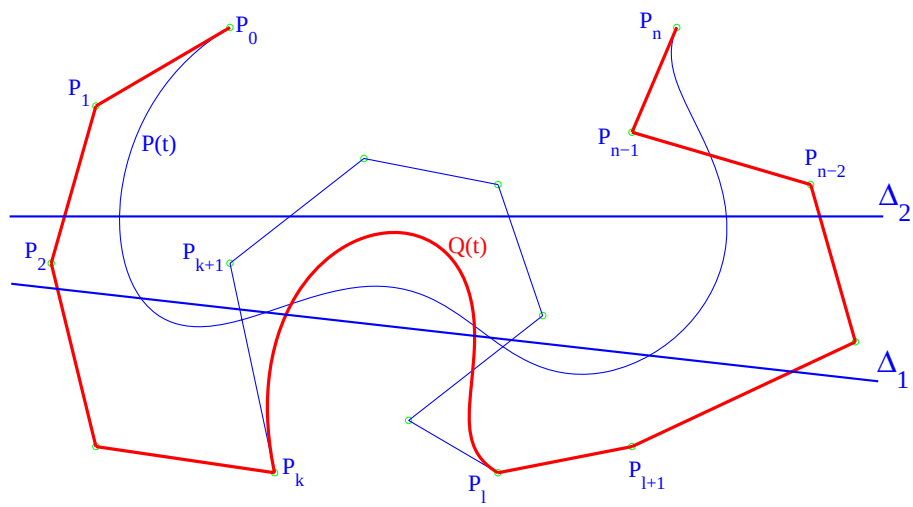

Fig. 4.3 - *An example of the refinement of the Variation Diminishing Property of Bézier Curves : The number of intersections of any straight line Δ with the Bézier curve in blue does not exceed the number of intersections of the line with the red curve (in bold).*

• Example 2. The following Fig. 4.4 exhibits a refinement of the variation diminishing property of Bézier curves : the number of intersections of any line Δ with the blue curve $F(t)$ does not exceed the number of intersections of that same line with the piecewise curve in red and bold. Furthermore, considering the two lines Δ_i, $i = 1, 2$, we deduce that the number of intersections of these lines with the Bézier curve $F(t)$ is at most one, since the lines does not intersect the control polygon of the polar derivative $F_\zeta(t)$. Naturally, we can reach the same conclusion by just applying De Casteljau subdivision over the two intervals $[0, \zeta]$ and $[\zeta, 1]$. However, with the refinement of the variation diminishing property, we can iterate the process, with different poles at each stage, thereby leading to a strategy with complexity $O(n)$ instead of $O(n^2)$ obtained using De Casteljau algorithm.

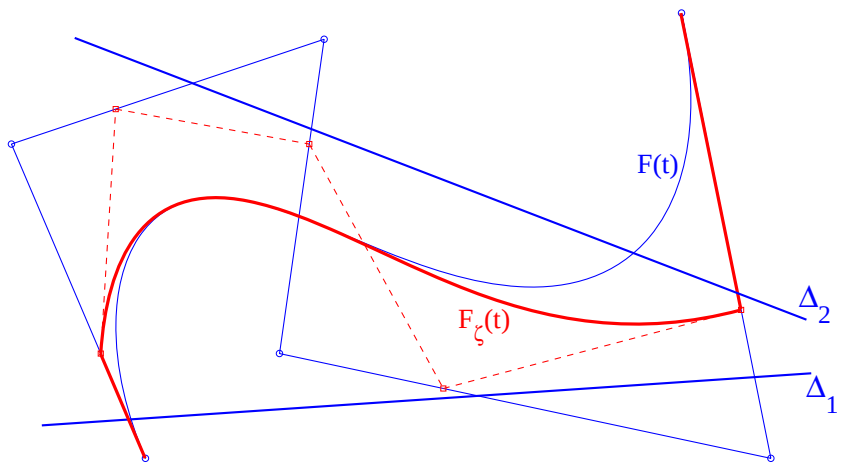

Fig. 4.4 - *A refinement of the variation diminishing property of Bézier curves. The polar derivative is performed with respect to the pole $\zeta = 1/3$.*

4.4 Future work

For algorithms aimed at localizing the real roots of polynomials, by subdivision of the control polygon and elimination of the intervals in which the control points have the same sign, this refinement of the variation diminishing property have the potential of speeding up the algorithm with more efficient detection of the interval in which the polynomial has not roots. Such algorithms will improve on applications in intersection detection.

As an example, consider the following direct application of the previous results. *Let $F(t) = \sum_{i=0}^{n} F_i B_i^n(t)$ be a parametric polynomial curve of degree n defined on an interval $[a, b]$ and denote by $f(u_1, u_2, \ldots, u_n)$ its blossom. Let Δ be an affine line. Then, for any set of n real numbers ζ_i, $i = 1, \ldots, n$ in the interval $[a, b]$, we have*

$$Z_{\Delta,[a,b]}\Big(\sum_{i=0}^{n} F_i B_i^n(t)\Big) \;\leq\; S_\Delta(R_n, R_{n-1}, \ldots, R_1, R_0 = S_0, S_1, \ldots, S_{n-1}, S_n),$$

where

$$\begin{array}{lll} R_n = f(a^n) = F_0\,, & R_i = f(a^i, \zeta_1, \ldots, \zeta_{n-i}) & i = 0, \ldots, n-1\,, \\ S_n = f(b^n) = F_n\,, & S_i = f(b^i, \zeta_1, \ldots, \zeta_{n-i}) & i = 0, \ldots, n-1\,. \end{array}$$

An interesting choice of the parameters ζ_i are the ones in which the successive polar derivative of the polynomial $F(t)$ vanishes. As an illustrative example, consider the polynomial function $F(t)$ defined in Fig. 4.5. Let ζ_1 and ζ_2 the real numbers in the interval $[0, 1]$ such that $f(0, 0, 0, 0, \zeta_1) = 0$ and $f(0, 1, 1, \zeta_1, \zeta_2) = 0$. Then, with $\zeta_3 = \zeta_4 = \zeta_5 = 1$, we have $Z_{[a,b]}(F(t)) \leq S(r_5, 0, r_3, r_2, 0, r_0 = s_0 = s_1 = s_2 = s_3, s_4, s_5) = 2$. Nevertheless, for a small perturbation of parameters ζ_1 and ζ_2, the sign change in r_4 disappears whereas the sign change in r_1 always remains. Which leads to $Z_{[a,b]}(F(t)) \leq 1$, which is an optimal bound since the polynomial $F(t)$ has only one real root in the interval $[0, 1]$.

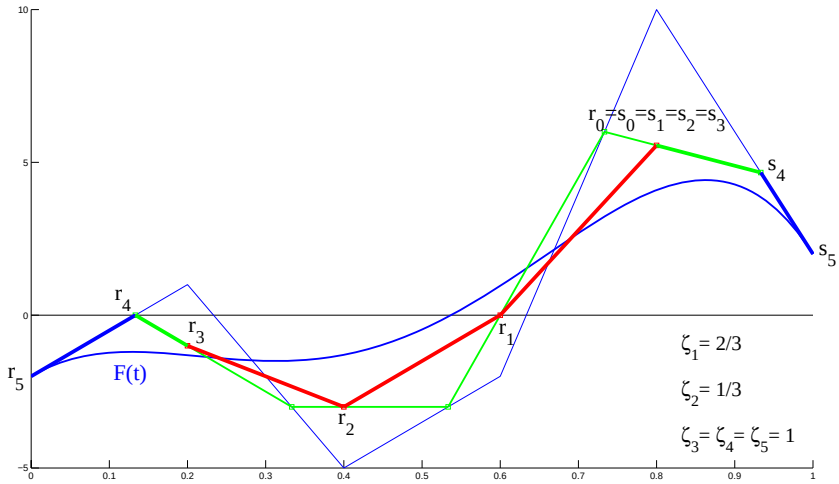

Fig. 4.5 - *A refinement of the variation diminishing property : the number of intersections of any line with the polynomial curve in blue does not exceed the number of intersections of the same line with the piecewise linear polygon in bold.*

Bibliography Chapter 4

[1] Ait-Haddou R., and W. Herzog, Convex subdivision of a Bézier curve, *Computer Aided Geometric Design, 8, pp. 663-671, 2002.*

[2] Ait-Haddou Rachid, Taishin Nomura and Luc Biard, A Refinement of the Variation Diminishing Property of Bézier Curves, *on Revision, Comput. Aided Geom. Design, May 2009.*

[3] Farin G., Curves and Surfaces for CAGD, *Fifth Edition, Academic Press, 2002.*

[4] Goodman T. N. T., Shape preserving representations, *in Mathematical methods in Computer Aided Geometric Design, T. Lyche and L. L. Schumaker (eds.), Academic Press, New York, 333-357, 1989.*

[5] Karlin, S., Total Positivity, *Stanford University Press, Stanford, 1968.*

[6] Marden, M., Geometry of Polynomials, 2nd ed., *Amer. Math. Soc., Providence, 1966.*

[7] Ramshaw, L., Blossoms are polar forms, *Computer Aided Geometric Design, Vol. 6, Issue 4, pp. 323-358, 1989.*

Chapter 5

Industrial activities

This chapter is concerned with wave propagation in homogeneous media. We took advantage of planar offsetting techniques presented in Chapter 1 for industrial applications in a seismological context : ELF EP [3] and TOTAL FINA ELF S.A. [3]. In this context, the standard Euclidean approach corresponds to isotropic homogeneous media, while the Minkowski-plane approach [1, 2] conveniently and rigorously extends the exploding-reflector method to include anisotropic-homogeneous media. Nevertheless, the anisotropic-homogeneous case has not been implemented in the following application.

Our participation split into two parts : the approximation and reconstruction of the interfaces by quadrics (N. Szafran, B. Lacolle) and the propagation of waves (L. Biard). Even though these works are confidential, it is possible to outline the main ideas of the method.

• **The method**.

We essentially treated the 2D case (planar propagated waves) but some attempts with 3D waves have also been considered. The propagated waves are modeled as offset curves. More precisely, the method can be summarized as follows.

1. The propagated waves are approximated by planar offset. Precisely, if $C_0(u)$ is an approximation of the initial waves, the propagated wave at time t is defined by

   $$C_t(u) = C_0(t) + t\,N(u)\,,$$

   where $N(u)$ is the unit normal to the curve C_0.

   The relation between the time t and and the distance covered by the waves during a fixed time is assumed by the norm of the plane. For an isotropic homogeneous media we consider the Euclidean plane with a sphere as indicatrix.

2. For simplicity, we consider rational parametric approximation of the waves. Since the approximation depends on the time t, we shall consider PH approximation of the propagated waves.

   More precisely, we consider G^1 PH splines, i.e., rational PH curves of class 3 with G^1 contact. Furthermore we consider the dual Bézier characterization of these PH curves by using a generating circle. Notice that this construction give a free parameter α for each PH curve of class 3.

3. Thus, the propagated waves in an uniform medium are obtained by just translating the dual control structures of the PH curves. It can be noticed that this process preserves G^1 continuity.

4. For reflection/transmission through an interface separating two homogeneous media, the reflection/transmission of the dual control structure of the PH curves produces an approximation of the reflected/transmitted waves which is, generally, no more a PH curve. Thus, we consider again a G^1 PH approximation of the reflected/transmitted waves after subdivision of the initial propagated wave. Then, the free parameters allow to improve the approximation by least square method.

   Notice that a major difficulty is to control the regularity of the produced PH curves.

• **Dual Bézier construction of PH curves**.

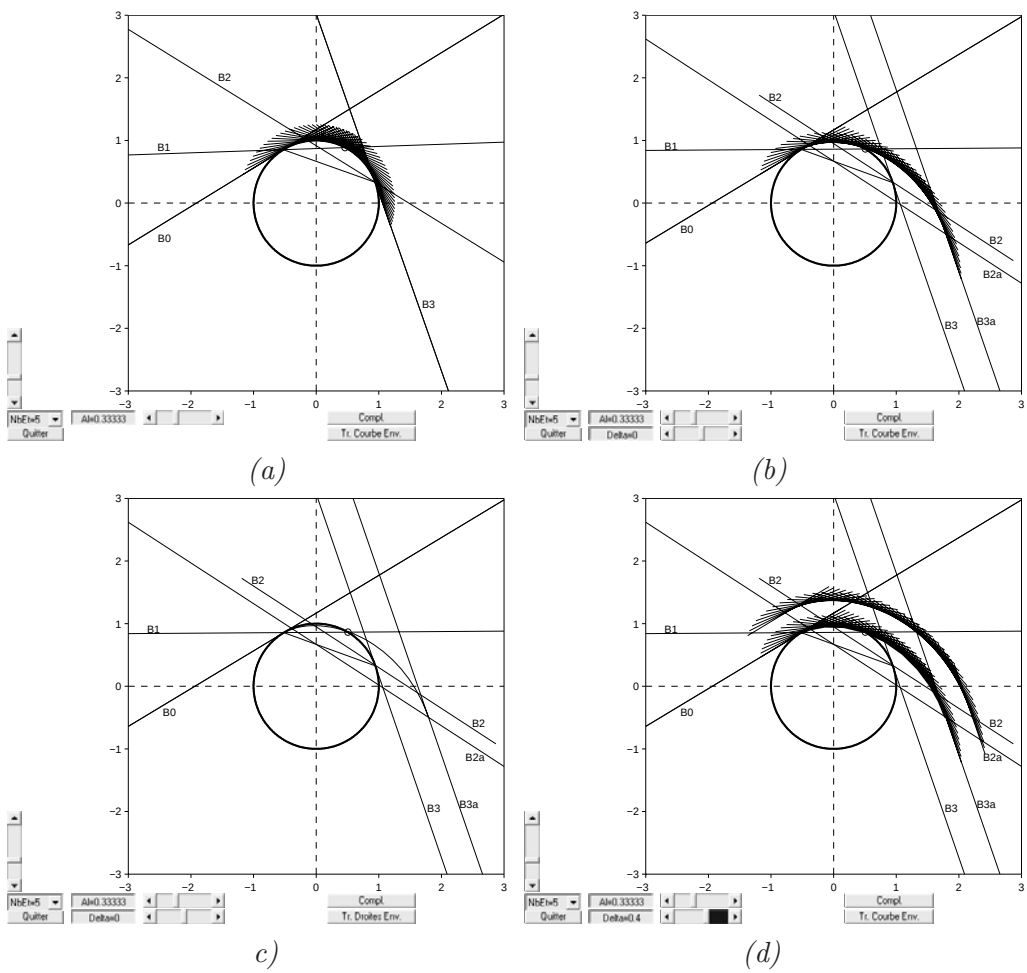

Fig. 5.1 - *Dual Bézier representation of PH curves of class 3 and of their offsets.*

The dual-Bézier control structure of a rational curve [5, 6] provides a natural tool for the construction of rational curves with a G^1 contact. Precisely, for two such curves of class 3, with Bézier lines B_i and b_i, $i = 0, ..., 3$, the G^1 contact is realized if and only if

$$B_3 \equiv b_0 \quad \text{and} \quad B_2 \cap B_3 = M = b_0 \cap b_1 \,.$$

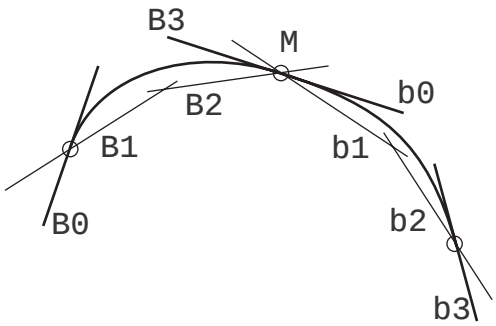

Fig. 5.2 - *G^1 continuity for curves in their dual-Bézier representation.*

• **Direct propagation in the same media**.

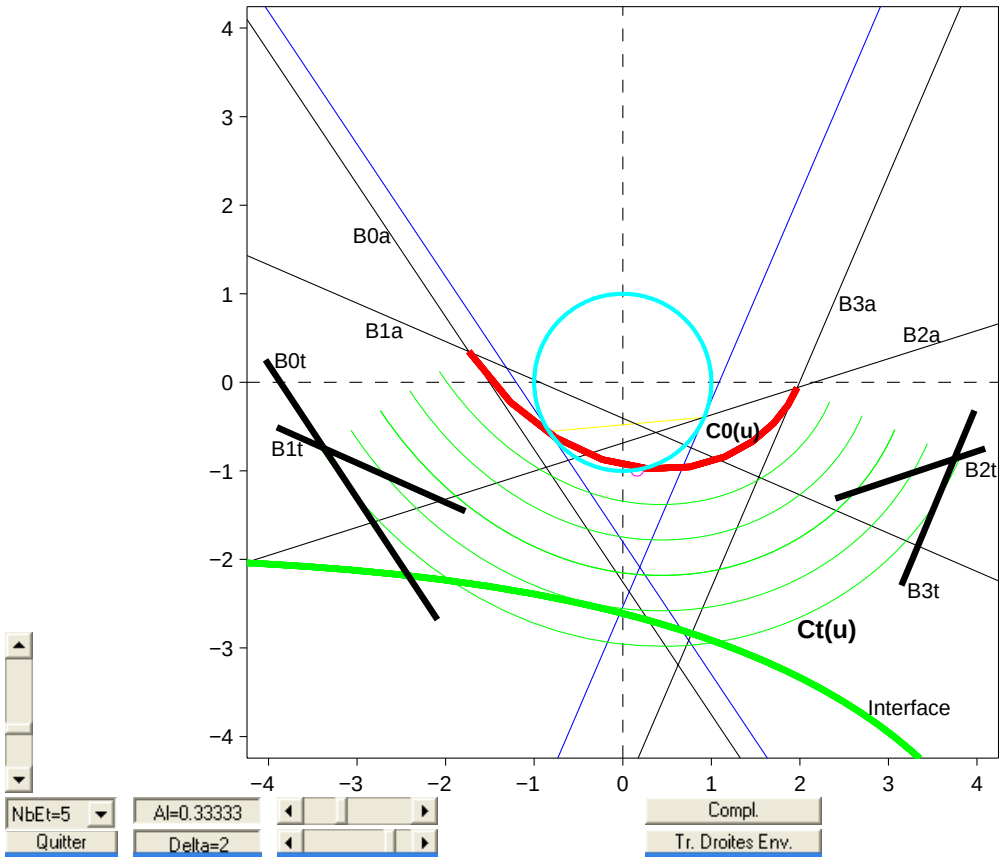

Fig. 5.3 - *Direct propagation of an initial PH wave front $C_0(u)$. The dual control structure of the propagated wave $C_t(u)$ is deduced from the initial dual control structure by a simple translations.*

• **Reflection and transmission**.

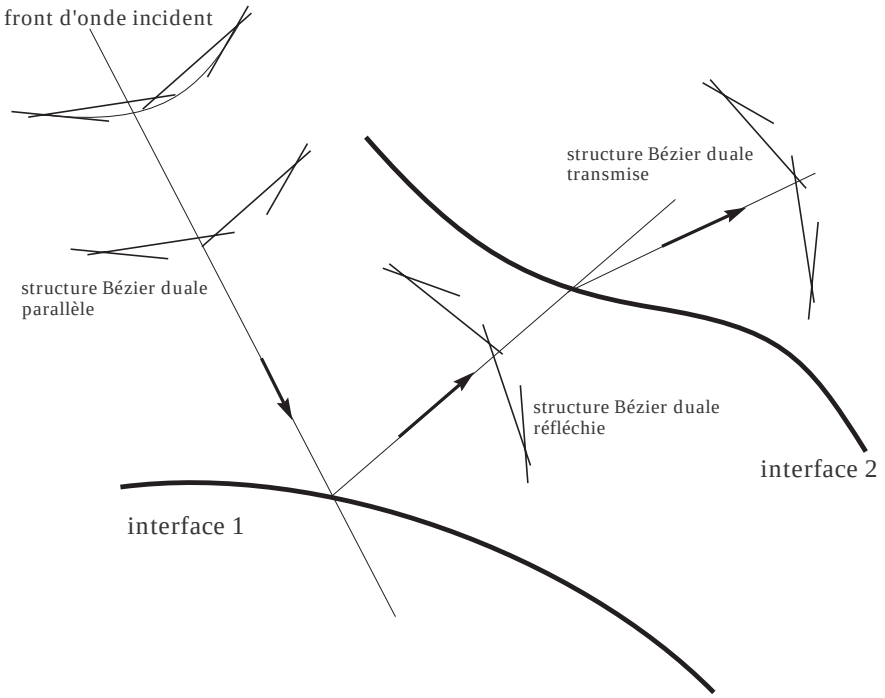

Fig. 5.4 - *Reflection and transmission.*

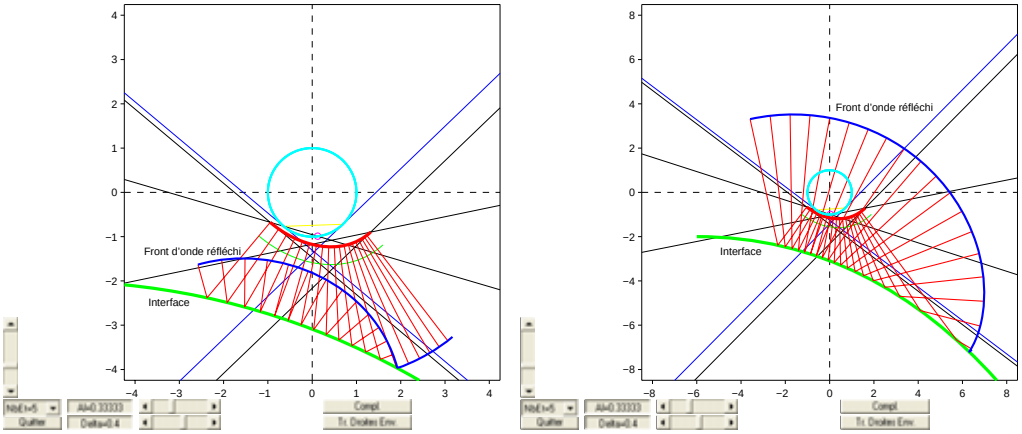

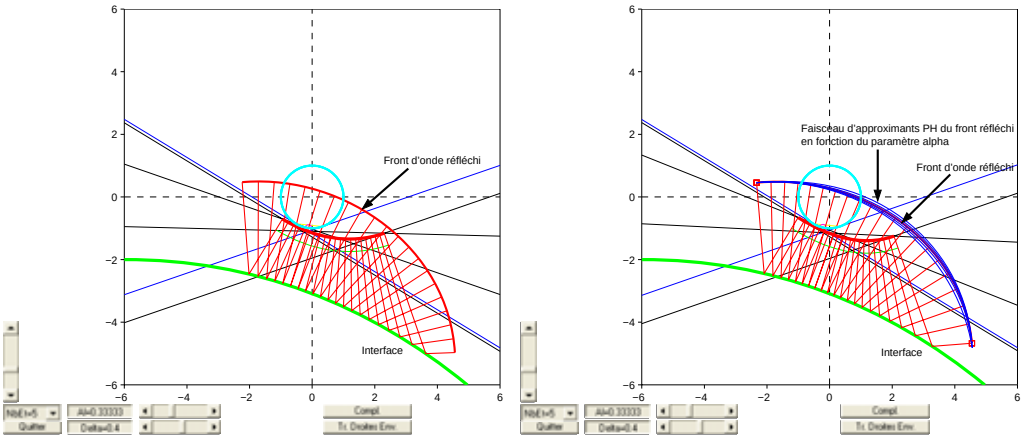

(a) (b)

Fig. 5.5 - *Reflection of the wave front and its approximation by a PH curve.*

We can see in Fig. 5.5 - (b), that the exact reflected front wave is correctly approximated by the one parameter family of PH curves depending on the free parameter α. The best approximation can be evaluated from a mid-point of the curve and least square method.

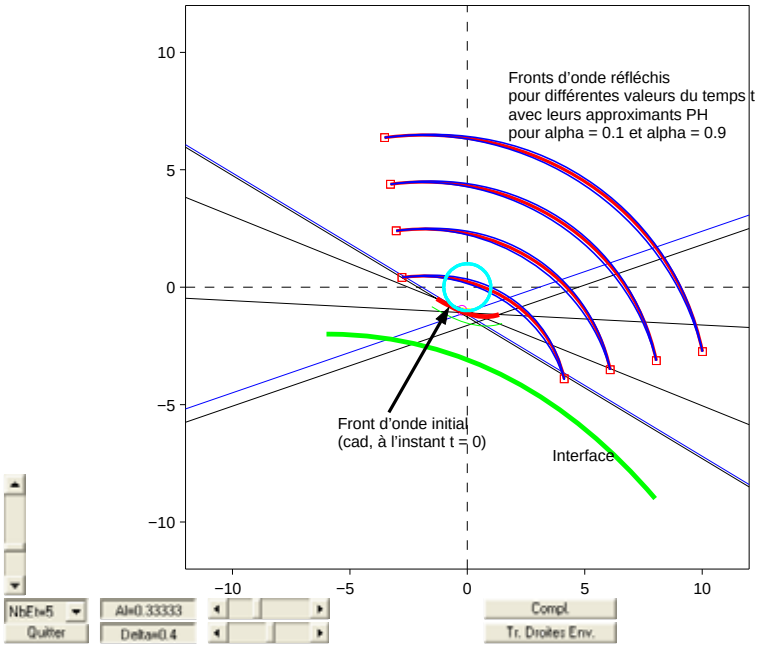

Fig. 5.6 - *Then, after reflection, the propagation of the front wave is straightforward.*

• **Subdivision**.

In order to increase the precision of the approximation of the different propagated waves, we perform a subdivision of each PH curve of class 3 for each reflection/transmission.

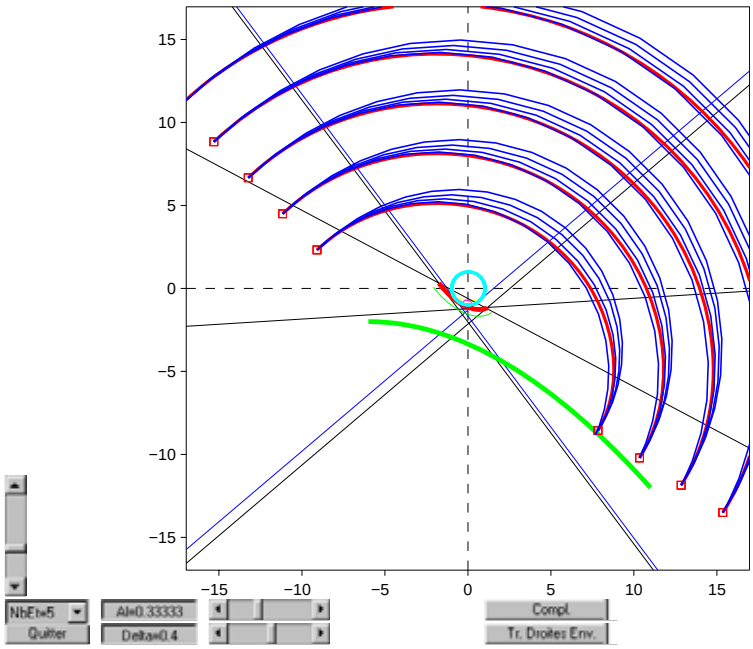

(a) : before subdivision of the one parameter family of PH-approximating curves.

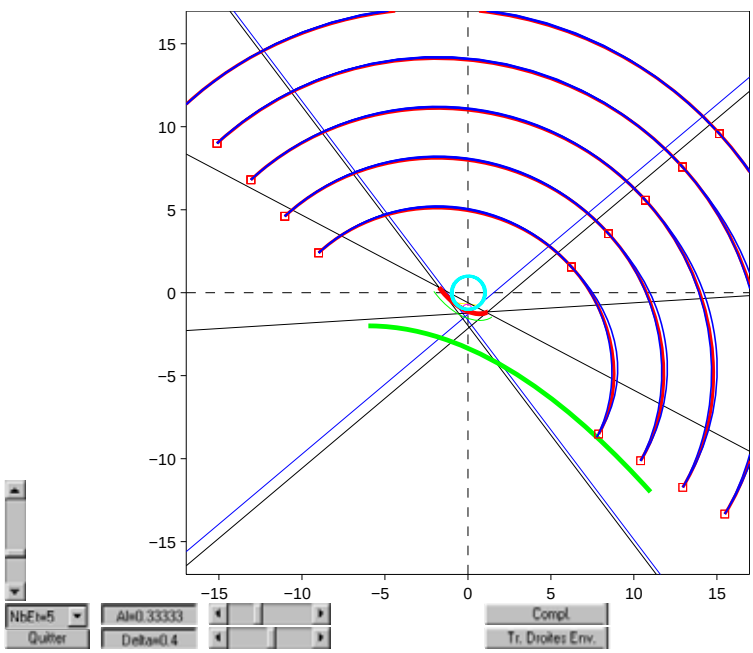

(b) : after subdivision of the one parameter family of PH-approximating curves.

Fig. 5.7 - *Subdivision of the propagated wave.*

• **Conclusion**.

As noticed above, the implementation of such an algorithm is somewhat technical. Notice that the need to control singularities of the approximating curves lead us not to consider PH curves of higher degree.

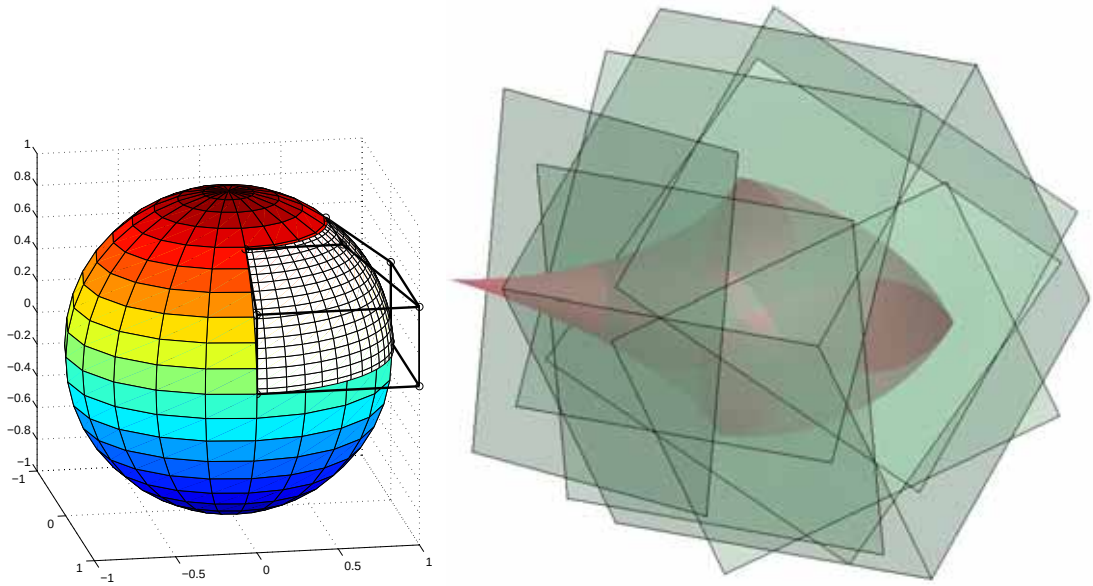

Fig. 5.8 - *Offset surface.*

Finally, we made some attempts to model offset surfaces deduced from a sphere as proposed by Pottmann [5, 6]. But, this approach appears to be to much intricate for such an application.

Bibliography Chapter 5

[1] Ait-Haddou Rachid, PhD Thesis,
Courbes à hodographe pythagorien en géométrie de Minkowski et modélisation géométrique, *Applied Mathematics, University Joseph Fourier, Laboratory LMC-IMAG, 6 septembre 1996.*

[2] Ait-Haddou, R., L. Biard and M. A. Slawinski, Minkowski isoperimetric-hodograph curves, *in Comput. Aided. Geom. Design, vol 17, issue 9, October 2000, pp 835-861.*

[3] Lacolle B., N. Szafran, L. Biard, Approximations adaptatives par des quadriques et modélisation géométrique des interfaces en liaison avec le contexte optique, *Rapport de contrat TOTAL FINA ELF S.A., Juillet 2004.*

[4] Lacolle B., N. Szafran and L. Biard, Modélisation par paraboloïdes et Modélisation par surfaces duales, *Rapport de contrat ELF EP n° 11985, CNRS n° 721671/00, UJF n° 9025, Mars 2001.*

[5] Pottmann, H., Rational curves and surfaces with rational offsets, *Comp. Aided Geom. Design* **12**, *(1995), 175–192.*

[6] Pottmann, H., Curve design with rational Pythagorean-hodograph curves, *Advances in Computational Mathematics, Vol. 3, pp.147–170, 1995.*